

TJ778

.M41

.G24

no. 197

AERO

MIT LIBRARIES



3 9080 00601 1164

**INDUCED STRAIN ACTUATION
OF COMPOSITE PLATES**

by

**Kenneth B. Lazarus
Edward F. Crawley**

GTL Report #197

March 1989

APR 24 1990



**GAS TURBINE LABORATORY
MASSACHUSETTS INSTITUTE OF TECHNOLOGY
CAMBRIDGE, MASSACHUSETTS**

**INDUCED STRAIN ACTUATION
OF COMPOSITE PLATES**

by

**Kenneth B. Lazarus
Edward F. Crawley**

GTL Report #197

March 1989

This research was sponsored by General Dynamics Corporation, Michael Love and Jon Bohlmann, technical monitors. Additional funding was provided by the Allison Gas Turbine division of General Motors Corporation.

ABSTRACT

Two models of induced strain plate actuator/substrate systems are developed and verified experimentally. Equations relating the actuation strains produced by the strain actuators to the induced strains found in the system are derived for both models. In addition, the plate strain energy relations are also developed.

Exact and approximate solutions are formulated for isotropic and anisotropic plate systems. Exact solutions are found for actuator/substrate systems with free-free, free-free boundary conditions, and a general procedure for solving the strain energy equations with a Rayleigh-Ritz approximate solution is formulated for systems with arbitrary boundary conditions and external loads. Specific solutions are detailed for cantilever plate systems, including a discussion of the assumed modes selected.

A model for predicting the actuation strains produced by a specific class of induced strain actuators, piezoceramic actuators, is also developed. The non-linear properties of piezoceramics are discussed and the important effects of such non-linearities are accounted for by developing a strain dependent model for the actuation strains created in piezoceramics.

The models developed were verified through experimentation via two sets of plate test articles. The first set of simple test articles were used to verify the accuracy of the basic induced strain actuation models, the strain dependence of piezoceramic actuation strains, and a semi-empirical solution procedure. The second, more representative, set of large cantilever plate test articles verified the ability of the models to predict the strains induced in systems with extensive stiffness couplings and complicated boundary conditions, and the Ritz model. Agreement between the solutions predicted by the induced strain actuator models and the experimentally measured deformations was excellent, verifying the effectiveness of using induced strain actuation for shape control of structures such as aeroelastic lifting surfaces and components of intelligent structures.

ACKNOWLEDGEMENTS

This research was sponsored by the General Dynamics corporation with Michael Love and Jon Bohlmann serving as technical monitors.

Additional funding was provided by the Allison Gas Turbine division of the General Motors Corporation.

Their support is greatly appreciated.

TABEL OF CONTENTS

List of Symbols	6
List of Figures	8
List of Tables	11
Chapter 1. Introduction	12
Background and Objective	14
Approach and Outline	15
Chapter 2. Analytical Models of Induced Strain Actuators	17
2.1 Introduction	17
2.2 "Pin" Force Model in One Dimension	18
Induced Strain Actuation in Extension	19
Induced Strain Actuation in Bending	22
2.3 Review of Thin Plate Theory	27
2.4 Development of the "Pin" Force Plate Model	31
Plate Actuation in Extension	33
Plate Actuation in Bending	34
2.5 Development of the Consistent Plate Model	36
Governing Equations	37
Strain Energy Relations	40
2.6 Conclusions	42
Chapter 3. Solutions to the Analytical Models	44
3.1 Introduction	44
3.2 Exact Solutions of Induced Strain Actuator Models	45
"Pin" Force Plate Model Solutions	45
Consistent Plate Model Solutions	51
3.3 Ritz Formulation for Approximate Solutions	55
Ritz Assumed Mode Method	55
Assumed Mode Selection	59
Simplifications for Design	62

3.4	Conclusions	69
Chapter 4.	Piezoceramic Induced Strain Actuators	71
4.1	Introduction	71
4.2	Piezoceramic Actuation Strain Model	72
	Effects of Limited Orthotropy	77
	Effects of Creep and Hysteresis	78
	Strain Dependence of the Mechanical/Electrical Coupling Coefficient	81
4.3	Semi-Empirical Iterative Solution Procedure	85
	Solution Convergence	78
4.4	Conclusions	89
Chapter 5.	Testing of the Sandwich Articles	90
5.1	Introduction	90
5.2	Construction of the Sandwich Articles	91
5.3	Experimental Procedure and Results	92
5.4	Comparison of Experimental Results with Theoretical Predictions	95
	Isotropic Sandwich Actuator Systems	95
	Orthotropic Sandwich Actuator Systems	97
5.5	Conclusions	98
Chapter 6.	Testing of the Cantilever Plate Articles	100
6.1	Introduction	100
6.2	Construction of the Cantilever Plate Articles	101
6.3	Experimental Procedure and Results	106
	Static Mode Shape Tests	108
	Deflection versus Applied Field Tests	114
6.4	Conclusions	121
Chapter 7.	Conclusions and Recommendations	122
References		126

LIST OF SYMBOLS

Variables

A	Extensional Stiffness
B	Coupling Stiffness
b	Bar Width
C	Transverse Plate Dimension
D	Bending Stiffness Element
<i>D</i>	Derivative Operator
d	Mechanical/Electrical Coupling Coefficient
\mathcal{E}	Applied Electric Field
F	Force
H	Mode Shape Matrix
I	Beam Area Moment Of Inertia
K	Modal Stiffness
L	Longitudinal Plate Dimension
M	Moment Per Unit Length
N	Force Per Unit Length
<i>p</i>	External Plate Forces
Q	Reduced Stiffness, Modal Forcing
<i>t</i>	Plate Thickness
U	Total Strain Energy
α	Geometric Constant
η	Distance From Neutral Axis To "Pin" Location
ϵ	Induced Strain
ϕ	Assumed Mode
Λ	Actuation Strain

Subscripts

<i>a</i>	Actuator
<i>k</i>	Externally Applied
<i>o</i>	Residual Strain
<i>p</i>	At The "Pins"
<i>s</i>	Substrate
<i>neg</i>	Strains Recorded With The Field
<i>pos</i>	Strains Recorded Against The Field

Superscripts

*	Average Definition
+	One-Sided Definition (Against The Field)
-	One-Sided Definition (With The Field)

LIST OF FIGURES

1.1	Example induced strain actuation actuator/substrate system.	13
2.1	Symmetric actuator/substrate geometry and "pin" force model idealization.	19
2.2	Free body diagram of the symmetric actuator/substrate system modelled by the "pin" force model.	20
2.3	"Pin" force model assumed strain distribution.	23
2.4	Selected actuator configurations and geometric constants.	26
2.5	Thin plate coordinate system and sign conventions.	29
2.6	Free body diagram of a plate system modelled by the "pin" force plate model.	32
2.7	Consistent plate model with assumed strain distribution for extensional and bending actuation.	38
3.1	Plot of strain ratio versus moduli ratio for an orthotropic system actuated in extension.	51
3.2	Plot of the ratio of curvatures predicted by the "pin" force plate and the consistent plate model versus thickness ratio for bending actuation.	54
3.3	Assumed mode shapes of a free plate actuator/substrate system.	60
3.4	Assumed mode shapes of a cantilever plate actuator/substrate system.	61
4.1	Piezoceramic plate poled through the thickness.	74
4.2	Experimentally measured actuation strains created in several piezoceramic plate actuator test specimens.	76
4.3	Plot of experimentally measured actuation strains versus applied field showing the limited orthotropy of piezoceramics.	77
4.4	Applied field/induced strain hysteresis loops from an unconstrained piezoceramic.	79

4.5	Plot of induced strain versus applied field measured in an unconstrained piezoceramic with curve fit.	81
4.6	Plot of induced strain versus applied field for the aluminum sandwich with 0.32 mm thick substrates. Figure compares strains predicted with an assumed strain dependent and field dependent coupling coefficient.	83
5.1	Sandwich actuator/substrate specimen geometry.	91
5.2	Plot of induced strain versus applied field for the aluminum sandwich with 0.84 mm thick substrates.	96
5.3	Plot of induced strain versus applied field for the aluminum sandwich with 0.51 mm thick substrates.	96
5.4	Plot of induced strain versus applied field for the graphite/epoxy sandwich.	98
6.1	Cantilever plate symmetric actuator/substrate specimen configuration.	101
6.2	Cantilever plate symmetric actuator/substrate specimen wiring schematic.	103
6.3	Cantilever plate symmetric actuator/substrate specimen actuator groupings.	104
6.4	Cantilever plate symmetric actuator/substrate specimen non-contacting proximity sensor target locations.	107
6.5	Aluminum plate longitudinal bending mode shape.	109
6.6	Aluminum plate transverse bending mode shape.	109
6.7	Graphite/epoxy $[\pm 45/0]_s$ plate longitudinal bending mode shape.	110
6.8	Graphite/epoxy $[\pm 45/0]_s$ plate twist mode shape.	111
6.9	Graphite/epoxy $[\pm 45/0]_s$ plate transverse bending mode shape.	111
6.10	Graphite/epoxy $[30_2/0]_s$ plate longitudinal bending mode shape.	112
6.11	Graphite/epoxy $[30_2/0]_s$ plate twist mode shape.	113
6.12	Graphite/epoxy $[30_2/0]_s$ plate transverse bending mode shape.	113
6.13	Graphite/epoxy $[+45_3/-45_3]$ plate twist mode shape.	114

6.14	Longitudinal bending deflection versus applied field for the aluminum plate symmetric system.	116
6.15	Transverse bending deflection versus applied field for the aluminum plate symmetric system.	117
6.16	Longitudinal bending deflection versus applied field for the graphite/epoxy $[\pm 45/0]_s$ plate symmetric system.	118
6.17	Transverse bending deflection versus applied field for the graphite/epoxy $[\pm 45/0]_s$ plate symmetric system.	118
6.18	Longitudinal bending deflection versus applied field for the graphite/epoxy $[30_2/0]_s$ plate symmetric system.	119
6.19	Twist deflection versus applied field for the graphite/epoxy $[30_2/0]_s$ plate symmetric system.	119
6.20	Twist deflection versus applied field for the graphite/epoxy $[+45_3/-45_3]$ plate symmetric system.	120

LIST OF TABLES

5.1	Sandwich specimen dimensions and material properties.	92
5.2	Sandwich specimen experimental and theoretical results at an applied field of 551 V/mm.	94
6.1	Cantilever plate specimen dimensions and material properties.	105
6.2	Cantilever plate specimen experimental and theoretical results at an applied field of 315 V/mm.	116

CHAPTER 1

INTRODUCTION

Induced strain actuators apply localized strains which can be used to control the deformations of structural elements without producing rigid body forces and torques or inertial loads. Induced strain actuation is a desirable means for the control of plate like-structures. It allows for the direct control of plate extension, bending, and twisting. Induced strain actuation has advantages over other types of actuation because the actuators can be easily integrated with load bearing structures and are, in general, light weight and do not significantly alter the passive static or dynamic stiffness characteristics of the structures.

Used in conjunction with advanced composite materials with inherent directional stiffness, control of specific mode shapes (static or dynamic) can be greatly enhanced, and precision static control can be effected. Isotropic and anisotropic plates with distributed induced strain actuators could be used for the pointing of precision instruments or the control of aeroelastic lifting surfaces [Crawley, Warkentin, and Lazarus, 1988], optical system mirror or reflector shape control [Chiarappa and Claysmith, 1981], and the active acoustical control of structure borne noise [Atluri and Amos ed., 1988]. Such deformation control is ideal for the accurate shape regulation required for pointing precision space or ground based optical packages, and machining, soldering, or placing high fidelity components by robotic machinery. Shape control through induced strain actuation is also ideal for large scale applications such as attaining control authority of an aerodynamic body by altering the twist curvature and camber of aeroelastic lifting surfaces, and improving the performance of an optical surface by precisely controlling the mirror contour.

An example induced strain actuator/substrate system is displayed in Fig. 1.1. Although the particular application of the systems shown is for the control of an aeroelastic lifting surface, this system is typical of most systems which utilize induced strain actuation. The cross-section in Fig. 1.1 shows

induced strain actuators bonded to an elastic load bearing substrate, and protective substrates bonded to the actuators. The actuators of such a system can be used to alter the shape of the lifting surface, thereby changing the lift on the vehicle. Thus control is effected without the use of articulated structures and mechanical linkages necessary for conventional aerodynamic control. Aeroelastic applications of this induced strain system include the quasi-static control of the camber and twist of aerodynamic control surfaces in supersonic and hypersonic flight when separate articulated lift control devices are undesirable.

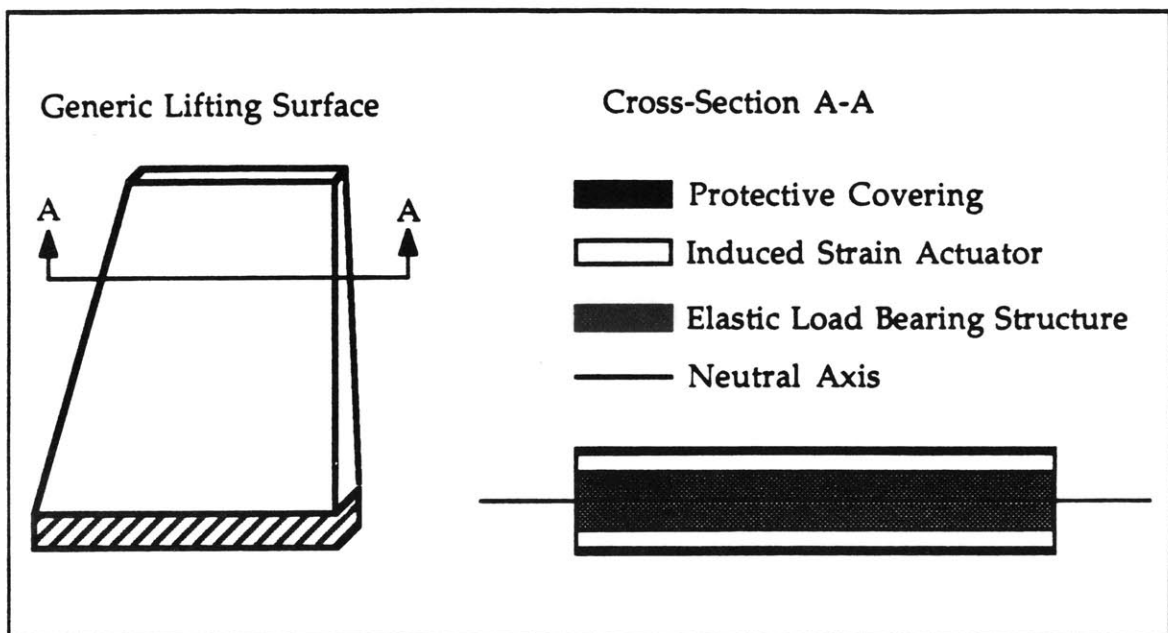


Figure 1.1 Example induced strain actuator/substrate system in an aeroelastic application. Figure shows a generic lifting surface and the system cross-section.

Another application for such induced strain actuation is in the control of an optical surface. An optical surface control system could be constructed of an optical surface affixed to a load bearing substrate covered with induced strain actuators. Such a system would be capable of altering its shape to attain a range of desired mirror curvatures. Hence the focal length or pointing direction of the mirror could be quickly and accurately changed. Similar induced strain actuation systems could be conceived to meet the needs of the other applications mentioned above.

Background and Objective

Any actuator capable of creating actuation strains can, in principle, be thought of as an induced strain actuator. Actuation strain is the general term for all sources of strain which enter the constitutive relations, other than those due to mechanical stress. Actuation strains may be due to a variety of effects such as thermal expansion [Jones, 1975], piezoelectricity [Crawley and de Luis, 1987], electrostriction [Uchino, 1986], material phase change [Shimizu, *et al.*, 1986], magnetostriction [Butler, 1988], or moisture absorption [Tsai and Hahn, 1980]. The actuation strain is the mechanism by which induced strain actuators induce strain and therefore effect control. The components of an induced strain actuator/substrate system are the induced strain actuators and the structural plates which provided support, directional stiffness, and protection. These components are assembled into systems either by surface bonding any number of induced strain actuators to the structural plates or embedding the actuators within the structural plates themselves [Crawley and de Luis, 1987].

Currently, the most researched and used induced strain actuators are piezoceramic. Typical of most induced strain actuators, piezoceramics are simple, compact, light weight structures which can be incorporated easily into induced strain actuator/substrate systems. Piezoceramics produce actuation strains in response to applied electric fields. Because the piezoceramic actuation strains are proportional to an applied field, piezoceramic induced strain actuators allow for implementation of a variety of control schemes.

To date, detailed models of induced strain actuator/substrate systems are limited. Models of strain actuators coupled with simple beams [Forward and Swigert, 1981; Hanagud and Obal, 1985; Crawley and de Luis, 1987; and Burke and Hubbard, 1987] and plates [Crawley, Warkentin, and Lazarus, 1988; and Crawley *et al.*, 1988], and models of isolated piezoelectric plates [Boriseiko *et al.*, 1972; and Antonyak and Vassergiser, 1980] currently exist. There exists a need for a model of plates, with various boundary conditions and externally applied loads, coupled with general induced strain actuators. Such induced strain plate actuator models should treat isotropic and anisotropic plates which are entirely or partial covered with piezoelectric actuators at various orientations. The models should incorporate surface bonded and embedded

actuators, and be accurate for both static and dynamic applications. It is the objective of this work to develop and verify such a modeling capability.

Approach and Outline

To meet the above needs two types of models of the induced strain actuation of thin flat plates will be developed. The models which will be developed include a "pin" force plate model, and a consistent plate model. The models will be developed and verified for quasi-static actuation. Although there are numerous important dynamic induced strain actuation applications, it is essential to first understand and be able to predict the static behavior. Thus the focus of this report will be on the modelling, analysis, and experimental verification of quasi-static systems.

The "pin" force plate model conceptually models the induced strain actuators and the structural substrates to be separate components, and can be used to evaluate the effectiveness of simple induced strain systems, and to provide insight into the physics of the induced strain actuation problem. The more inclusive consistent plate model depicts the actuators and the substrates to be one integrated structure. The consistent plate model relations lead to direct formulation of the plate equations of elasticity and strain energy equations. Thus, this model can be used to obtain a limited number of exact solutions, and to obtain approximate solutions of the strain energy equations. The later are important in the analysis of systems with complex directional stiffness couplings, boundary conditions, and externally applied loads.

The "pin" force plate model and the consistent plate model will be derived in Chapter 2. And, solutions to the governing equations derived for these models will be developed in Chapter 3. Specifically, exact solutions will be found to systems for which such solutions are obtainable and a general Rayleigh Ritz solution will be developed to analyze more complicated induced strain actuation systems.

Due to the wide spread used of piezoceramics, and because the induced strain systems built and tested in this research incorporated piezoceramic actuators, models for predicting the actuation strains produced by these

actuators will then be developed. The piezoceramic actuation strain models will include important non-linear effects such as hysteresis and the strain dependence [Aronov, 1980] of the mechanical/electrical coupling coefficient. And, the effects of these, and other, characteristics of piezoceramic actuators on the prediction of the induced strains produced in induced strain actuator/substrate systems will be discussed. Piezoceramic actuation strain models will be developed in Chapter 4.

Finally, the models and solutions developed will be verified through experimentation. Model induced strain actuator/substrate systems will be built and the induced strains and deformations found in such systems will be measured experimentally. The testing for in-plane strains of simple induced strain plate actuator/substrate systems will be discussed in Chapter 5, and the testing of more representative cantilever plate systems for mode shape and deflection information will be discussed in Chapter 6. The results of the experiments performed on these test specimens will be used to show the validity of the models developed, and the effectiveness of using induced strain actuation for shape control of elastic structures.

CHAPTER 2

ANALYTICAL MODELS OF INDUCED STRAIN ACTUATOR SYSTEMS

2.1 Introduction

In this chapter two separate models of induced strain actuator/substrate systems are developed. These models differ primarily in the strain distributions assumed in each component of the system and the ability to model specific systems, but are complimentary in the design and analysis process. The first model discussed, the "pin" force model, conceptually models the actuators and substrates to be separate structures linked together by pins, which can carry only point loads, at the edges of the actuators. The second model, referred to as the consistent plate model, considers the actuators and the substrates to be one integrated structure. The governing equations which relate the strains created in the induced strain actuators (actuation strains) to the resultant total strains found in the system will be derived for both models.

In the derivation of the "pin" force model, equations relating the actuation strains to the resultant total strains are obtained directly. The "pin" force model equations lead to relatively simple formulation of explicit solutions, and reveal parameters that determine the actuator effectiveness for simple actuator/substrate systems. This model is extremely valuable for understanding the physics of induced strain actuation and in the preliminary design process, and it yields accurate results for a variety of cases. The "pin" force model will be reviewed for one dimensional systems in section 2.2 and the "pin" force plate model will be developed for plate systems in section 2.4.

Some actuator system configurations are not easily described by the "pin" force model. In particular modeling of arbitrary boundary conditions and anisotropic stiffness couplings in the substrates is awkward. This motivates the development of the more encompassing consistent plate model. The consistent plate model integrates the actuators and the substrates into a unified laminated plate. This allows easy application of classical

laminated plate theory and plate strain energy concepts in order to analyze systems with arbitrary boundary conditions, complicated stiffness couplings, and a variety of externally applied forces. In addition, formulation of the problem in this manner allows for well known approximate solution techniques to be conveniently applied. The equations governing the relationship between the actuation strains and the resultant total strains will be derived for the consistent plate model in section 2.5, and the consistent plate model strain energy relations will be formulated in section 2.5 as well.

2.2 "Pin" Force Model in One Dimension

In order to become acquainted with the mechanism by which induced strain actuation is affected, the "pin" force model will first be developed for simple one dimensional actuator/substrate systems. The physics involved in using induced strain actuators for the purpose of control of static or dynamic displacements can best be understood by examining such simple systems. The most basic induced strain actuator/substrate systems are those composed of one dimensional linear elastic bars actuated in an extensional mode, and beams actuated in bending. The extensional actuation of a bar will be discussed first. Then the "pin" force will be utilized to develop relations for a beam actuated in bending. This model will be reviewed for the symmetric actuator system shown in Fig. 2.1. The symmetric actuator system consists of an induced strain actuator bonded to the upper and lower surface of a substrate. Other simple systems with different actuator/substrate configurations will also be discussed.

The "pin" force model considers the actuators and the substrates to be separate elastic bodies. The extensional forces produced by the strain actuators are transferred to the substrates by "pins" at the edges of the actuators [de Luis and Crawley]. Fig. 2.1 displays the idealized "pin" force model concept. This model of force transfer from actuator to substrate is consistent with the assumption of perfect bonding between the actuator and the substrate. Under the condition of perfect bonding the shear stress σ_{xz} is concentrated in an infinitesimal zone at the end of the actuator, modelled here by the "pins." The principal implication of the pinned assumption is that the strain in the

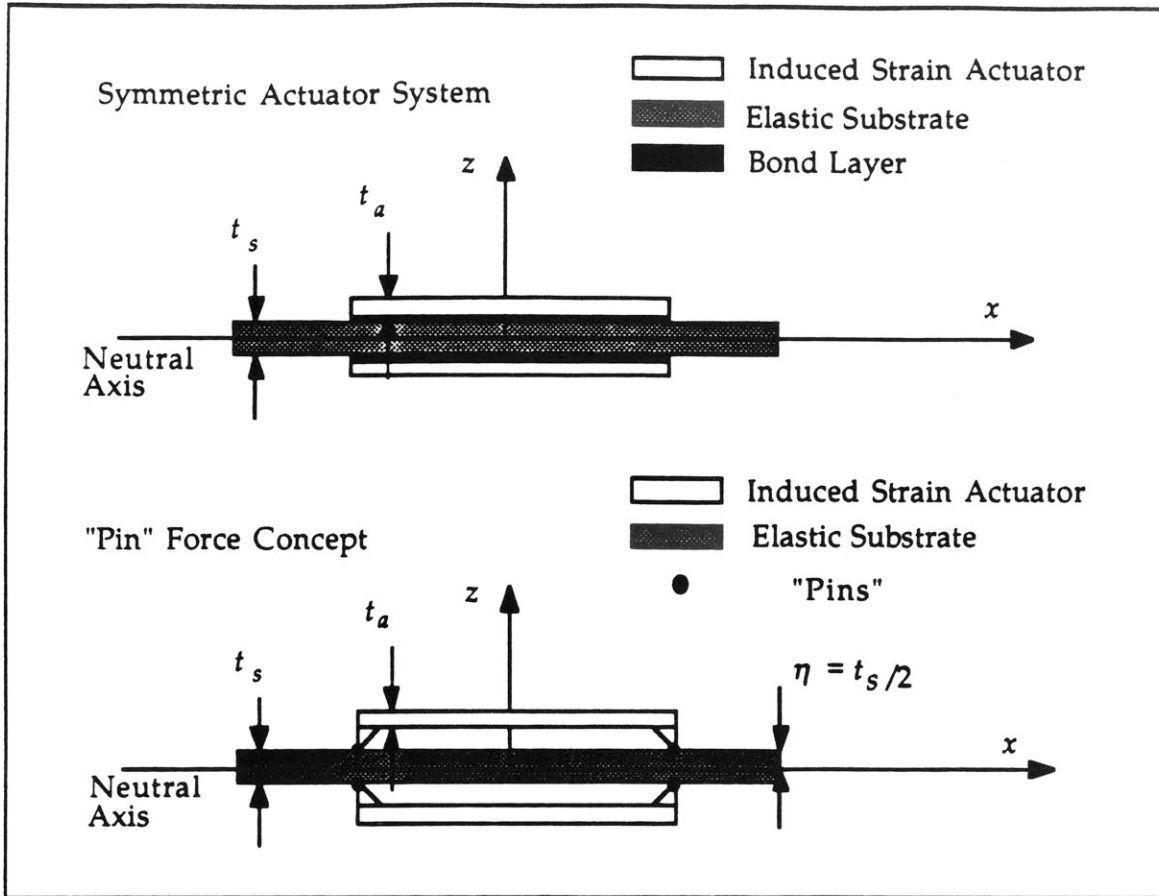


Figure 2.1 Symmetric actuator/substrate geometry, and "pin" force model idealization.

actuators and substrates can be modelled independently, so long as compatibility is assumed at the location of the pins.

Induced Strain Actuation of a Bar in Extension

Figure 2.2 shows the free body diagram of a symmetric actuator system actuated in extension. Pure extension is created in the substrate by commanding the actuation strain in both actuators to be in extension. In this mode of actuation, the "pin" force model assumes the strain distribution to be constant with respect to the thickness of both the actuators and the substrate, as shown in Fig 2.3.

Following the derivation of Crawley and de Luis [1987], an equation which relates the actuation strain to the resultant total strain created in the bar is now developed. The stress-strain relationships for the actuator (denoted by subscript a) and the substrate (subscript s) are

$$\epsilon_a = \frac{\sigma_a}{E_a} + \Lambda \quad (2.1)$$

$$\epsilon_s = \frac{\sigma_s}{E_s} \quad (2.2)$$

where ϵ is the resultant total strain, which is comprised of the mechanical strain and the actuation strain Λ . The actuation strain Λ enters into the equations in the same manner as does thermal strain, and the actuation strain is the strain which causes, physically, induced strains to be produced. This strain can be due to thermal expansion, piezoelectricity, electrostriction, magnetostriction, material phase changes, or moisture absorption. It is the mechanism by which induced strain actuators work.

The equilibrium equations for the extensional case can be found by inspection of Fig. 2.2 to be

$$\sigma_a = -\frac{F}{bt_a} \quad (2.3)$$

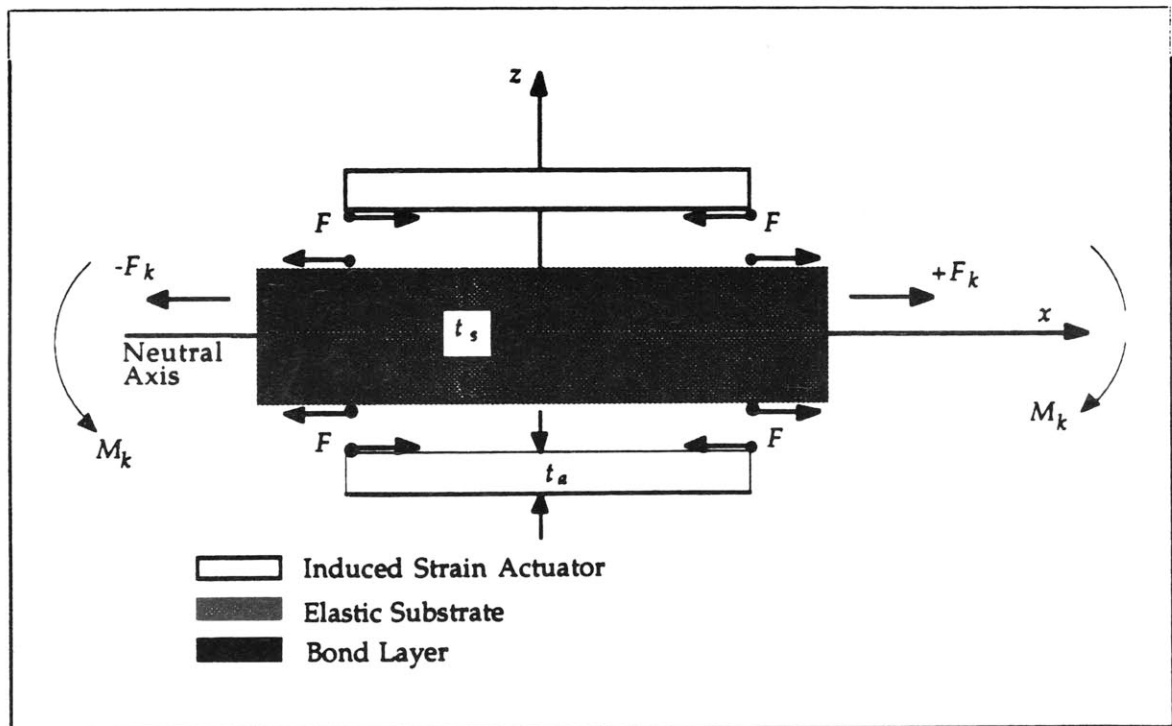


Figure 2.2 Free body diagram of the symmetric actuator/substrate system modelled by the "pin" force model.

$$\sigma_s = \frac{2F}{bt_s} + \frac{F_k}{bt_s} \quad (2.4)$$

where the substrate or actuator thickness is represented by t , and b is the bar width. In these equilibrium expressions σ is the stress which develops in the actuators or the substrate, F is the force on the "pins," and F_k represents an external load independent of the force applied by the actuator. This external load may be composed of forces which develop at the boundaries or from an externally applied force. Determination of this applied load will be discussed later in this chapter and in chapter 3.

By applying compatibility ($\epsilon_a = \epsilon_s$, at the actuator/beam interface), substituting the equilibrium relationships (Eqs. 2.3 and 2.4) into the stress-strain equations (Eqs. 2.1 and 2.2), and manipulating, the "pin" force can be calculated. This force is related to the actuation strain and externally applied load as

$$\frac{F}{b} = \left[\frac{1}{2 + \psi} \right] E_s t_s \Lambda - \left[\frac{1}{2 + \psi} \right] \frac{F_k}{b} \quad (2.5)$$

The non-dimensional parameter ψ , referred to as the relative stiffness ratio, represents the stiffness of the substrate compared to the actuator and is defined as

$$\psi = \frac{E_s t_s}{E_a t_a} \quad (2.6)$$

An explicit expression for the resultant total strain found in the actuator system can now be found by substituting the "pin" force expression (Eq. 2.5) back into the equilibrium equations (Eqs. 2.3 and 2.4), and subsequently combining this result with the original strain relations (Eqs. 2.1 and 2.2). The resultant total strain is found to be

$$\epsilon_s = \left[\frac{2}{2 + \psi} \right] \Lambda + \left[\frac{\psi}{2 + \psi} \right] \frac{F_k}{E_s t_s b} \quad (2.7)$$

The total strain in the substrate is the sum of the induced strain and the strain produced by the external load. The induced strain is the strain induced in the

substrate as a result of the actuation strain commanded in the actuator, and is equal to the first term in Eq. 2.7 for the system under consideration.

The above equation can be generalized to the form

$$\epsilon_s = \left[\frac{\alpha}{\alpha + \psi} \right] \Lambda + \left[\frac{\psi}{\alpha + \psi} \right] \frac{F_k}{E_s t_s b} \quad (2.8)$$

where α is a constant which depends on the geometry of the system, and the mode of actuation. If no external load is present, *i.e.*, F_k equals zero, the resultant total strain equals the induced strain, and is a function of only the actuation strain, the relative stiffness ratio ψ , and the geometry of deformation,

$$\epsilon_s = \left[\frac{\alpha}{\alpha + \psi} \right] \Lambda \quad (2.9)$$

For any given actuator configuration, the induced strain in the substrate can be increased by either decreasing the stiffness of the substrate relative to the actuator or by increasing the actuation strain.

Induced Strain Actuation of a Beam in Bending

Development of the bending model parallels that of the extensional model. The substrate is now assumed to be a beam which can deform only in bending, and the symmetric actuator system of Fig. 2.1 is commanded to produce a pure moment. This is accomplished by actuating the two induced strain actuators, which are equal distance from the neutral axis, in equal and opposite senses. One actuator produces an extensional actuation strain while a compressive actuation strain is produced by the other. Because the substrate bends, the assumed strain distribution is no longer constant through the substrate thickness. Fig. 2.3 illustrates the assumed strain of the system for the bending configuration. The strain in the substrate is assumed to vary linearly through the thickness, as in Bernoulli-Euler beam theory. The strain in the actuator is constant through the thickness, as in the extensional case.

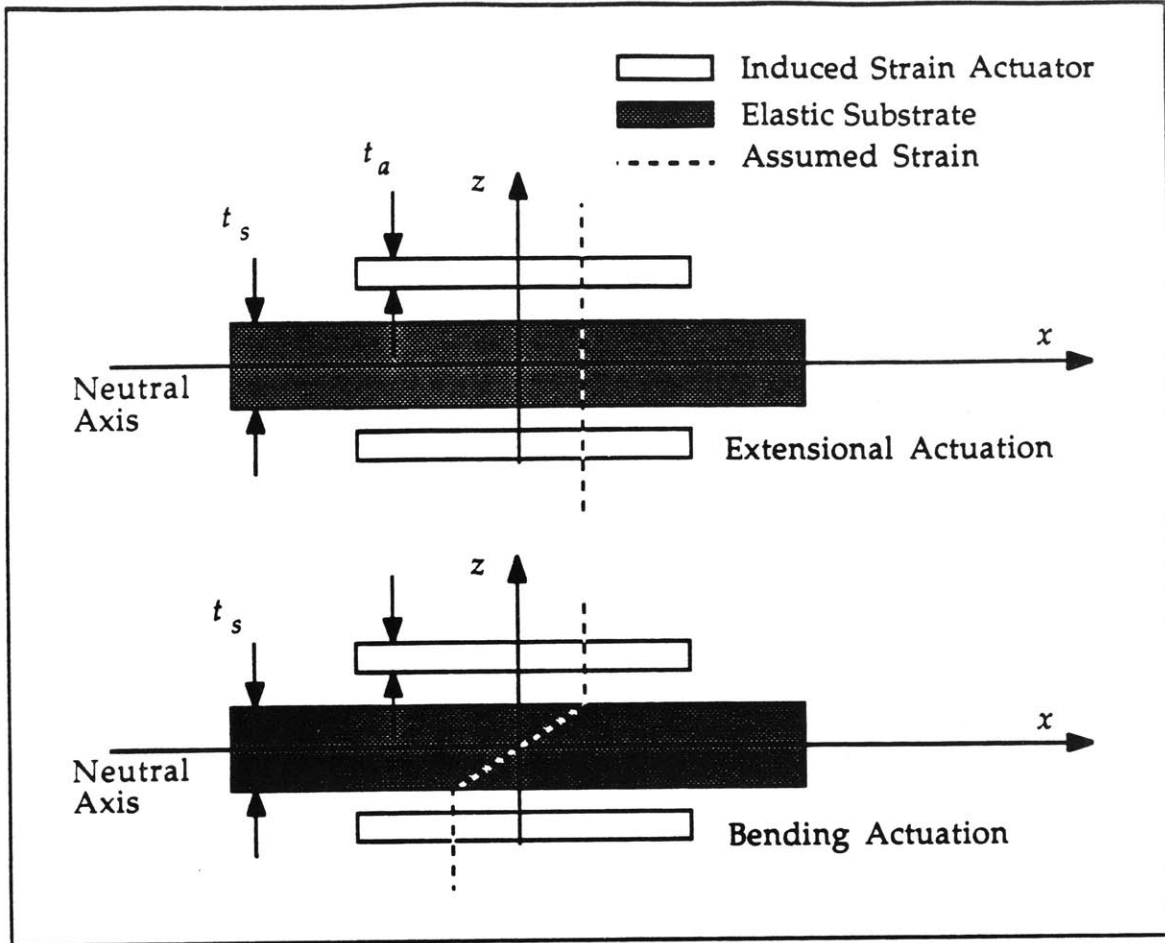


Figure 2.3 Strain distribution assumed by the "pin" force model model for extensional and bending actuation.

As a result of the assumptions made above, the "pin" force below the neutral axis will be equal and opposite to the "pin" force above the neutral axis, and a new equilibrium equation for the substrate is valid, which can be found by examining Fig. 2.2

$$\sigma_s = \frac{12Fz}{bt_s^2} + \frac{M_k z}{I} \quad (2.10)$$

where I is the moment of inertia of the substrate cross section, z is the distance from the neutral axis at which the stress is evaluated, and the external load is a moment M_k which may be due to moments produced at the boundaries or externally applied moments. These moments are defined so that a positive moment produces positive strain above the neutral axis. This

convention is adopted to be consistent with plate theory since the "pin" force model will be extended to the "pin" force plate model in section 2.4.

To apply compatibility, the stress and strain must be evaluated at the actuator/substrate interface. The distance from the neutral axis of the substrate to the interface with the actuator, or the "pins", is defined as $\eta = t_s/2$. The stress at the interface η is

$$\sigma_s|_{\eta} = \frac{6F}{bt_s} + \frac{M_k t_s}{2I} \quad (2.11)$$

The equilibrium equation for the actuator is the same as found previously (Eq. 2.3), as are the stress-strain relations (Eqs. 2.1 and 2.2). Applying these relations, the "pin" force can be determined in a manner analogous to the procedure used for the extensional actuator. The "pin" force which results is

$$\frac{F}{b}|_{\eta} = \left[\frac{1}{6 + \psi} \right] E_s t_s \Lambda - \left[\frac{1}{6 + \psi} \right] \frac{M_k t_s^2}{2I} \quad (2.12)$$

and by substituting this "pin" force into the equilibrium relations (Eqs. 2.3 and 2.11) and the stress-strain equations (Eqs. 2.1 and 2.2) as above. The total strain at the interface is found to be

$$\epsilon_s|_{\eta} = \left[\frac{6}{6 + \psi} \right] \Lambda + \left[\frac{\psi}{6 + \psi} \right] \frac{M_k t_s}{2E_s I} \quad (2.13)$$

and the curvature in the beam is

$$\kappa = \frac{2}{t_s} \left[\frac{6}{6 + \psi} \right] \Lambda + \left[\frac{\psi}{6 + \psi} \right] \frac{M_k}{E_s I} \quad (2.14)$$

where the curvature is defined so that positive moments produce positive curvatures, consistent with plate theory convention. Eq. 2.13 can be compared with Eq. 2.8 to see that once again, the total strain induced in the substrate depends on the induced strain and the strain produced by the applied load. In the absence external loads Eq. 2.14 reduces to Eq. 2.9 repeated here

$$\epsilon_s|_{\eta} = \left[\frac{\alpha}{\alpha + \psi} \right] \Lambda \quad (2.15)$$

Equation 2.9 or Eq. 2.14 reveal the fundamental parameters governing the effectiveness of induced strain actuator systems. Obtaining these parameters is the reason for analyzing the simple one dimensional systems. Eq 2.9 or Eq. 2.14 determine the ability of an actuator system to induce strains in the substrate from commanded actuation strains. In the absence of external loads, the strain induced in the substrate is a function of the actuation strain Λ , the relative stiffness ratio ψ , and the geometric constant α . For bending actuation, α equals 6 while α was equal to 2 for extensional actuation. Therefore, it is evident that the form of the equation which governs the transfer of actuation strain to induced strain is identical for extensional and bending actuation, but the exact strain values for the two systems differ because of the geometry of the deformations.

Actuator systems with configurations other than the symmetric actuator of Fig. 2.1 will still be governed by Eq. 2.9 or Eq. 2.15. The geometric constant associated with each system will depend on the system configuration and the mode of actuation. Selected actuator geometries and their corresponding geometric constants are displayed in Fig. 2.4.

It should be noted that no assumptions have been made with regards to the boundary conditions of the actuator system. Thus Eqs. 2.7, 2.13, and 2.14 are in principle general and can be used for any set of boundary conditions. The boundary conditions enter the problem through the external load term which consists of forces and moments generated at the boundaries as well as by externally applied forces and moments. Therefore, in order to determine the induced strains produced, both the forces and moments at the boundary, and the forces and moment applied externally must be known. This subject will be discussed further in chapter 3.

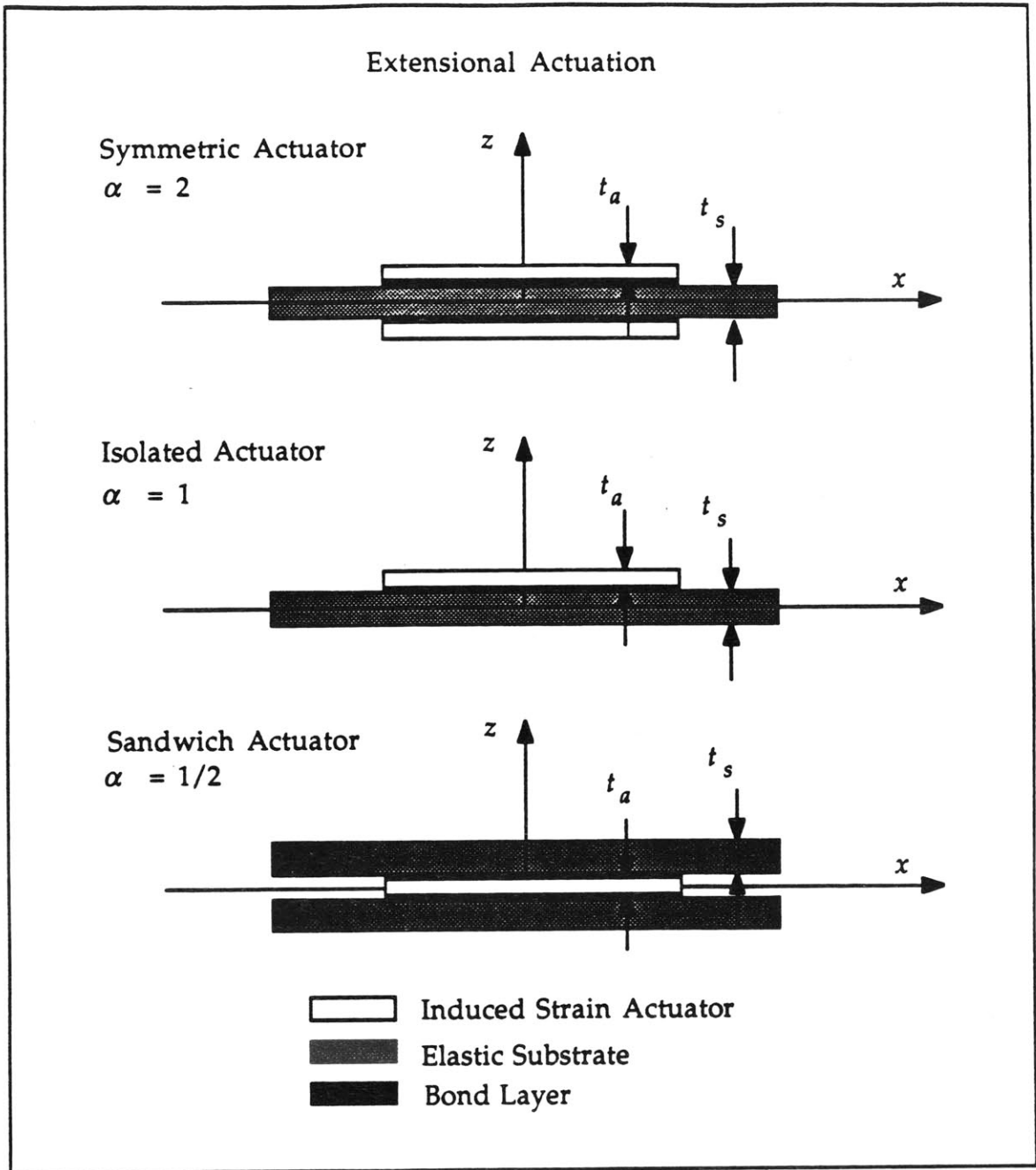


Figure 2.4 Selected actuator configurations and their "pin" force model geometric constants for extensional actuation.

2.3 Review of Thin Plate Theory

Before deriving the governing equations for induced strain plate actuation, a brief review of thin plate theory is presented for completeness. These equations will be used in extending the one dimensional "pin" force model to the "pin" force plate model, and in deriving the consistent plate model. This review is based on classical Kirchhoff thin plate theory [Ashton and Whitney, 1970; and Jones, 1975].

The coordinate axis and plate dimensions are defined in Fig. 2.5. A plate may be considered to be either uniform though the thickness or composed of several laminate plies. The basic assumption used in thin plate theory is that the total plate thickness h is much smaller than the longitudinal L or transverse C dimensions, thus the stresses acting on the surface parallel to the mid-plane σ_z are small compared to the in-plane membrane and bending longitudinal σ_x and transverse σ_y stresses. Also, plane sections are assumed to remain plane and normal to the mid-plane during deformation which requires the shear strains γ_{xz} and γ_{yz} to be zero. Due to these assumptions the plate deforms in an approximate state of plane stress. Additionally, it is required that the in-plane strains are small compared to unity so that second order non-linear terms may be neglected.

Thin plate theory requires the out-of-plane deformations to be a function of only the longitudinal x and transverse y coordinates, therefore the bending strains and curvatures, as well as the membrane strains, can be fully described by derivatives with respect to these coordinates. The total strain of a thin plate is composed a mid-plane strain ϵ^0 and a curvature component κ . The strain is defined by the following strain-displacement relation

$$\epsilon = \epsilon^0 + z \kappa \quad (2.16)$$

where z is the out-of-plane coordinate axis, and the strains and curvatures are defined in engineering notation as

$$\begin{aligned}
\varepsilon &= \begin{bmatrix} \varepsilon_x \\ \varepsilon_y \\ \gamma_{xy} \end{bmatrix} & \varepsilon^o &= \begin{bmatrix} \varepsilon_x^o \\ \varepsilon_y^o \\ \gamma_{xy}^o \end{bmatrix} & \kappa &= \begin{bmatrix} \kappa_{xx} \\ \kappa_{yy} \\ \kappa_{xy} \end{bmatrix} \\
\begin{bmatrix} \varepsilon_x^o \\ \varepsilon_y^o \\ \gamma_{xy}^o \end{bmatrix} &= \begin{bmatrix} \frac{\partial u}{\partial x} \\ \frac{\partial v}{\partial y} \\ \frac{\partial u}{\partial y} + \frac{\partial v}{\partial x} \end{bmatrix} & \begin{bmatrix} \kappa_{xx} \\ \kappa_{yy} \\ \kappa_{xy} \end{bmatrix} &= \begin{bmatrix} -\frac{\partial^2 w}{\partial x^2} \\ -\frac{\partial^2 w}{\partial y^2} \\ -2\frac{\partial^2 w}{\partial x \partial y} \end{bmatrix}
\end{aligned} \tag{2.17}$$

In Eq. 2.17 the mid-plane strains are the usual membrane normal and shear strains, and κ_{xx} , κ_{yy} , and κ_{xy} represent the longitudinal, transverse, and twist curvature respectively.

The stress-strain relation for a homogeneous plate, or for any ply of a laminated plate is

$$\sigma = Q (\varepsilon - \Lambda) = Q\varepsilon - Q\Lambda \tag{2.18}$$

where the stress vector and the actuation strain vector are defined as

$$\sigma = \begin{bmatrix} \sigma_x \\ \sigma_y \\ \tau_{xy} \end{bmatrix} \quad \Lambda = \begin{bmatrix} \Lambda_x \\ \Lambda_y \\ \Lambda_{xy} \end{bmatrix}$$

The matrix Q is the transformed reduced stiffness of the plate or one of its plies in the plate axis system [Jones, 1975]. The first term $Q\varepsilon$ of the stress-strain equation (Eq. 2.18) represents the normal stress-strain relations for plane stress in a plate [Ashton and Whitney, 1970]. The second term $Q\Lambda$ represents the stress which is created as a result of the actuation strains. The actuation strain vector Λ , which is analogous to the one dimensional actuation strain term of Eq. 2.1, contains in-plane normal and shear strain components. Again these actuation strains can develop from the same induced strain mechanisms discussed for one dimensional actuators in section 2.2.

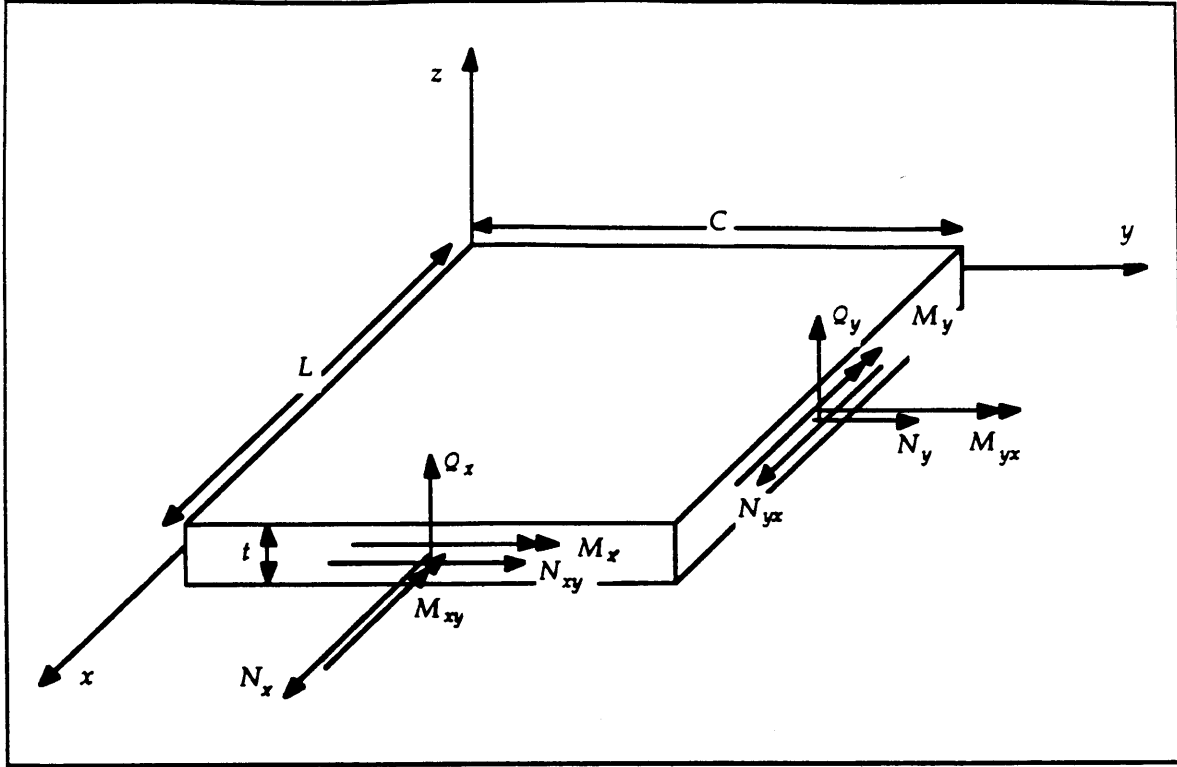


Figure 2.5 Thin plate with coordinate axis, dimensions, and sign conventions shown.

The plate constitutive relations can be found by substituting the strain-displacement equations (Eqs. 2.16 and 2.17) into the stress-strain equation (Eq. 2.18) and integrating through the thickness of the plate. The constitutive equations relate the resultant forces and moment in the plate to the plate stiffnesses, strains and curvatures, and actuator forces as follows

$$\begin{aligned}\bar{N}_x &= A_{11}\epsilon_x^o + A_{12}\epsilon_y^o + A_{16}\gamma_{xy}^o \\ &+ B_{11}\kappa_{xx} + B_{12}\kappa_{yy} + B_{16}\kappa_{xy} - (N_\Lambda)_x\end{aligned}$$

$$\begin{aligned}\bar{N}_y &= A_{21}\epsilon_x^o + A_{22}\epsilon_y^o + A_{26}\gamma_{xy}^o \\ &+ B_{21}\kappa_{xx} + B_{22}\kappa_{yy} + B_{26}\kappa_{xy} - (N_\Lambda)_y\end{aligned}$$

$$\begin{aligned}\bar{N}_{xy} &= A_{61}\epsilon_x^o + A_{62}\epsilon_y^o + A_{66}\gamma_{xy}^o \\ &+ B_{61}\kappa_{xx} + B_{62}\kappa_{yy} + B_{66}\kappa_{xy} - (N_\Lambda)_{xy}\end{aligned}$$

$$\begin{aligned}\bar{M}_x &= B_{11}\epsilon_x^o + B_{12}\epsilon_y^o + B_{16}\gamma_{xy}^o \\ &+ D_{11}\kappa_{xx} + D_{12}\kappa_{yy} + D_{16}\kappa_{xy} - (M_\Lambda)_x\end{aligned}$$

$$\begin{aligned}
\bar{M}_y &= B_{21}\varepsilon_x^o + B_{22}\varepsilon_y^o + B_{26}\gamma_{xy}^o \\
&\quad + D_{21}\kappa_{xx} + D_{22}\kappa_{yy} + D_{26}\kappa_{xy} - (M_\Lambda)_y \\
\bar{M}_{xy} &= B_{61}\varepsilon_x^o + B_{62}\varepsilon_y^o + B_{66}\gamma_{xy}^o \\
&\quad + D_{61}\kappa_{xx} + D_{62}\kappa_{yy} + D_{66}\kappa_{xy} - (M_\Lambda)_{xy}
\end{aligned} \tag{2.19}$$

In formulation of the resultants, advantage has been taken of contracted notation for the fourth order stiffness tensors [Jones, 1975]. Arranging these six equations into matrix notation leads to the plate constitutive relations in a compact form

$$\begin{bmatrix} \bar{\mathbf{N}} \\ \bar{\mathbf{M}} \end{bmatrix} = \begin{bmatrix} \mathbf{A} & \mathbf{B} \\ \mathbf{B} & \mathbf{D} \end{bmatrix} \begin{bmatrix} \boldsymbol{\varepsilon}^o \\ \boldsymbol{\kappa} \end{bmatrix} - \begin{bmatrix} \mathbf{N}_\Lambda \\ \mathbf{M}_\Lambda \end{bmatrix} \tag{2.20}$$

The force and moment resultants, are defined as forces and moments per unit length, and are

$$\bar{\mathbf{N}} = \int_{-\frac{t}{2}}^{\frac{t}{2}} \boldsymbol{\sigma} dz \quad \bar{\mathbf{M}} = \int_{-\frac{t}{2}}^{\frac{t}{2}} \boldsymbol{\sigma} z dz \tag{2.21}$$

The matrixes \mathbf{A} , \mathbf{B} , and \mathbf{D} are respectively called the extensional stiffness, coupling stiffness, and bending stiffness of the plate, and are defined by the following relations

$$\mathbf{A} = \int_{-\frac{t}{2}}^{\frac{t}{2}} \mathbf{Q} dz \quad \mathbf{B} = \int_{-\frac{t}{2}}^{\frac{t}{2}} \mathbf{Q} z dz \quad \mathbf{D} = \int_{-\frac{t}{2}}^{\frac{t}{2}} \mathbf{Q} z^2 dz \tag{2.22}$$

Finally, the actuator forces \mathbf{N}_Λ and moments \mathbf{M}_Λ per unit length which are created by the actuation strains are defined as

$$\mathbf{N}_\Lambda = \int_{-\frac{t}{2}}^{\frac{t}{2}} \mathbf{Q} \boldsymbol{\Lambda} dz \quad \mathbf{M}_\Lambda = \int_{-\frac{t}{2}}^{\frac{t}{2}} \mathbf{Q} \boldsymbol{\Lambda} z dz \tag{2.23}$$

These are the equivalent mechanical forcing terms which result from the commanded actuation strains.

The equilibrium equations for a thin laminated plate are defined in terms of the average stress equilibrium relations and are

$$\begin{aligned}\frac{\partial \bar{N}_x}{\partial x} + \frac{\partial \bar{N}_{xy}}{\partial y} &= -p_x \\ \frac{\partial \bar{N}_{xy}}{\partial x} + \frac{\partial \bar{N}_y}{\partial y} &= -p_y \\ \frac{\partial^2 \bar{M}_x}{\partial x^2} + 2\frac{\partial^2 \bar{M}_{xy}}{\partial x \partial y} + \frac{\partial^2 \bar{M}_y}{\partial y^2} &= -p_z\end{aligned}\tag{2.24}$$

where the force p is a force per unit area applied to the plate. The complete governing equations can be obtained by substituting the force and moment resultants (Eq. 2.20) into these equilibrium equations (Eq. 2.24). This yields a set of highly coupled equations that cannot be solved in a general sense.

2.4 Development of the "Pin" Force Plate Model

The purpose of this section is to obtain an induced strain actuation model for plates in extension and bending by extending the one dimensional "pin" force model to a two dimensional "pin" force plate model. Models for plates in extension and bending will be developed.

As in the one dimensional case, the "pin" force plate model assumes the actuators and substrates are pinned, so that the forces produced by the actuators are transferred to the substrates by "pins" at the edges of the actuators. The strain distributions assumed for the "pin" force plate model parallel those assumed in the one dimensional case. The assumed strains in the actuators are always constant through the thickness, while the assumed strains in the substrates are constant in the extension mode and linear in the bending mode through the thickness.

It will further be assumed that the actuator and the substrate are thin isotropic or anisotropic plates which can be described by the equations of

section 2.3, but without any extension/bending ($\mathbf{B}=0$) coupling. Uncoupling extension from bending allows for the separate development of the governing equations for extensional and bending actuation.

Equations which relate actuation strains to induced strains for the "pin" force plate model will now be derived using the same procedure developed in section 2.2, except that the scalar quantities for stress, strain, force and stiffness are now vector quantities for stress, strain, force per length and a matrix for the anisotropic plate stiffness. The geometry, coordinate system, and free body diagram of a symmetric plate actuator system is displayed in Fig. 2.6. In this configuration there is an induced strain plate actuator symmetrically positioned on either side of a laminated plate substrate. This geometry is the two dimensional equivalent of the symmetric actuator system discussed in section 2.2.

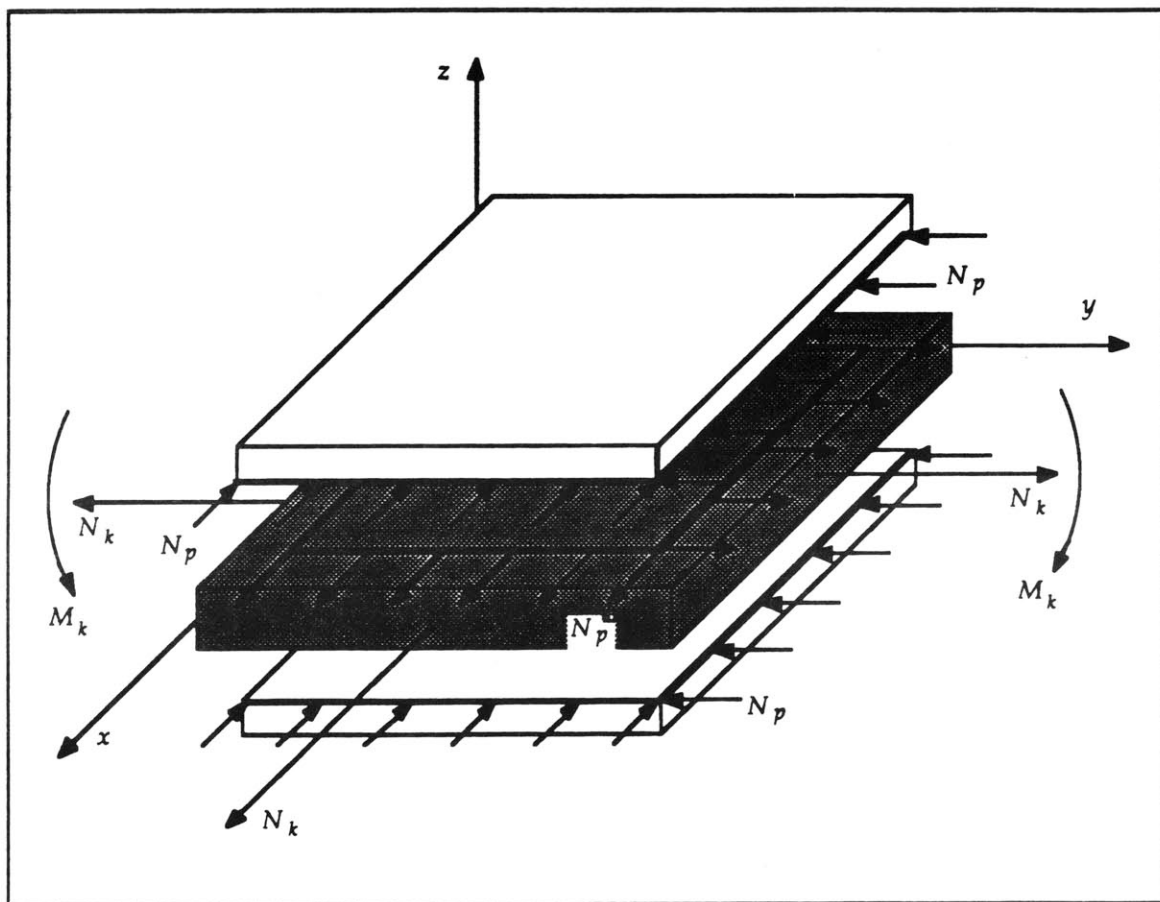


Figure 2.6 Free body diagram of the symmetric plate actuator/substrate system used for the "pin" force plate model analysis.

Plate Actuation in Extension

Like the one dimensional case, pure extension is created by commanding extensional actuation strains in both plate actuators. In this mode of actuation, the induced strain actuators as well as the substrate behave like membranes in extension, and have assumed strain distributions which are constant though the thickness.

An expression for the induced strains in the plate substrate will now be derived. Integrating the stress-strain relation (Eq. 2.18) individually over the thickness of the actuators and the substrate results in the following independent constitutive relations for each component

$$\bar{\mathbf{N}}_s = \mathbf{A}_s (\boldsymbol{\varepsilon}_s - \boldsymbol{\Lambda}) \quad (2.25)$$

$$\bar{\mathbf{N}}_s = \mathbf{A}_s (\boldsymbol{\varepsilon}_s) \quad (2.26)$$

where $\bar{\mathbf{N}}$ is resultant force per unit length in the actuator or substrate, and $\boldsymbol{\Lambda}$ is the actuation strain vector. Examination of the free body diagram in Fig. 2.6 provides the following equilibrium relations

$$\bar{\mathbf{N}}_s = -\mathbf{N}_p \quad (2.27)$$

$$\bar{\mathbf{N}}_s = \mathbf{N}_p + \mathbf{N}_k \quad (2.28)$$

In the relations above, \mathbf{N}_k and \mathbf{N}_p are respectively the external loads and the "pin" forces defined per unit length. As in the one dimensional case, the external loads \mathbf{N}_k consist of forces produced at the boundaries and externally applied forces. The forces at the edges of the actuator, or "pin" forces \mathbf{N}_p , can be found by combining the constitutive (Eqs. 2.25 and 2.26) and equilibrium (Eqs. 2.27 and 2.28) relations, and applying compatibility at the actuator/substrate interface. After some manipulation, it is found that the resulting expression for the "pin" forces is proportional to the actuation strains and the external loads, and is a function of the stiffness properties of the system.

$$\mathbf{N}_p = [\mathbf{A}_a^{-1} + \mathbf{A}_s^{-1}]^{-1} \boldsymbol{\Lambda} - [\mathbf{A}_a^{-1} + \mathbf{A}_s^{-1}]^{-1} \mathbf{A}_s^{-1} \mathbf{N}_k \quad (2.29)$$

The resultant total strains in the substrate can be found by back substitution of the "pin" forces into the equilibrium (Eqs. 2.27 and 2.28) and constitutive (Eqs. 2.25 and 2.26) relations

$$\varepsilon_s = \mathbf{A}_s^{-1} [\mathbf{A}_s^{-1} + \mathbf{A}_a^{-1}]^{-1} \Lambda + \left(\mathbf{I} - \mathbf{A}_s^{-1} [\mathbf{A}_s^{-1} + \mathbf{A}_a^{-1}]^{-1} \right) \mathbf{A}_s^{-1} \mathbf{N}_k \quad (2.30)$$

Since the strains were assumed to be uniform through the thickness of the actuator and the substrate, this one equation describes the total resultant strains in the entire system. The magnitude of the total strains are once again found to be proportional to the actuation strains and the external loads, and are functions of the relative stiffness of the substrate \mathbf{A}_s and the actuator \mathbf{A}_a .

Plate Actuation in Bending

Bending actuation of an anisotropic flat plate is now considered. Pure bending is created by commanding extensional actuations strains in one of the symmetric actuators and compressive actuation strains in the other. As in the one dimensional case, the actuators are assumed to have constant strain through the thickness, while the substrate is assumed to deform as a thin plate with strains that vary linearly through the thickness. In addition, it will be assumed that the substrate has no coupling stiffness ($\mathbf{B}=0$) terms, and that the actuators are placed symmetrically about the mid-plane.

With these assumptions, integration through the thickness of the actuators and the substrate leads to the following constitutive relations

$$\bar{\mathbf{N}}_s = \mathbf{A}_s (\varepsilon_s - \Lambda) \quad (2.31)$$

$$\bar{\mathbf{M}}_s = \mathbf{D}_s \kappa_s \quad (2.32)$$

An expression relating the strain at the actuator/substrate interface to the substrate moment resultant can be found by substituting the strain-displacement relation (Eq. 2.16) into the moment curvature equation (Eq. 2.32) and evaluating at the interface $\eta = t_s/2$

$$\bar{\mathbf{M}}_s|_{\eta} = \frac{1}{\eta} \mathbf{D}_s \varepsilon_s \quad (2.33)$$

In Eq. 2.33 the constant η represents the distance from the neutral axis of the substrate to the interface as defined in section 2.2.

The equilibrium equation for the actuator remains unchanged

$$\bar{N}_a = -N_p \quad (2.34)$$

and the substrate equilibrium at the interface can be found by examining Fig. 2.6.

$$\bar{M}_s|_{\eta} = \eta N_p + M_k \quad (2.35)$$

In Eq. 2.35, M_k is an external load vector with dimensions of moment per unit length. Notice that by thin plate theory convention a positive bending moment produces positive curvatures, and tensile stresses and extensional strains above the neutral axis.

Combining the constitutive (Eqs. 2.31 and 2.33) and equilibrium (Eqs. 2.34 and 2.35) relations and applying compatibility yields an expression for the forces on the "pins"

$$N_p = [A_a^{-1} + \eta^2 D_s^{-1}]^{-1} \Lambda - \eta [A_a^{-1} + \eta^2 D_s^{-1}]^{-1} D_s^{-1} M_k \quad (2.36)$$

By back substitution of the "pin" forces into the equilibrium (Eq. 2.35) and the constitutive (Eq. 2.33) relations, the total strain at the actuator/substrate interface can be found

$$\varepsilon_s|_{\eta} = \eta^2 D_s^{-1} [A_a^{-1} + \eta^2 D_s^{-1}]^{-1} \Lambda + \eta \left(I - \eta^2 D_s^{-1} [A_a^{-1} + \eta^2 D_s^{-1}]^{-1} \right) D_s^{-1} M_k \quad (2.37)$$

The plate curvatures are then found directly from the strain displacement relations (Eq. 2.16)

$$\kappa = \eta D_s^{-1} [A_a^{-1} + \eta^2 D_s^{-1}]^{-1} \Lambda + \left(I - \eta^2 D_s^{-1} [A_a^{-1} + \eta^2 D_s^{-1}]^{-1} \right) D_s^{-1} M_k \quad (2.38)$$

From Eq. 2.38 it can be seen that if the actuator bonded to the upper surface of the substrate is actuated in extensional, positive curvature will be induced in

the plate. Also, the expression in the parenthesis will be positive for most system configurations, so that a positive external load will produce positive curvature as well.

Upon examination of Eqs. 2.30, 2.37, and 2.38, it is obvious that the degree of strain and curvature obtainable from the induced strain actuators is proportional to the maximum actuation strain. The deformations are also proportional to the external loads. In addition, the magnitude of the strains and curvatures induced in the substrate are a function of the relative stiffness of the actuators versus the substrate and of the system geometry. Unfortunately, the complicated (algebraic) nature of the plate actuator relations obscures the important parameters which determine the effectiveness of induced strain actuator/substrate systems. In order to extract this information, specific systems will be analyzed for which closed form solutions can be found and design parameters can be obtained. These solutions will be discussed in section 3.2.

As in the one dimensional case the ability to obtain explicit solutions to the "pin" force plate model equations depends on the nature of the boundary conditions and the externally applied loads. Unfortunately, solutions for plate systems are difficult to obtain in closed form. This difficulty is one of the prime motivating factors behind developing the consistent plate model. This model is advantageous because, as will be seen, the consistent plate model formulates the induced strain problem in a manner which can easily be solved using approximate solution techniques.

2.5 Development of the Consistent Plate Model

The second, more comprehensive, model which will be used to analyze induced strain actuator/substrate systems is the consistent plate model. The consistent plate model considers both the actuators and the structural plate substrates to be plies of a laminated plate. The assumptions on symmetry of the actuator placement, their placement only at the surface of the substrate, and the uncoupled bending/extension nature of the substrate will be relaxed. This model offers great flexibility in that any number of

arbitrarily positioned and oriented actuators, including embedded actuators and protective coverings, combined with a substrates of arbitrary stiffness properties can be modelled conveniently.

The name *consistent plate model* comes from the assumption of consistent deformations in the actuators and substrates. For systems actuated in extension, the strains will be assumed constant through the thickness of the entire actuator/substrate system. Likewise, for systems actuated in bending, it will be assumed that the strain varies linearly through the thickness of the entire system. Fig. 2.7 displays a typical actuator/substrate system modeled by the consistent plate model and a cross-section of the assumed strain distribution for the system actuated in extension and bending. Comparing this strain distribution with that of the "pin" force model assumed strain of Fig. 2.3 illustrates the difference between the two models.

Incorporating each component of the actuator/substrate system as plies of a single laminated plate with a consistent strain distribution allows for straight forward development of the governing equations. The strain and curvature relations, and the appropriate strain energy expressions can be found in a manner similar to classical laminated plate theory. In addition to yielding more accurate results for some systems, it is the straight forward formulation of the plate strain energy relations which makes the consistent plate model so attractive. However, because the entire system has been condensed into one laminated plate, finding exact solutions, discussed in the following chapter, may require additional effort.

Governing Equations

The governing equations for the consistent plate model will now be developed. Except for modelling the system as a thin laminated plate with a consistent strain distribution, no further assumptions will be imposed on this model other than those used in the development in section 2.3.

The stress-strain relation for each ply of a laminated plate was assumed in section 2.3 to be

$$\sigma^k = Q^k (\epsilon - \Lambda) \quad (2.39)$$

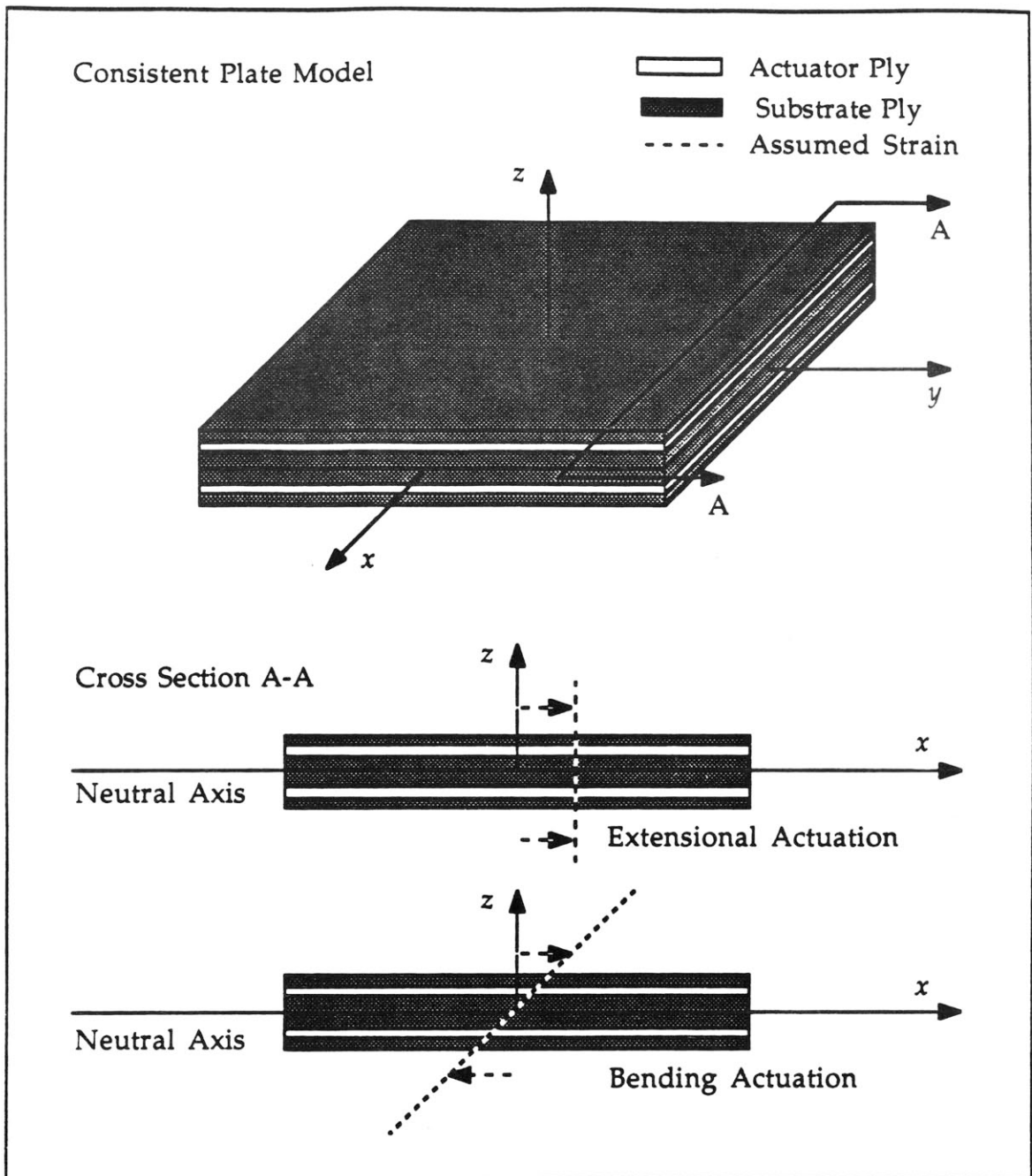


Figure 2.7 Consistent plate model and assumed strain distributions for extensional and bending actuation.

where the superscript k represents the ply number considered. In the actuator plies the actuation strain vector Λ will have some non-zero components, while all elements of Λ will be zero in the substrate plies. The actuation strain term is treated exactly as thermal strains would be handled in classical laminated plate theory.

The consistent plate model constitutive relations are found by integrating Eq. 2.39 through the thickness of each ply over the entire system. The resultant forces and moments are found to be

$$\begin{bmatrix} \bar{\mathbf{N}} \\ \bar{\mathbf{M}} \end{bmatrix} = \begin{bmatrix} \mathbf{A} & \mathbf{B} \\ \mathbf{B} & \mathbf{D} \end{bmatrix} \begin{bmatrix} \boldsymbol{\varepsilon}^o \\ \boldsymbol{\kappa} \end{bmatrix} - \begin{bmatrix} \mathbf{N}_\Lambda \\ \mathbf{M}_\Lambda \end{bmatrix} \quad (2.40)$$

Although these resultants are simply those found for a general laminated plate (Eq. 2.20) care must be taken in performing the necessary integrations to obtain the correct stiffness and actuator forcing terms. Both actuator and substrate plies will contribute to the stiffness matrixes \mathbf{A} , \mathbf{B} , and \mathbf{D} , while only actuator plies will contribute to the actuator forcing vectors \mathbf{N}_Λ and \mathbf{M}_Λ . In addition, the elements of the actuator forcing vectors will depend on both the actuator stiffness Q^k and the actuation strain vector Λ .

The actuator forcing vectors are manifest as actual forces and moments only when the plate is completely restrained. This concept is equivalent to the force which develops when a bar is constrained by two solid walls and subjected to a temperature change which would cause the bar to expand in an unconstrained situation.

Equation 2.40 relates the resultant total strains and curvatures found in the actuator/substrate system to the actuation strains, external loads, and the stiffness properties of the system. This expression sacrifices insight concerning induced strain actuators, which is present in the less comprehensive "pin" force results (Eqs 2.30, 2.37, and 2.38), but obtains an expression which is general and compact; however, some observations can be made. The presence of numerous coupling terms shows that it is possible to create a variety of deformations (bending or twisting), using several different actuation modes (extension or bending), provided the correct directional stiffnesses are incorporated into the plate. In particular, twisting can be induced by commanding bending if the plate is designed to embody bending/twisting coupling (D_{16} and D_{26} terms non-zero), or by commanding extension if extension/twisting (B_{16} and B_{26}) coupling terms are present. Thus, by careful selection of the laminate plies an actuator system can be designed to take advantage of one, many, or none of the aforementioned couplings.

Under special limited circumstances, closed form solutions of these plate models can be determined. When the equilibrium relations are satisfied such that the force and moment resultants are identically zero, the strains and curvatures in the plate can be solved directly from the constitutive relationship. Such situations will be discussed in Chapter 3. If the resultants are not zero everywhere, then the externally applied loads and the loads produced at the boundaries must be known in order to obtain a solution. This difficulty is true of both the "pin" force plate model and the consistent plate models presented. Therefore, the closed form solutions for the strains and curvatures cannot be found in general. Unfortunately, in most practical cases the complete laminated plate equilibrium equations (Eq. 2.24) must be solved, with the appropriate boundary conditions, in order to be able to specify the external loads on the actuator/substrate system. Solutions to such cases are usually not available, thus approximate solution techniques must be developed.

Strain Energy Relations

The difficulties involved in solving the general governing equations describing a laminated plate, indicates the necessity to derive approximate methods based on the strain energy relations for induced strain actuator/substrate systems. Using the consistent plate model, the system will be considered a laminated composite plate with induced strain actuator and substrate plies. It will be assumed that the thin plate assumptions used previously, once again apply, and that the plate geometry remains unchanged from that of Fig. 2.7. All other assumptions remain identical to those imposed in formulating the consistent plate model.

The incremental strain energy associated with extension, shear, bending, and twisting of a thin plate is given by

$$\delta U = \int \int \int_{\text{volume}} \{ \sigma_x \delta \epsilon_x + \sigma_y \delta \epsilon_y + \tau_{xy} \delta \gamma_{xy} \} d(\text{volume}) \quad (2.41)$$

This differential strain energy relation can be manipulated into a form which allows for straight forward derivation of the plate strain energy in an extremely useful and compact matrix form. Such a plate strain energy

equation, which includes actuation strain terms from induced strain actuators is developed below.

After partitioning the integral into an integral through the thickness t and over the surface A , and rewriting the stresses and strains in matrix notation, the following relation is obtained from Eq. 2.41

$$\delta U = \int_A \int_t \left\{ \int_t [\sigma^T \delta \epsilon] dz \right\} d(A) \quad (2.42)$$

Substitution of the thin plate stress-strain relation (Eq. 2.18) yields the following differential strain energy expression

$$\delta U = \int_A \int_t \left\{ \int_t [(\mathbf{Q}^k \epsilon)^T \delta \epsilon - (\mathbf{Q}^k \Lambda)^T \delta \epsilon] dz \right\} d(A) \quad (2.43)$$

where Λ is the actuation strain vector. Taking the transpose of the quantities in the parenthesis yields

$$\delta U = \int_A \int_t \left\{ \int_t [\epsilon^T \mathbf{Q}^k \delta \epsilon - \Lambda^T \mathbf{Q}^k \delta \epsilon] dz \right\} d(A) \quad (2.44)$$

since the transformed reduced stiffness matrix is symmetric ($\mathbf{Q} = \mathbf{Q}^T$). It can be seen that the first term in the equation above represents the internal energy of the plate, and the second term represents the energy associated with the actuation strain.

The next step toward deriving the full plate strain energy expression is to substitute the strain-displacement relations (Eq. 2.16) into the energy equation. After manipulating, the strain energy can be written as

$$\delta U = \int_A \int_t \left\{ \int_t \left[\begin{matrix} \epsilon^{\circ T} & \kappa^T \end{matrix} \right] \begin{bmatrix} \mathbf{Q}^k & z \mathbf{Q}^k \\ z \mathbf{Q}^k & z^2 \mathbf{Q}^k \end{bmatrix} \begin{Bmatrix} \delta \epsilon^{\circ} \\ \delta \kappa \end{Bmatrix} - \Lambda^T [\mathbf{Q}^k \ z \ \mathbf{Q}^k] \begin{Bmatrix} \delta \epsilon^{\circ} \\ \delta \kappa \end{Bmatrix} \right] dz \right\} d(A) \quad (2.45)$$

Examination of Eq. 2.45 indicates that the differential energy expression is in a form which can be integrated through the thickness since the in-plane strains and the curvatures are independent of z . Integration results in a strain energy

relation in terms of the stiffness matrixes (**A**, **B**, and **D**), and the induced strain actuator forcing terms (\mathbf{N}_A and \mathbf{M}_A) defined in section 2.2

$$\delta U = \int \int_A \left\{ \begin{Bmatrix} \varepsilon^{\circ T} & \kappa^T \end{Bmatrix} \begin{bmatrix} \mathbf{A} & \mathbf{B} \\ \mathbf{B} & \mathbf{D} \end{bmatrix} \begin{Bmatrix} \delta \varepsilon^{\circ} \\ \delta \kappa \end{Bmatrix} - \begin{bmatrix} \mathbf{N}_A & \mathbf{M}_A \end{bmatrix} \begin{Bmatrix} \delta \varepsilon^{\circ} \\ \delta \kappa \end{Bmatrix} \right\} d(A) \quad (2.46)$$

Finally, integration of the differential strain energy expression from a zero strain state to the induced strain state is carried out to arrive at the plate strain energy equation,

$$U = \frac{1}{2} \int \int_A \left\{ \begin{Bmatrix} \varepsilon^{\circ T} & \kappa^T \end{Bmatrix} \begin{bmatrix} \mathbf{A} & \mathbf{B} \\ \mathbf{B} & \mathbf{D} \end{bmatrix} \begin{Bmatrix} \varepsilon^{\circ} \\ \kappa \end{Bmatrix} \right\} d(A) - \int \int_A \begin{bmatrix} \mathbf{N}_A & \mathbf{M}_A \end{bmatrix} \begin{Bmatrix} \varepsilon^{\circ} \\ \kappa \end{Bmatrix} d(A) \quad (2.47)$$

Eq. 2.47 represents the total potential energy stored in a laminated plate. This energy expression is made up of strain energy due to in-plane, out-of-plane, and coupled deformations. The strain energy equation along with approximate solution methods will be used in the next chapter to solve for the strains and curvatures induced in plate actuator/substrate systems.

2.6 Conclusions

In summary, two models of induced strain actuation systems have been presented. The models included a "pin" force model and a consistent plate model. Expressions were first found for the induced strain and curvature in a system using the one dimensional "pin" force model. The expressions showed that the actuation strain, relative stiffness ratio, and geometry of deformation determined the effectiveness of the transfer of actuation strain to induced strain in the substrate. Expressions for strains and curvatures were also found using the "pin" force plate model, however in the plate case the equations are more complicated, and the parameters become obscured in the algebra.

The consistent plate model was developed to allow actuation systems with more complex configurations to be analyzed. The consistent plate model analyzes complex induced strain actuator/substrate systems by

modelling each component of the system as a laminate ply, and because this model treats the system as one integrated structure, the assumed strain distributions of the actuators and substrates are identical. The consistent plate model was used to derive an expression for the strains and curvatures induced in actuator/substrate systems.

For both the "pin" force plate model and the consistent plate model the external loads dictated whether explicit expressions could be found. And since these loads are a complicated function of the boundary conditions and the full plate equilibrium equations, they cannot be determined exactly for most systems. Therefore, the plate strain energy relations were developed using the consistent plate model in order to be able to take advantage of approximate solution techniques.

CHAPTER 3

SOLUTIONS TO THE ANALYTIC MODELS

3.1 Introduction

Solutions to the governing equation derived in the previous chapter are discussed below. Cases for which closed form solutions can be obtained are presented for both the "pin" force plate model and the consistent plate model. In addition a general solution procedure for induced strain plate actuator/substrate systems, with arbitrary boundary conditions and externally applied forces and moments, is developed. This general solution makes use of the consistent plate model strain energy relations and approximate solution techniques. Finally, specific solutions for the geometries of the experimental test specimens, which are described in Chapters 5 and 6, are detailed.

As discussed in Chapter 2, explicit solutions for the induced strains and curvatures found in an actuator/substrate system can only be calculated in closed form when the external loads, which result from the boundary conditions as well as any externally applied forces and moments, can be determined exactly. Situations when the external loads can be determined in closed form will be discussed, and the solutions which result from the "pin" force plate model and the consistent plate model will be examined and compared. For most real systems the applied loads cannot be determined exactly. Thus the strain energy relations and approximate solution techniques will be utilized to solve for the induced strains and curvatures of general induced strain actuator/substrate systems.

For the solutions presented in this chapter, it will be assumed that the actuation strain vector is that which would be generated by an isotropic induced strain actuator, and the stiffness properties of the actuator are that of an isotropic material. In this model, the actuation strain vector takes the form of

$$\Lambda = \begin{bmatrix} \Lambda_x \\ \Lambda_y \\ 0 \end{bmatrix} \quad (3.1)$$

Although the actuator model is isotropic and actuation strains of unconstrained induced strain actuators are generally isotropic as well, actuation strains which differ in the longitudinal Λ_x and transverse Λ_y directions may develop as a result of anisotropic coupling effects from the substrates. This result is due to the substrates effect on the properties of some induced strain actuators, which will be discussed in detail in section 4.2. The realism of the isotropic actuator model will also be discussed in detail in section 4.2. Finally, it should be noted that the isotropic actuator model (Eq. 3.1) assumes no actuation shear strains are produced.

3.2 Exact Solutions of Induced Strain Actuator Models

Actuator configurations for which the induced strains and curvatures can be calculated in closed form are now presented. As mentioned previously, closed form solutions can be found when the external loads on the system are known exactly. One actuator configuration for which the external loads can be determined explicitly is the totally unconstrained case, such as the free-free, free-free plate system. The external loads generated by free-free, free-free boundary conditions are zero everywhere. Thus external loads will only result from externally applied forces and moments and for the purpose of analyzing the transfer of actuation strains to induced strains in actuator systems, the externally applied forces and moments will be set to zero. Solutions for totally unconstrained systems, with no externally applied loads, are now developed.

"Pin" Force Plate Model Solutions

"Pin" force plate model solutions for actuation systems with free-free, free-free boundary conditions and no externally applied forces or moments are detailed below. The same symmetric actuator/substrate plate system (Fig. 2.6) used to develop the "pin" force plate model in chapter two will be analyzed. Induced strain actuator systems with isotropic substrates will be

considered first. Solutions will be found for systems actuated in extension and in bending. Following this analysis, systems with anisotropic substrates will be discussed.

The equations which relate the actuation strains to the total strains found in the system were given by the "pin" force plate model in Eq. 2.30 for actuation in the extensional mode. The configuration of the system is such that no external loads are generated by the boundary conditions and it has been assumed that there are no externally applied forces or moments. Thus, the relations for the "pin" forces (Eq. 2.29) and the total strains (Eq. 2.30), which are equal to the induced strains under these conditions, reduce to

$$\mathbf{N}_p = [\mathbf{A}_s^{-1} + \mathbf{A}_s^{-1}]^{-1} \Lambda \quad (3.2)$$

$$\boldsymbol{\varepsilon} = \mathbf{A}_s^{-1} [\mathbf{A}_s^{-1} + \mathbf{A}_s^{-1}]^{-1} \Lambda \quad (3.3)$$

The extensional stiffness matrix \mathbf{A} for an isotropic plate is found by integration, as defined in section 2.3, of the two dimensional isotropic reduced stiffness matrix

$$\mathbf{Q}_{isotropic} = \frac{1}{1-\nu^2} \begin{bmatrix} E & \nu E & 0 \\ \nu E & E & 0 \\ 0 & 0 & E \frac{(1-\nu)}{2} \end{bmatrix} \quad (3.4)$$

where E is the modulus of elasticity and ν is Poisson's ratio. After integrating the reduced stiffness matrix to find the extensional stiffness matrix, combining this result with the "pin" force (Eq. 3.2) or the induced strain expression (Eq. 3.3), and manipulating, the forces at the "pins" and the induced strains can be expressed as follows

$$\mathbf{N}_p = \frac{1}{1-\nu} \left[\frac{1}{\alpha + \psi} \right] \begin{bmatrix} 1 & 0 & 0 \\ 0 & 1 & 0 \\ 0 & 0 & 1 \end{bmatrix} \Lambda \quad (3.5)$$

$$\boldsymbol{\varepsilon} = \frac{\alpha}{\alpha + \psi} \begin{bmatrix} 1 & 0 & 0 \\ 0 & 1 & 0 \\ 0 & 0 & 1 \end{bmatrix} \Lambda \quad (3.6)$$

where $\alpha = 2$ for this symmetric actuator geometry since there are two induced strain actuators and one structural plate. It should be noted that since the substrate as well as the actuators have been assumed to be isotropic, the actuation strain will be equal in the longitudinal Λ_x and transverse Λ_y directions. Thus the actuation strain vector becomes

$$\Lambda = \begin{bmatrix} \Lambda \\ \Lambda \\ 0 \end{bmatrix} \quad (3.7)$$

And, the "pin" forces and strains can be written

$$\begin{aligned} (N_p)_x &= \frac{1}{1-\nu} \left[\frac{1}{\alpha + \psi} \right] \Lambda \\ (N_p)_y &= \frac{1}{1-\nu} \left[\frac{1}{\alpha + \psi} \right] \Lambda \\ (N_p)_{xy} &= 0 \end{aligned} \quad (3.8)$$

$$\begin{aligned} \epsilon_x &= \frac{\alpha}{\alpha + \psi} \Lambda \\ \epsilon_y &= \frac{\alpha}{\alpha + \psi} \Lambda \\ \epsilon_{xy} &= 0 \end{aligned} \quad (3.9)$$

Similar expressions can be found for the same isotropic symmetric system actuated in bending. As above, the boundary conditions are given as free-free, free-free and no externally applied forces or moments are present. Also, both the substrate and the actuators are assumed to be isotropic, thus the actuation strain vector is isotropic as above (Eq. 3.7).

Expressions for the induced strains (Eq. 2.37) and curvatures (Eq. 2.38) were found in chapter 2 for the "pin" force plate model. Setting the applied loads to zero, these expressions become

$$\epsilon_s|_{\eta} = \eta^2 \mathbf{D}_s^{-1} [\mathbf{A}_s^{-1} + \eta^2 \mathbf{D}_s^{-1}]^{-1} \Lambda \quad (3.10)$$

$$\kappa = \eta \mathbf{D}_s^{-1} [\mathbf{A}_s^{-1} + \eta^2 \mathbf{D}_s^{-1}]^{-1} \Lambda \quad (3.11)$$

for actuation in the bending mode. Similar to the isotropic extensional stiffness matrix \mathbf{A} , the isotropic bending stiffness matrix is found from the isotropic reduced stiffness matrix $\mathbf{Q}_{\text{isotropic}}$

$$\mathbf{D} = \begin{bmatrix} D & \nu D & 0 \\ \nu D & D & 0 \\ 0 & 0 & D \frac{(1-\nu)}{2} \end{bmatrix} \quad \text{where} \quad D = \frac{E_s t_s^3}{12(1-\nu^2)} \quad (3.12)$$

By substituting the isotropic stiffness relations into the strain (Eq. 3.10) and curvature (Eq. 3.11) relations, and manipulating, the resulting induced strains and curvatures reduce to

$$\varepsilon_s|_{\eta} = \frac{\alpha}{\alpha + \psi} \begin{bmatrix} 1 & 0 & 0 \\ 0 & 1 & 0 \\ 0 & 0 & 1 \end{bmatrix} \Lambda \quad (3.13)$$

$$\kappa = \frac{2}{t_s} \left[\frac{\alpha}{\alpha + \psi} \right] \begin{bmatrix} 1 & 0 & 0 \\ 0 & 1 & 0 \\ 0 & 0 & 1 \end{bmatrix} \Lambda \quad (3.14)$$

where $\alpha = 6$ for this system actuated in the bending mode.

Notice that the strain equations for extensional (Eq. 3.6) and the curvature relations for bending (Eq. 3.14) actuation are uncoupled due to the assumption of isotropy of the actuator and the plate, and closely resemble the equations derived for a bar in extension (Eq. 2.9) and a beam in bending (Eq. 2.14) respectively. The geometric constants α , which was found to equal 2 in the extensional mode and 6 in the bending mode, are identical to the one dimensional cases. Also, the effectiveness of the induced strain actuation systems, and hence the magnitude of the strains and curvatures depend on the same factors - actuation strain Λ , relative stiffness ratio ψ , and geometry α . It is clear that as the plate stiffness decreases, the effectiveness of the actuator strain transfer, from actuation strain to induced extensional or bending strain, is increased. And, increasing the actuation strain will increase the induced strain. These trends which govern the transfer of actuation strain to induced strain apply to the actuator systems with other geometries, and different geometric constants, presented in Fig. 2.4.

It is interesting that Poisson's ratio has disappeared from the problem. It can be seen from Eq. 3.8 that the forces produced at the "pins" have increased by a factor of $1/(1-\nu)$, in the case of the two dimensional plate compared to the one dimensional bar, due to Poisson's effect in the plate. However, the plate stiffness has also been increased by the same factor, and the two factors cancel in the resulting strain equation (Eq. 3.9). As a result of this cancellation, Poisson's ratio is not present in the solution for the induced strains (Eqs. 3.9 and 3.13) and curvatures (Eq. 3.14), and the strains and curvatures in the two orthogonal directions are uncoupled. This interesting result is true only of isotropic plates.

In the above analysis closed form solutions for isotropic, unconstrained, unforced systems were presented. As shown, elegant solutions can be found for such systems. However, this is not the case for systems with anisotropic substrates. In anisotropic systems, Poisson's ratio plays an important role determining the induced strains and curvatures, and the equations are highly coupled. Such anisotropic systems are now discussed. As before, a symmetric plate system with free-free, free-free boundary conditions and no externally applied forces or moments will be considered. The actuator will again be assumed to be isotropic, but the substrate will have orthotropic properties. Further it will be assumed that the induced strain actuator is isotropic and is unaffected by the orthotropic substrate, so the actuation strain is given by Eq. 3.7.

The "pin" force plate relations for the induced strain of an unconstrained, unforced, symmetric plate actuator system were given by Eq. 3.4 for actuation in the extensional mode. Some effects of the orthotropic substrate can be found by assuming that the substrate has a longitudinal x to transverse y Poisson's ratio ν_{yx} equal to the Poisson's ratio of the actuator ν , and no extension/bending coupling ($B=0$). Thus the substrate extensional stiffness matrix becomes

$$\mathbf{A}_s = \begin{bmatrix} \frac{E_x}{1-\nu\nu_{yx}} & \frac{\nu E_y}{1-\nu\nu_{yx}} & 0 \\ \frac{\nu E_y}{1-\nu\nu_{yx}} & \frac{E_y}{1-\nu\nu_{yx}} & 0 \\ 0 & 0 & G_{xy} \end{bmatrix} \quad (3.15)$$

where the transverse Poisson's ratio is

$$\nu_{yx} = \nu \frac{E_y}{E_x} \quad (3.16)$$

and G_{xy} is the shear modulus of the substrate.

After substitution of Eq. 3.15 into Eq. 3.4 and much algebraic manipulation the induced strains are found to be

$$\begin{aligned} \varepsilon_x &= \left[\frac{\alpha}{\alpha + \psi} \right] \Lambda \\ \varepsilon_y &= \left[\frac{\alpha \left[\nu \left(\frac{1}{\gamma} (\alpha + \psi) - \left(\frac{\alpha}{\gamma} + \psi \right) \right) + \left(\frac{1}{\gamma} - \nu^2 \right) (\alpha + \psi) \right]}{(\alpha + \psi) \left(\frac{\alpha}{\gamma} + \psi \right) - \nu^2 (\alpha + \psi)^2} \right] \Lambda \\ \varepsilon_{xy} &= 0 \end{aligned} \quad (3.17)$$

where γ is the ratio of the transverse elastic modulus to the longitudinal elastic modulus E_y/E_x , and the relative stiffness ratio ψ is now given by E_{xts}/E_{ata} .

It can be seen that anisotropic strains will be induced in the actuator system. The degree of anisotropy of the induced strains will depend on the ratio of the plate stiffness in the longitudinal and transverse directions γ . Also, because the actuation strains were assumed to be isotropic and it was assumed that the substrate had no extension/shear coupling, no shear strain will be induced in the substrate.

A good measure of the anisotropic behavior of this system can be seen by examining the ratio of induced strains in the longitudinal and transverse directions. Fig. 3.1 shows a plot of the strain ratio versus γ for several values of the relative stiffness ψ with Poisson's ratio set to 0.3. From Fig. 3.1 it can be seen that the induced strain ratio increases as γ decreases, and that the relative stiffness effects the magnitude of the substrate strains.

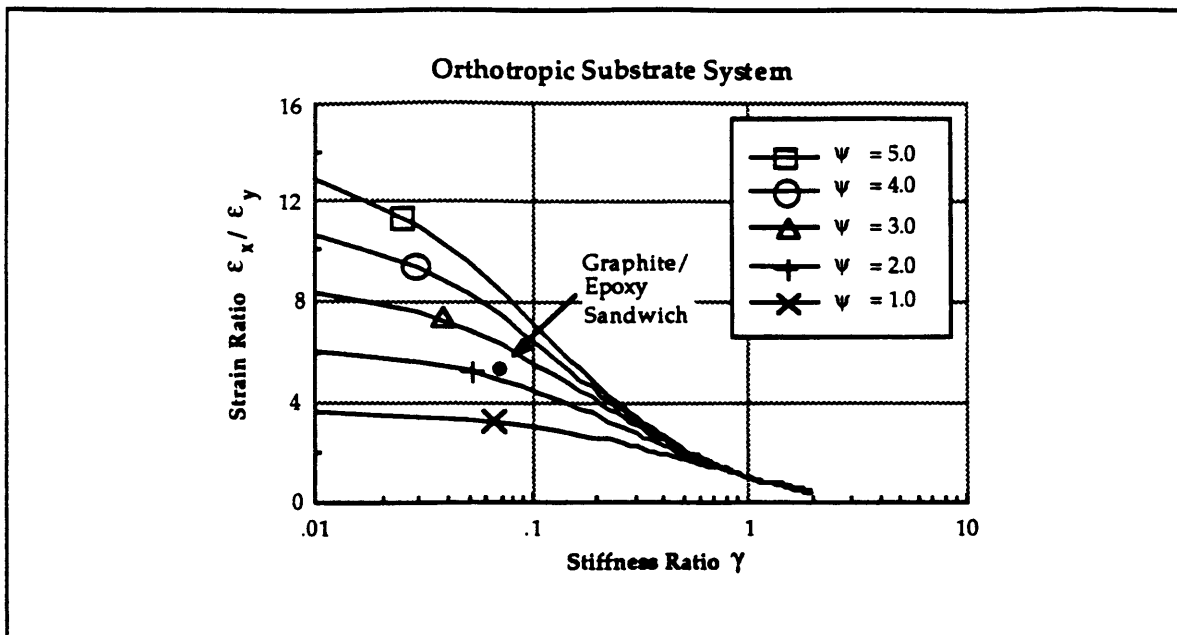


Figure 3.1 Plot of strain ratio versus moduli ratio in the transverse and longitudinal directions.

The orthotropic substrate system presented above is relatively simple but has important ramifications for the design of induced strain actuator systems. The importance lies in the fact that a goal of many actuator designs is to induce a specific shear strain or twist curvature. Since isotropic symmetric actuators in combination with orthotropic substrates do not inherently produced shear strain, such deformations can only be obtained by taking advantage of substrates with extension/shear, extension/twist, and bending/twist coupling. The degree of such coupling is dependent on two factors: the ratio of the transverse to longitudinal stiffness γ , and the orientation, or ply angle, of the substrate. Thus, both factors must be considered in designing an induced strain actuator/substrate system to deform in shear or twist.

Consistent Plate Model Solutions

In a manner similar to the procedure used to find the "pin" force plate model solutions, exact solutions can be found for actuator systems described by the consistent plate model. Closed form solutions will found using the consistent plate model for the same symmetric plate actuator/substrate system analyzed above, and the results will be compared to the "pin" force

plate model solutions. Solutions for systems with isotropic actuators and substrates will be detailed, and solutions for systems with anisotropic substrates will be discussed.

As before, an unconstrained symmetric plate actuator system with no externally applied forces or moments will be considered. The resultant forces and moments in this actuator system are again zero everywhere, and the consistent plate model relations for the induced strains and curvatures (Eq. 2.40) reduce to

$$\begin{bmatrix} \epsilon^\circ \\ \kappa \end{bmatrix} = \begin{bmatrix} \mathbf{A} & \mathbf{B} \\ \mathbf{B} & \mathbf{D} \end{bmatrix}^{-1} \begin{bmatrix} \mathbf{N}_\Lambda \\ \mathbf{M}_\Lambda \end{bmatrix} \quad (3.18)$$

The induced strains and curvatures can be found for an isotropic system by inserting the isotropic extensional stiffness and isotropic bending stiffness matrixes into Eq. 3.18 and performing the necessary algebra. This results in the uncoupled induced strain and curvature relations given below

$$\begin{bmatrix} \epsilon \\ \kappa \end{bmatrix} = \begin{bmatrix} \frac{\alpha_1}{\alpha_1 + \psi} \begin{bmatrix} 1 & 0 & 0 \\ 0 & 1 & 0 \\ 0 & 0 & 1 \end{bmatrix} \Lambda & [0] \\ [0] & \frac{2}{t_s} \left[\frac{1}{T} + 1 \right] \frac{\alpha_2}{\alpha_2 K + \psi} \begin{bmatrix} 1 & 0 & 0 \\ 0 & 1 & 0 \\ 0 & 0 & 1 \end{bmatrix} \Lambda \end{bmatrix} \quad (3.19)$$

where $T = \frac{t_s}{t_a}$ and $K = \frac{4}{3} \left(\frac{1}{T} \right)^2 + 2 \left(\frac{1}{T} \right) + 1$

Notice that there is no cross coupling between the in-plane strains and the curvatures because all elements of the coupling stiffness matrix \mathbf{B} are zero for isotropic materials and the actuators are symmetric. In Eq. 3.19 the values of the geometric constants, $\alpha_1 = 2$ and $\alpha_2 = 6$, are identical to those found in the corresponding "pin" force solution. It is interesting that the extensional strains predicted by the consistent plate model are identical to those found from the plate "pin" force model. This result is due to the strain distributions assumed in each model, which are the same for actuation in the extensional mode as shown in Figs. 2.3 and 2.7.

In contrast, the strain distributions are different when considering actuation in bending, and this difference is reflected in the curvature solutions. By comparing the curvatures predicted by Eq. 3.14 for the "pin" force plate model and Eq. 3.19 for the consistent plate model, the following ratio can be formulated.

$$\frac{\kappa_{\text{Consistent}}}{\kappa_{\text{"Pin" Force}}} = \left[\frac{1}{T} + 1 \right] \frac{\alpha + \frac{E_s T}{E_a}}{\alpha K + \frac{E_s T}{E_a}} \quad (3.20)$$

Fig. 3.2 displays a graph of Eq. 3.20 versus the ratio of the substrate to actuator thickness (t_s/t_a) for various to actuator stiffness ratios (E_s/E_a). It can be readily seen that as the thickness ratio (t_s/t_a) increases, the two solutions become the same. This is because the assumed strain distributions become nearly identical as the thickness ratio increases. As the thickness ratio decreases and becomes small (substrate thickness roughly equal to the actuator thickness) the "pin" force model deviates from the more precise consistent plate model because of increasing discrepancies in the assumed strain distributions. Experimental results of actual plate actuator systems actuated in bending, discussed in Chapter 6, indicate that the consistent plate model is the more accurate of the two models.

Equations. 3.14 and 3.19 show that the amount of bending or twist curvature obtainable from an induced strain actuation system is inversely proportional to the substrate thickness. Hence, if the purpose of an actuator/substrate system is to obtain relatively large deflections or curvatures, the substrate thickness should be small and the consistent plate model should be used to obtain accurate result.

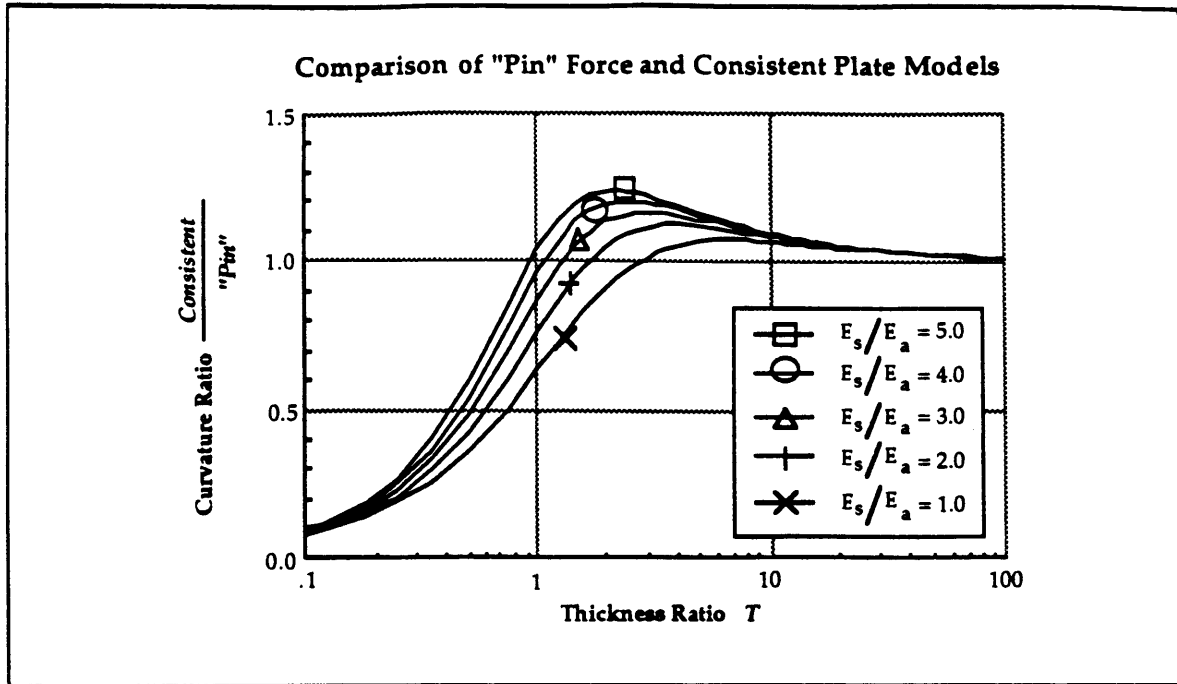


Figure 3.2 Plot of the ratio of curvatures predicted by the "pin" force plate and consistent plate model versus thickness ratio of a symmetric actuator/substrate system.

In the above analysis, closed form solutions were found for an unconstrained, unforced, isotropic, symmetric system using the consistent plate model. Closed form solutions for this system with orthotropic components can be found, but as can be inferred from Eq. 3.17 the addition of orthotropic properties cause such solutions to become algebraically prohibitive. For components constructed from a general composite laminate, Eq. 3.18 indicates that a fully populated six by six element stiffness matrix must be inverted. It can be seen from this equation that shear strain will be induced in systems with extension/shear coupling (A_{16}) and twist curvature will be induced in systems with extension/twist coupling (B_{16}) when actuated in extension, and twist curvature will be induced in systems with bending/twist (D_{16}) coupling when actuated in bending. But, no further insight is found by attempting to invert the stiffness matrix. In addition to being difficult to solve algebraically, Eq. 3.18 is valid only for an extremely limited class of actuator systems which are defined by the assumptions made above with respect to the boundary conditions and externally applied forces. It is because of these difficulties that approximate solutions to the consistent plate model strain energy equations are attractive.

3.3 Ritz Formulation for Approximate Solutions

Closed form solutions, such as those found above, cannot be found for the majority of induced strain actuator configurations. For systems with arbitrary boundary conditions and externally applied loads, such as an aeroelastic lifting surface or a structure used to control the pointing of a precision optical package, approximate solution methods must be utilized. Approximate solutions must also be used for dynamic analysis. The two most prominent solution techniques are the Rayleigh-Ritz assumed mode method and the Finite Element method. A Ritz solution is derived below because it requires less computation, and provides more insight into the physics of induced strain actuation.

The strains and curvatures in an induced strain actuator system can be solved using a Ritz technique by substituting assumed modes into the plate strain energy equations and applying Lagrange's equations of motion. In this section a general Ritz approximate solution is outlined. In addition the selection of mode shapes will be discussed, specifically for the geometries of the test articles constructed. Finally, simplifications will be made which reveal important design and performance parameters. Matrix notation is adopted which leads to compact representations and simplifies the algebra required considerably.

Ritz Assumed Mode Method

The plate systems which will be considered have both in-plane and out-of-plane displacements, therefore the displacement vector is defined as

$$\mathbf{u} = \{u \ v \ w\}^T \quad (3.21)$$

where u and v are the longitudinal and transverse in-plane displacements respectively, and w is the out-of-plane displacement. It is important that the correct mode shapes are assumed for the in-plane as well as the out-of-plane displacements for two reasons. First, solutions are desired for the extensional strains of test articles actuated in the extensional mode. Since some of the systems are anisotropic and have extension/shear coupling, in-plane modes must be assumed which capture the behavior of these specimens. Second,

solutions for plate articles with extension/twist as well as bending/twist coupling will be sought. It is essential that the in-plane as well as the out-of-plane modes are adequately represented in order to correctly predict the twist and bending curvatures of these specimens when actuated in either extension or bending.

Using the above representation for the displacements (Eq. 3.21), the strains and curvatures can be expressed as

$$\begin{Bmatrix} \varepsilon^o \\ \kappa \end{Bmatrix} = [\mathcal{D}]\{\mathbf{u}\} \quad (3.22)$$

where \mathcal{D} is a derivative operator matrix

$$\mathcal{D} = \begin{bmatrix} \frac{\partial}{\partial x} & 0 & 0 \\ 0 & \frac{\partial}{\partial y} & 0 \\ \frac{\partial}{\partial y} & \frac{\partial}{\partial x} & 0 \\ 0 & 0 & -\frac{\partial^2}{\partial x^2} \\ 0 & 0 & -\frac{\partial^2}{\partial y^2} \\ 0 & 0 & -2\frac{\partial^2}{\partial xy} \end{bmatrix}$$

and the strains and curvatures are defined by Eq. 2.17.

The modes assumed for the displacements will depend on the geometry, boundary conditions, and forcing of each individual system, but in a general sense the displacements can be written as

$$u = \sum_{i=1}^m \phi_{u_i} q_i \quad v = \sum_{j=1}^n \phi_{v_j} q_{m+j} \quad w = \sum_{k=1}^p \phi_{w_k} q_{m+n+k} \quad (3.23)$$

where ϕ_{u_i} , ϕ_{v_j} , and ϕ_{w_k} are the longitudinal in-plane, transverse in-plane and out-of-plane assumed mode shapes respectively. And, \mathbf{q} represents the generalized coordinate vector. The assumed modes can be written in a

convenient form by replacing the above summation notation with matrix notation such that

$$\{u\} = [H]q \quad (3.24)$$

$$H = \begin{bmatrix} [\phi_{u_1}, \phi_{u_2}, \dots, \phi_{u_m}] & [0] & [0] \\ [0] & [\phi_{v_1}, \phi_{v_2}, \dots, \phi_{v_n}] & [0] \\ [0] & [0] & [\phi_{w_1}, \phi_{w_2}, \dots, \phi_{w_p}] \end{bmatrix}$$

The matrix, H, is a 3 by r dimensional mode shape matrix where r equals the total number of modes ($m+n+p$). Substitution of Eq. 3.24 into Eq. 3.22 leads to a matrix expression for the strain and curvatures as follows

$$\begin{Bmatrix} \epsilon^o \\ \kappa \end{Bmatrix} = (\mathcal{D}H)\{q\} \quad (3.25)$$

Eq. 3.25 represents an expression for the strains and curvatures in the plate in terms of the modal displacements. The derivative mode shape matrix $\mathcal{D}H$ has dimensions of 6 by r , and when multiplied by the generalized coordinate vector (r by 1), the 6 by 1 strain and curvature vector is recovered.

The above expression for the strains and curvatures (Eq. 3.25) can be substituted directly into the strain energy equation (Eq. 2.47) in order to obtain the modal strain energy equation

$$U = \frac{1}{2} \int \int_A \{(\mathcal{D}H)q\}^T \begin{bmatrix} A & B \\ B & D \end{bmatrix} \{(\mathcal{D}H)q\} d(A) - \int \int_A \{N^T_\Lambda M^T_\Lambda\} \{(\mathcal{D}H)q\} d(A) \quad (3.26)$$

This energy relation can be rewritten with the order of the matrixes in the second term reversed and the generalized coordinate vector q taken outside the integral. This yields

$$U = \frac{1}{2} q^T \left[\int \int_A (\mathcal{D}H)^T \begin{bmatrix} A & B \\ B & D \end{bmatrix} (\mathcal{D}H) d(A) \right] q - \left[\int \int_A (\mathcal{D}H)^T \begin{Bmatrix} N_\Lambda \\ M_\Lambda \end{Bmatrix} d(A) \right] q \quad (3.27)$$

The above manipulations may be affected, since the order of multiplication is immaterial for matrixes which produce a scalar quantity, and the generalized coordinate vector is independent of the integration. Finally, the energy equation can be written

$$U = \frac{1}{2} \mathbf{q}^T \mathbf{K} \mathbf{q} - \mathbf{Q}_A \mathbf{q} \quad (3.28)$$

$$\mathbf{K} = \int_A \int (\mathcal{D}\mathbf{H})^T \begin{bmatrix} \mathbf{A} & \mathbf{B} \\ \mathbf{B} & \mathbf{D} \end{bmatrix} (\mathcal{D}\mathbf{H}) d(A)$$

$$\mathbf{Q}_A = \int_A \int (\mathcal{D}\mathbf{H})^T \begin{Bmatrix} \mathbf{N}_A \\ \mathbf{M}_A \end{Bmatrix} d(A)$$

In the energy expression above \mathbf{K} is the usual r by r modal stiffness matrix, and \mathbf{Q}_A can be described as the r by 1 modal actuation strain forcing matrix since it represents the modal forces and moments which develop from the actuation strains.

In a static analysis, Lagrange's equations of motion reduce to

$$\frac{\partial U}{\partial q_i} = Q_k \quad (3.29)$$

where Q_i is the modal external forcing matrix which is non-zero when true externally applied forces or moments are present, and is equal to the integral of the applied forces and moments over each mode. Substituting the energy expression in the form of Eq. 3.28 into Lagrange's equations (Eq. 3.29) yields

$$\mathbf{K} \mathbf{q} = \mathbf{Q}_A + \mathbf{Q}_k \quad (3.30)$$

Eq. 3.30 is the governing equation for the modal amplitudes and represents the complete solution for any actuator/substrate system. Once the modal amplitudes are known, the strains and curvatures can be found directly from Eq. 3.25. All that remains to be done in order to obtain a solution for a particular actuator/substrate system is to choose a set of assumed mode shapes.

Assumed Mode Selection

The key step to the solution of the Ritz equations is the selection of the assumed mode shapes. This is not a trivial procedure, and requires careful study of the physical nature of each system. The mode shapes must match the geometric, or displacement, boundary conditions, and some insight into the behavior of the system is required to find mode shapes which accurately describe the system. In addition, it is desirable to meet the above requirements with the smallest possible number of, and the most basic mode shapes possible, to keep the problem manageable (in terms of understanding the physics, as well as minimizing the computation). The assumed modes for a free-free, free-free, and a cantilevered, free-free induced strain plate actuator system are presented below.

For a system which is totally unconstrained and has no externally applied forces or moments, the strain and curvature distributions will be constant along the length and width of the plate when actuated statically in extension or bending. The mode shapes chosen are displayed in Fig. 3.3. The four in-plane modes represent the normal extension and shear strain expected in such a plate, and have no functional dependence on the longitudinal or transverse plate dimensions. Likewise, the three out-of-plane modes are those of constant plate curvatures. These modes represent longitudinal bending, transverse bending, and twist, and have no functional dependence on the plate length or width as well.

The mode shapes for a cantilever plate system are shown in Fig. 3.4. The difference between these mode shapes and those of the unconstrained plate reflect the difference in the geometric boundary conditions. That is, the deflections and the out-of-plane slopes must be zero at the cantilevered edge. Strictly meeting these conditions would require complicated functions, however a few simple mode shapes can be found which adequately describe the system and approximate the conditions at the boundary. It will be shown in Chapters 5 and 6 that the simple mode shapes chosen, which are described in detail below, provide for accurate solutions.

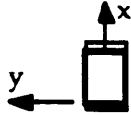
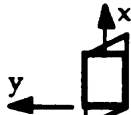
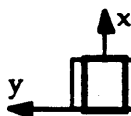

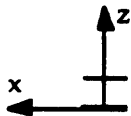
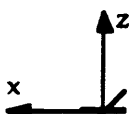
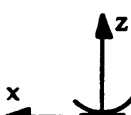
Mode	Deflection	Function	Shape
<i>In-Plane Modes</i>			
1	Long. Extension	$u = x/L$	
2	Long. Shear	$u = y/C$	
3	Trans. Extension	$v = y/C$	
4	Trans. Shear	$v = x/L$	
<i>Out-Of-Plane Modes</i>			
5	Long. Bending	$w = (x/L)^2$	
6	Twist	$w = xy/LC$	
7	Trans. Bending	$w = (y/C)^2$	

Figure 3.3 Assumed mode shapes of a free plate actuator/substrate system.

Referring again to Fig. 3.4, the clamped boundary condition has been enforced for the longitudinal in-plane modes to the extent that displacements are constrained at the fixed edge. The same normal in-plane strain in the longitudinal x direction (mode 1), assumed in the free case, satisfies the clamped condition, while the longitudinal component of the shear strain (mode 2) can be approximated as a linear function in x such that the u displacement goes to zero at the clamped edge. The transverse y component of the normal strain (mode 3) is unconstrained over the majority of the plate,

but drops off to zero at the clamped edge. A higher order function would be required to capture the rapid decrease in normal strain near the fixed edge, but to first order this mode can be approximated by the same mode shape as in the unconstrained case, a uniform strain in y . This is approximately correct since extension in the transverse direction is actually unconstrained (not effected by the clamped edge) over most of the length of the plate. The transverse component of the shear strain (mode 4) is unaffected by the cantilever boundary condition.

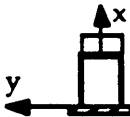

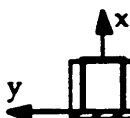

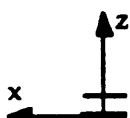


Mode	Deflection	Function	Shape
<i>In-Plane Modes</i>			
1	Long. Extension	$u = x/L$	
2	Long. Shear	$u = xy/LC$	
3	Trans. Extension	$v = y/C$	
4	Trans. Shear	$v = x/L$	
<i>Out-Of-Plane Modes</i>			
5	Long. Bending	$w = (x/L)^2$	
6	Twist	$w = xy/LC$	
7	Trans. Bending	$w = (x/L)(y/C)^2$	

Figure 3.4 Assumed mode shapes of a cantilever plate actuator/substrate system.

The four modes presented above account for the complete distribution of in-plane strain. The out-of-plane strains, which arise due to plate bending and twisting are now considered. The boundary condition will be rigorously enforced so that the out-of-plane deflection w is zero at the fixed edge. The slope boundary condition will be enforced for longitudinal bending, but not for twist or transverse bending. The distribution of longitudinal bending (mode 5) also can be approximated as being unaffected by the cantilevered boundary condition, so long as the displacement w and slope $\partial w/\partial x$ are zero at the clamped end. In contrast, the twist deformation (mode 6) and transverse bending (mode 7) are significantly effected by the fixed edge. These modes can be approximated by a linear function in x such that displacements are zero at the clamped edge and a maximum at the free end. This approximation is very accurate for the twisting mode, with only slight disagreement from the exact case due to the non-zero slope at the cantilevered end. The transverse bending mode would, like the transverse normal strain mode, require a higher order function to model exactly, but can also be approximated by assuming the transverse curvature varies linearly in the x direction.

The mode shapes chosen above were intended to provide a first order estimate of the problem. But the actual mode shapes measured turned out to be described quite accurately by the modes assumed above. Consequently, these modes were used in the analytical determination of the strains, curvatures, and deflections presented in Chapters 5 and 6.

Simplifications for Design

The mode shapes chosen above are all needed to accurately predict the strains and curvatures of induced strain actuator/substrate system with the boundary conditions specified. As can be seen upon examination of Eq. 3.30, solving for the static modal amplitudes requires the inversion of a 7 by 7 element matrix. This inversion can be easily performed by a digital computer, but cannot be found algebraically in general. Solving for the modal amplitudes in closed form is desirable for the purpose of designing an actuator system to induce specific desired strains or deformations. Also much insight can be gained and important design parameters are revealed by such an explicit solution.

It is possible to obtain closed form solutions by reducing the assumed modes to some minimal number. Enough modes must be retained to provide a rough approximation of the mode of actuation (extension or bending) and the resulting deformation. For most practical systems the minimum number of assumed modes was found to be three; the modes are longitudinal extension x , longitudinal x bending, and twist. Using only these modes is equivalent to assuming that the actuator/substrate system is rigid in transverse extension and transverse bending, and the net shear strain in the plate is zero. Essentially, these three assumed modes reduce the system model to that of a beam which extends, bends, and twists. Solutions for the free-free, free-free system are developed below.

Explicit algebraic solution can now be easily found since the order of the system (of equations) has been reduced from 7 by 7 to 3 by 3 as a result of the assumptions stated above. After inserting modes 1 (extension), 5 (longitudinal bending), and 6 (twist), displayed in Fig. 3.3, into the modal strain energy equations (Eq. 3.28), and performing the necessary integrations, the modal stiffness matrix \mathbf{K} and the modal actuation strain forcing vector \mathbf{Q}_A are found to be

$$\mathbf{K} = \begin{bmatrix} A_{11} & -2\frac{1}{L}B_{11} & -2\frac{1}{C}B_{16} \\ -2\frac{1}{L}B_{11} & 4\frac{1}{L^2}D_{11} & 4\frac{1}{CL}D_{16} \\ -2\frac{1}{C}B_{16} & 4\frac{1}{CL}D_{16} & 4\frac{1}{C^2}D_{66} \end{bmatrix}$$

$$\mathbf{Q}_A = \begin{bmatrix} (N_A)_x L \\ 2(M_A)_x \\ 0 \end{bmatrix} \quad (3.31)$$

where L and C are the longitudinal and transverse plate dimensions respectively, and the stiffness and forcing elements are defined in section 2.3. The modal stiffness matrix is symmetric as expected and is fully populated in the general case. The rows of the modal induced strain forcing vector correspond to extensional strain, and bending and twist curvature. The twist forcing term, which is proportional to the actuation shear strain has been set to zero, since most induced strain actuators are incapable of producing any shear actuation strain. This point is discussed further in Chapter 4. The

generalized coordinate (modal amplitude) vector \mathbf{q} which pertains to the above stiffness matrix and forcing vector is defined as follows

$$\mathbf{q} = \begin{Bmatrix} q_1: \text{extension} \\ q_5: \text{bending} \\ q_6: \text{twist} \end{Bmatrix}$$

These modal amplitudes can be solved for using Eq. 3.30.

The modal stiffness matrix can now be further simplified for the purpose of obtaining design parameters. The magnitude of the extensional and bending modal amplitudes can be found by assuming the system has no stiffness cross coupling terms ($B_{11}=B_{16}=D_{16}=0$). This assumption uncouples the equations and the solution is found by inspection of Eq. 3.31.

$$\begin{aligned} q_1 &= L \frac{(N_\Lambda)_x}{A_{11}} \\ q_6 &= \frac{1}{2} L^2 \frac{(M_\Lambda)_x}{D_{11}} \end{aligned} \quad (3.32)$$

It should be noted that in these equations the stiffness terms are made up of stiffness contributions from the entire system (both actuator and substrate), while the forcing terms are proportional to only the actuator stiffness and the actuation strain. The extensional strain and bending curvature can be found directly from the modal amplitudes (Eq. 3.32) and Eq. 3.25

$$\begin{aligned} \epsilon_x &= \frac{(N_\Lambda)_x}{A_{11}} \\ \kappa_{xx} &= \frac{(M_\Lambda)_x}{D_{11}} \end{aligned} \quad (3.33)$$

In the absence of B_{16} , D_{16} , and Λ_{xy} , there is no twist induced in the system. The magnitude of the modal actuation strain forcing terms, N_Λ and M_Λ , depend on the actuation strain and the actuator stiffness. Therefore the strains and curvatures obtained from Eq. 3.33 are directly proportional to the actuation strain as was found previously. In addition, the amount of strain

and curvature induced in the system will depend on the same relative stiffness parameter ψ which was found to be an important parameter for determining the transfer of actuation strain to induced strain.

The role of the relative stiffness parameter can be clearly illustrated by manipulation of the strain relation in Eq. 3.33. Recognizing that

$$\begin{aligned} N_A &= (A_s)_{11} \Lambda_x \\ A_{11} &= (A_s + A_s)_{11} \\ \psi &= \left(\frac{A_s}{A_s} \right)_{11} \end{aligned}$$

it can be show that the extensional strain in Eq. 3.33 reduces to the familiar form

$$\epsilon_x = \frac{\alpha}{\alpha + \psi} \Lambda_x \quad (3.34)$$

where once again alpha is the geometric constant found for extensional actuation ($\alpha = 2$). It is not surprising that the strain relation reduces to Eq. 3.34 since the assumptions made above have effectively made the system being analyzed that of a one dimension bar in extension. Additionally, the mode shape assumed which corresponds to extensional strain is identical to the extensional strain assumed in the development of the "pin" force plate and consistent plate model. Hence all solutions presented yield the same answer to the extensionally actuated bar problem.

For the same system actuated in bending, the curvature relation in Eq. 3.33 can be shown, in a manner similar to the extensional case, to reduce to

$$\kappa_{xx} = \frac{2}{t_s} \left[\frac{1}{T} + 1 \right] \frac{\alpha}{\alpha K + \psi} \Lambda_x \quad (3.35)$$

where T and K are defined as in Eq. 3.19 and the geometric constant is now equal to 6. Notice that Eq. 3.35 is of the same form as the exact solution found for the consistent plate model (Eq. 3.19). This result was also expected since the strain energy relations were derived using the consistent plate model in-plane deformation assumptions, the bending mode shape chosen was that of

constant curvature, and the same isotropic actuator configuration assumptions were imposed in both instances.

An estimate of the magnitude of twist deformation which can be obtained from an induced strain actuation can be found in a similar manner. Twist can be induced by actuation either in the bending or the extensional mode. Each case will be examined and a comparison of the two methods will be made.

Twist curvature is induced as a result of bending actuation and the bending/twist coupling stiffness D_{16} of the system. The amount of twist curvature which results from this actuation mode can be found by setting the extension/bending B_{11} and extension/twist B_{16} coupling terms to zero. Elimination of these coupling terms reduces the modal stiffness matrix to

$$\mathbf{K} = \begin{bmatrix} A_{11} & 0 & 0 \\ 0 & 4\frac{1}{L^2}D_{11} & 4\frac{1}{CL}D_{16} \\ 0 & 4\frac{1}{CL}D_{16} & 4\frac{1}{C^2}D_{66} \end{bmatrix} \quad (3.36)$$

Inverting the matrix and solving for the modal twist amplitude gives

$$q_7 = -\frac{1}{2}CL \left[\frac{D_{16}}{D_{11}D_{66} - D_{16}^2} \right] (M_A)_x \quad (3.37)$$

from which the twist curvature can be obtained directly as above

$$\kappa_{xy} = -\frac{1}{2} \left[\frac{D_{16}}{D_{11}D_{66} - D_{16}^2} \right] (M_A)_x \quad (3.38)$$

Eq. 3.38 shows that the twist curvature is proportional to the actuation strain, which is an inherent part of the modal actuation strain actuator forcing term, and the system stiffness elements. A system which has a high degree of bending/twisting coupling will naturally produce large amounts of twist curvature, while a large bending or torsional stiffness will decrease the twist induced. It is evident that the twist curvature depends on the ratio of the coupling stiffness D_{16} to the bending stiffness D_{11} and the torsional stiffness

D_{66} , therefore it is convenient to define a bending/twist coupling parameter ψ_D as

$$\psi_D = \frac{D_{16}}{\sqrt{D_{11}D_{66}}} \quad (3.39)$$

This non-dimensional coupling parameter can be used to compare the relative amount of bending/twist coupling in various systems for the purpose of design or analysis. The bending/twist coupling parameter ψ_D is especially important for the design of systems subject to external out-of-plane loads such as in aeroelastic applications.

Alternatively, twist curvature can be induced from actuation in the extensional mode by utilizing the extension/twist coupling B_{16} term. An approximation of the effectiveness of obtaining twist in this manner can be found by setting the extension/bending B_{11} and the bending/twist D_{16} stiffness terms to zero. The resulting modal stiffness matrix becomes

$$\mathbf{K} = \begin{bmatrix} A_{11} & 0 & -2\frac{1}{c}B_{16} \\ 0 & 4\frac{1}{L^2}D_{11} & 0 \\ -2\frac{1}{c}B_{16} & 0 & 4\frac{1}{c^2}D_{66} \end{bmatrix} \quad (3.40)$$

The twist curvature can be solved for as above, and is

$$\kappa_{xy} = \frac{1}{2} \left[\frac{B_{16}}{A_{11}D_{66} - B_{16}^2} \right] (N_A)_x \quad (3.41)$$

Once again, it is found that the curvature depends on the actuation strain, the actuator stiffness, and some relation between the various system stiffness terms. In this mode of actuation the twist depends on the relationship between the extension/twist stiffness B_{16} , the extensional stiffness A_{11} , and the torsional stiffness D_{66} . This relationship can be characterized by an extension/twist coupling parameter ψ_B as follows

$$\psi_B = \frac{B_{16}}{\sqrt{A_{11}D_{66}}} \quad (3.42)$$

The extension/twist coupling parameter, like the bending/twist parameter, is a relative measure of the system extension/twist stiffness coupling, which can also be used for design and analysis. Besides serving as an indicator of the twist magnitude induced by extensional actuation, the extension/twist coupling parameter plays an important role in the design of systems with externally applied in-plane loads.

It should be pointed out that designing an induced strain actuator system which utilized the extension/twist coupling parameter ψ_B is a potentially desirable alternative to designing one which takes advantage of the bending/twist coupling parameter ψ_D . In many applications, the out-of-plane applied forces are significantly higher than the in-plane forces. It is often desirable to use bending/twist coupling to tailor a plate to utilize the out-of-plane forces to cause desirable deformations. If bending/twist coupling was used for tailoring, the combined actuation-tailoring problem would become over constrained. An obvious example of the above, would be the problem of using induced strain actuation to control an aeroelastic structure which has already been passively tailored using bending/twist coupling.

An additional benefit of utilizing extension/twist coupling can be found by careful examination of the extension/twist coupling parameter ψ_B . All of the stiffness elements of the bending/twist parameter ψ_D are proportional to the 3rd power of the plate thickness. In contrast, the numerator of the extension/twist coupling parameter is proportional to the plate thickness squared and one term in the denominator goes like the plate thickness while the other is proportional to the 3rd power of the plate thickness. This variation in the dependence of the stiffness elements in the extension/twist coupling parameter on thickness gives the designer of a stiffness coupled actuator/substrate system added flexibility.

In the above analysis, many simplifications have been made in order to reveal the stiffness parameters ψ_D and ψ_B , and the trends described. For example, the actual strains and curvatures induced in a real system are usually not constant, plates do not behave like beams (unless the plate is much longer than wide), and individual stiffness terms cannot be chosen arbitrarily. Poisson's effect causes transverse displacements, and the isotropic nature of most induced strain actuators requires that actuation is always two

dimensional. The elements of the stiffness matrixes (**A**, **B**, and **D**) are functions of the ply orientation, ply thickness, and laminate lay-up sequence. It may not be possible to build a laminate which has certain specified stiffness elements. However despite these drawbacks, the effects described by the stiffness parameters underlie the response of the structure. Thus, the parameters found and the implications drawn from the three mode analysis provide the designer of induced strain actuator/substrate systems with needed insight and solid design guidelines.

3.4 Conclusions

Solutions to the analytic models were presented in this chapter. Exact closed form solutions were found for particular system configurations. It was found that it is possible to obtain exact solutions for systems which are unconstrained. This is because no external loads are created by boundary conditions which are the free-free, free-free. These exact solutions can be expressed in an elegant explicit form for systems which are purely isotropic. The isotropic solutions revealed the parameters which are important for the transfer of actuation strains to induced strains and curvatures in the system. These parameters were found to be the actuation strain, the relative stiffness parameter ψ , and the geometric configuration of the system.

It was also found that the magnitude of the curvature induced by strain actuation is inversely proportional to the plate thickness. In addition, the solutions for isotropic plates showed that Poisson's effect, which normally plays an important role in plate problems, drops out of the equations. Because of the absence of any effects from Poisson's ratio, the equations uncouple and reduce to those found for one dimensional structures.

The analysis of anisotropic actuator/substrate systems was found to be more complex. The algebra required to obtain explicit exact solutions was prohibitive for all but the most simple cases, thus approximate solutions were developed. It was also found necessary to employ approximate solution techniques for the analysis of systems with boundary conditions other than the unconstrained case. Therefore, a detailed Ritz approximate solution was

developed, and the selection of the appropriate assumed mode shapes for particular systems were discussed. Finally, additional approximations were made which revealed the parameters important for inducing particular strains and curvatures in plate actuator systems. Specifically, the important parameters for inducing twist were found. These parameters were the bending/twist coupling parameter ψ_D and the extension/twist coupling parameter ψ_B .

The design parameters found from the analysis in this chapter were used to design the test articles constructed in this investigation. Likewise, the solutions presented were used to predict the deformations of these test articles. As will be shown, excellent correlation was found between the theoretical predictions and the experimental results.

CHAPTER 4

PIEZOCERAMIC INDUCED STRAIN ACTUATORS

4.1 Introduction

The analytic models developed in Chapter 2, and the solutions discussed in Chapter 3 are generally applicable to any type of induced strain actuator, in the sense that they apply to any method of induced strain actuation, whether it is due to thermal expansion, piezoelectricity, electrostriction, a material phase change, or moisture absorption. Regardless of the mechanism of induced strain actuation, the effects of the actuator can be incorporated into the models and solutions via the actuation strain term. However, the magnitude of the actuation strain must be known in order to obtain useful results, and the actuation strain will depend on various factors, depending on the type of induced strain actuator. In the experiments performed in this research effort, piezoceramic induced strain actuators were used. Therefore, further discussion of these actuators, and their actuation strains, is merited, and is the topic of this chapter.

Compared to servo-mechanisms, piezoceramics, or piezoelectric ceramics, make excellent induced strain actuators because of their simplicity. Piezoceramics are light weight and small in size, and can easily be incorporated into actuator systems through surface bonding or embedding techniques. Actuation strains can be commanded which are proportional to the applied electrical field and the mechanical/electrical coupling coefficient of the ceramic. Ideally the relationship between applied field and actuation strain is linear, and expressed by a single mechanical/electrical coupling coefficient. However, this mechanical/electrical coupling coefficient is not, in fact, a constant. Thus, the output (actuation strain) is not linearly proportional to the effort (applied electric field). It has been found in this work and by others [Aronov, 1980] that the coupling coefficient has a non-linear dependence on strain. In addition, experimental results indicate that piezoceramics exhibit limited anisotropy, creep, and hysteresis.

The behavior of piezoceramics, and the implications of this behavior for modelling the actuation strains, and obtaining solutions for induced strain actuator/substrate systems will be discussed. In section 4.2 a piezoceramic plate model will be developed for predicting actuation strains, and the non-linear behavior of piezoceramics will be discussed. Experimental results will also be presented.

As will be seen, the accurate prediction of actuation strains requires that second order non-linear terms be included in the calculation of the mechanical/electrical coupling coefficient. It will be shown that this coupling coefficient is a function of the induced strains in the system. Thus, an iterative solution procedure is required to solve the relations presented in Chapter 3 for the induced strains and curvatures. This solution procedure will be outlined and discussed in section 4.3.

4.2 Piezoceramic Actuation Strain Model

It is the purpose of this section to briefly describe the nature of piezoceramics with regard to their use as induced strain actuators, and to develop a model for predicting the actuation strains produced by piezoceramic plate actuators. A linear isotropic model will be described first, followed by models which incorporate the important non-linear effects of piezoceramics. The effects of limited anisotropy, creep, hysteresis, and a non-linear coupling coefficient will be discussed, and the relative importance of each effect will be evaluated.

For a plate actuator, the boundary conditions corresponding to the totally unconstrained state are free-free, free-free, and the actuation strains for a piezoceramic poled through the thickness are given by

$$\begin{bmatrix} \Lambda_x \\ \Lambda_y \\ \Lambda_z \\ \Lambda_{xz} \\ \Lambda_{yz} \\ \Lambda_{xy} \end{bmatrix} = \begin{bmatrix} 0 & 0 & d_{13} \\ 0 & 0 & d_{23} \\ 0 & 0 & d_{33} \\ 0 & d_{32} & 0 \\ d_{31} & 0 & 0 \\ 0 & 0 & 0 \end{bmatrix} \begin{bmatrix} \mathcal{E}_x \\ \mathcal{E}_y \\ \mathcal{E}_z \end{bmatrix} \quad (4.1)$$

where Λ is the actuation strain vector, d is the mechanical/electrical coupling coefficient matrix, and \mathcal{E} is the applied electrical field vector. Contracted notation has been used for the coupling coefficient tensor in Eq. 4.1.

A piezoceramic plate which has been poled through the thickness is shown in Fig. 4.1. The poling field, or poling direction, has been assumed to be positive along the positive z axis, and the actuation strains, which result from an applied electric field of opposite sense, are illustrated. An applied electric field of opposite sense from the poling direction is referred to as "against the field", while a field with the same sense as the poling direction is designated as "with the field." Electric fields which are applied against the poling field create extensional in-plane actuation strains, while fields applied with the poling field produce compressive actuation strains. The fields are applied to the piezoceramic with the aid of plated metallic electrodes which are extremely thin, less than 0.01 mm (0.05 mils) thick, compared to the nominal actuator thickness of 0.25 mm (10 mils). These electrodes are plated onto the upper and lower surfaces of the piezoceramic.

For a thin piezoceramic plate actuator as described above, the equation relating the actuation strain to the applied fields (Eq. 4.1) reduces to

$$\begin{bmatrix} \Lambda_x \\ \Lambda_y \\ \Lambda_{xy} \end{bmatrix} = \begin{bmatrix} 0 & 0 & d_{13} \\ 0 & 0 & d_{23} \\ 0 & 0 & 0 \end{bmatrix} \begin{bmatrix} 0 \\ 0 \\ \mathcal{E}_z \end{bmatrix} \quad (4.2)$$

where the actuation strains Λ are now the same actuation strains defined in Chapter 2 and used in Chapter 3. In Eq. 4.2 the same thin plate assumptions discussed in section 2.3 have been imposed on the piezoceramic plate actuator. The thin plate approximation is quite valid for the piezoceramics used in this research since the longitudinal x and transverse y dimensions were roughly 200 times the plate thickness as shown in Fig. 4.1. The results of assuming the actuator to be a thin plate poled through the thickness are a d matrix which has non-zero terms only in the column corresponding to the poling direction, and no shear strain/electric field coupling term, as seen in Eq. 4.2. Thus, no actuation shear strain will be produced by a piezoceramic plate actuator. This is the reason that the actuation shear strain was set to zero in Eqs. 3.1 and 3.7.

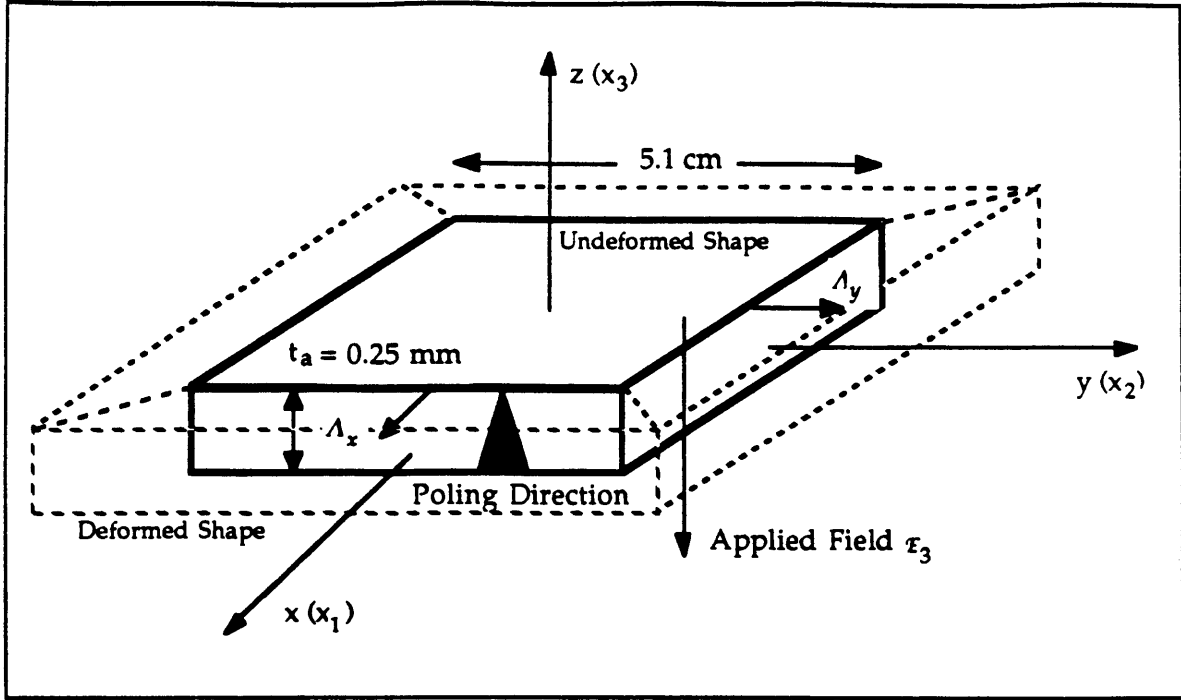


Figure 4.1 Piezoceramic plate poled through the thickness.

Assuming that the in-plane properties of the crystal are isotropic, the coupling coefficient matrix reduces to a single independent coefficient, d_{13} , which the manufacturers of piezoceramics commonly refer to as d_{31} . Thus, the equation relating the applied field to the actuation strains becomes

$$\Lambda = \begin{bmatrix} \Lambda \\ \Lambda \\ 0 \end{bmatrix} = \begin{bmatrix} 1 \\ 1 \\ 0 \end{bmatrix} d_{31} \mathcal{E}_z \quad (4.3)$$

where d_{31} is defined simply as the change in strain per change in applied field beginning at the zero applied field state, and \mathcal{E} is the field applied through the plate actuator thickness either with or against the field. Since there is only one independent coupling coefficient, Eq. 4.4 can be written as

$$\Lambda = \begin{bmatrix} \Lambda \\ \Lambda \\ 0 \end{bmatrix} = \begin{bmatrix} 1 \\ 1 \\ 0 \end{bmatrix} d \mathcal{E}_z \quad (4.4)$$

Eq. 4.4 is the linear isotropic relation for the actuation strains created in an unconstrained piezoceramic plate actuator. This equation shows that the

actuation strains are directly proportional the mechanical/electrical coupling coefficient d and the applied electrical field \mathcal{E} . Hence, the maximum value of the actuation strains obtainable will depend on the magnitude of the coupling coefficient and the maximum electrical field which can be sustained by the piezoceramic. This maximum field is known as the coercive field, and is the electric field which will depole the piezoceramic if applied against the poling field. Fields larger than the coercive field can be applied in the direction of the poling field.

Three different piezoceramic plate actuators were tested to determine which produced the largest actuation strains. The piezoceramics tested were a Piezoelectric Products G-1195, a Piezoelectric Products G-1278 and a Vernitron PZT-5H. Each had configurations and plate dimensions approximately equivalent to the piezoceramic actuator shown in Fig. 4.1. A BLH FAER-06B-35 S13 ET strain gage rosette was bonded to the surface of each piezoceramic, and the results of these tests are displayed in Fig. 4.2. Notice the dashed lines which denote the coercive field for fields applied against the poling field. There are no coercive fields for fields applied with the poling field. Therefore, when driving piezoceramic actuators with the poling field, the actuation strain is limited only by how much charge can be placed on the electrodes of the piezoceramic before arcing between the electrodes occurs. The coercive fields were found to range from 470 V/mm (12 V/mil) for the PZT-5H to 830 V/mm (21 V/mil) for the G-1195, and when excited with fields oriented in the poling direction, arcing occurred at about 1810 V/mm (46 V/mil).

The test results indicate that at low to medium applied fields the PZT-5H actuation strains were the highest. However, in the medium to high applied field (with the field) range the G-1275 piezoceramic actuation strains were higher than those created in the PZT-5H, and the actuation strains measured in the G-1195 actuator were found to be roughly equal to those created by the PZT-5H. In addition, the coercive field of the G-1195 piezoceramic was found to be significantly higher than the coercive field of the other two materials. Thus larger maximum strains were obtained from the G-1195 piezoceramic for applied fields against the poling direction. As a result of this experiment, the G-1195 piezoceramic was selected as the induced

strain actuator for the remainder of the experiments performed in this study. This piezoceramic was selected because inducing large strains and obtaining relatively large deflections from induced strain actuator/substrate systems was one of the goals of this research effort.

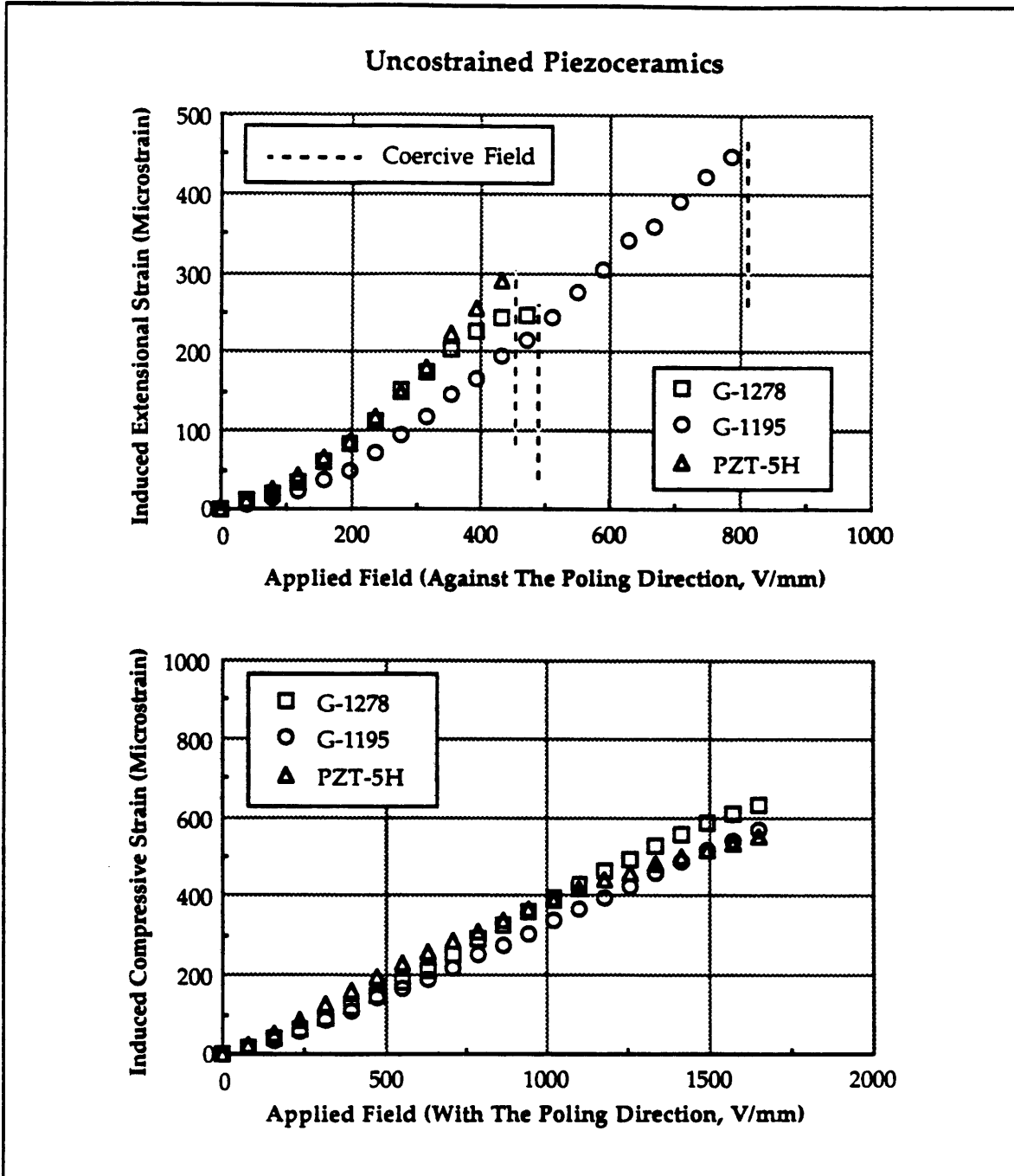


Figure 4.2 Maximum actuation strain data from several piezoceramic plate actuator test specimens.

Effects of Limited Orthotropy

Of course the isotropic linear actuation strain model developed above (Eq. 4.4) is an idealization. Actual piezoceramic actuators produce actuation strains which vary considerable between the longitudinal x and transverse y directions. Fig. 4.3 shows a plot of actuation strain versus applied field for a typical piezoceramic plate actuator. This figure clearly illustrates the orthotropic strains produced by piezoelectric actuators. The variation of the actuation strain in the longitudinal and transverse directions is about 18% of the average actuation strain value at 67% of the coercive field. In addition, the actuation strains produced by piezoceramics vary from actuator to actuator.

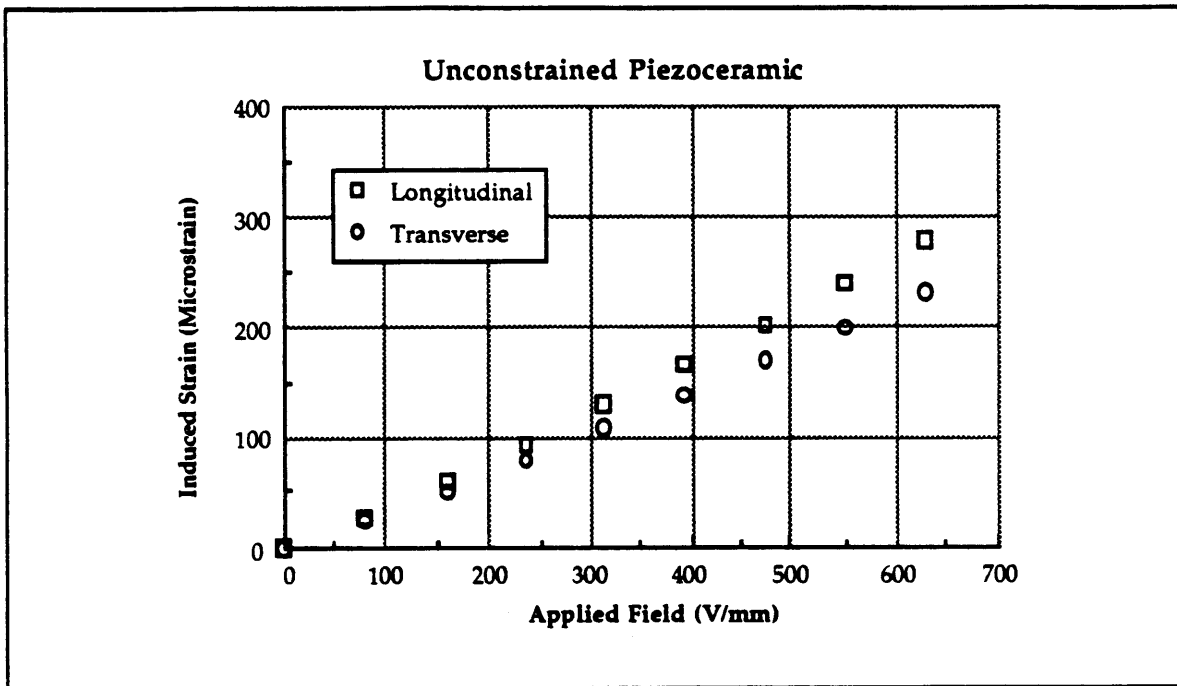


Figure 4.3 Plot of actuation strain in the longitudinal and transverse direction for an unconstrained piezoceramic.

This limited orthotropic nature, as well as the variation between piezoceramics, is thought to be due to the details of the manufacturing process, so its effects will not be modelled. Fortunately, these variations are significantly reduced when piezoceramics are constrained by elastic substrates, such as an aluminum plate. Test of the aluminum sandwich systems, described in Chapter 5, show that the strain variation in the longitudinal and

transverse directions is less than 5% of the average strain at 67% of the coercive field. Therefore, the effects of limited orthotropy will be ignored.

Effects of Creep and Hysteresis

Besides limited orthotropy, other effects cause the real piezoceramic behavior to deviate from the isotropic linear model. Two such effects are creep and hysteresis. The effects of creep on predicting the actuation strains are now discussed. In the piezoceramics tested, creep was clearly observed in the step response of strain to a step input of field. The time constant of the creep was found to be large (10 sec.) compared to the time constant of the electromechanical response itself. This later time constant is associated with the charging of the piezoceramic (which acts as a capacitor in steady state applications), and was found to be less than a millisecond. Therefore, in applications where the time constant is considerably shorter than 10 seconds or frequencies greater than 0.1 Hz the creep can be safely ignored. In addition, the magnitude of the strain associated with creep was observed to be a small portion (1-3 percent) of the nominal strain in free piezoceramics [Anderson, 1989], and piezoceramics bonded to constraining elastic substructures exhibited much less creep than in the unconstrained state. Therefore, although creep was observed, the magnitude of induced strain produced by creep was found to be sufficiently small in actuator systems so that its effects can be ignored even in long time scale applications.

Unlike the effects of creep, the hysteretic behavior of piezoceramic devices cannot be ignored. Fig. 4.4 shows typical hysteresis loops for an unconstrained piezoceramic plate with maximum applied fields of 30, 60, and 90% the coercive field. The strain values corresponding to zero applied field on the two sides of the 750 V/mm (19 V/mil) hysteresis loop differ by about 180 microstrain, roughly 60% of the maximum actuation strain. Because of hysteresis, the strain history of the piezoceramic must be known in order to produce consistent deformations, and to match the measured deformations to theoretical predictions. This can be accomplished by cycling the field applied to the piezoceramic from positive (against the poling direction) to negative several times before recording data. This cycling causes the loop to be centered symmetrically on true zero strain, and clearly establishes the position of the current field-strain state on the loop.

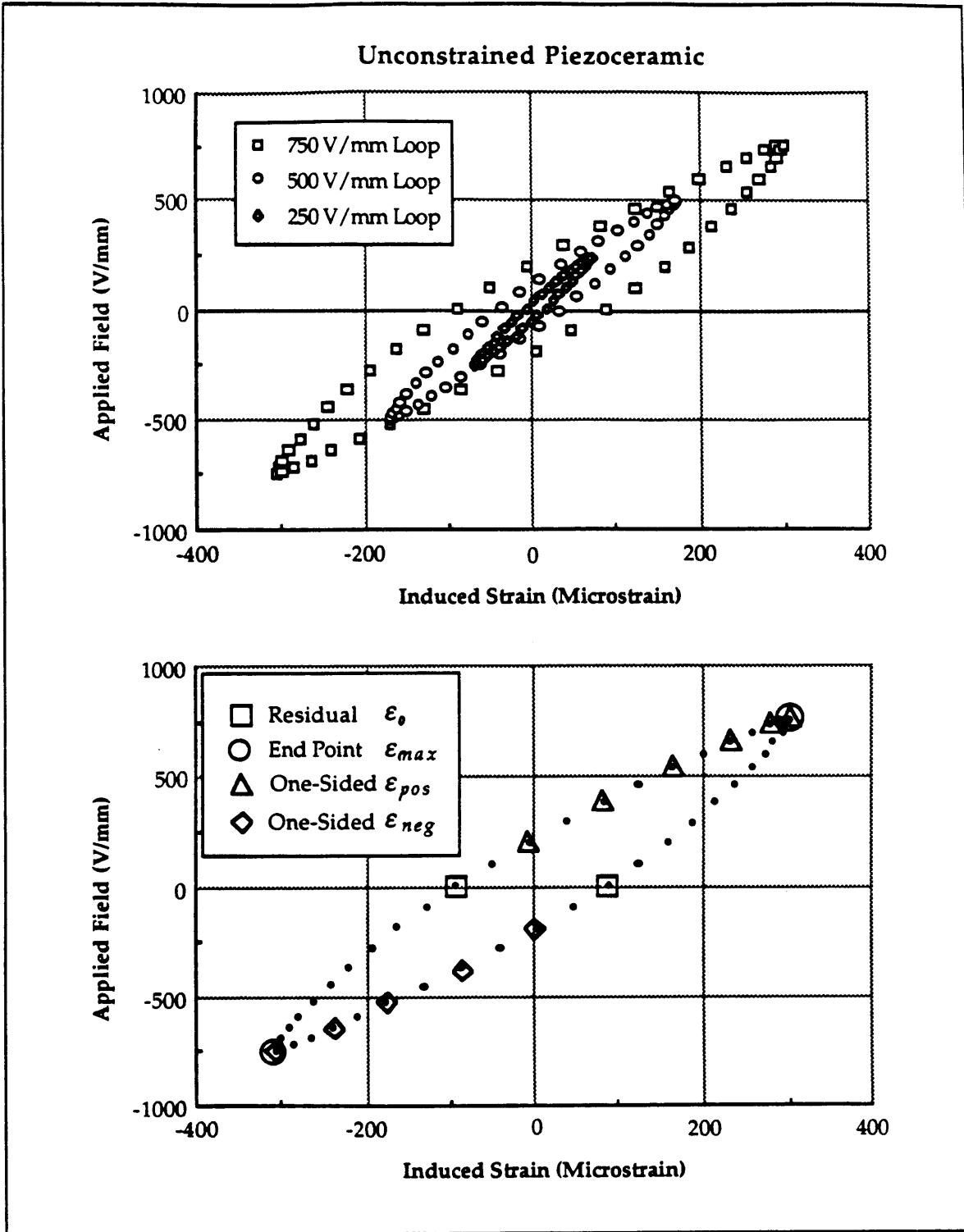


Figure 4.4 Applied field-induced strain hysteresis loops from an unconstrained piezoceramic plate actuator. Representative data points used in evaluating the mechanical/electrical coupling coefficient are indicated in the figure.

The hysteretic behavior of piezoceramics has important ramifications for the experimental determination of the mechanical/electrical coupling coefficient. Because of the complications of hysteresis, it is convenient to define two mechanical/electrical coupling coefficients: a one-sided secant coupling coefficient d^+ or d^- , and a symmetric or average secant coupling coefficient d^* . The one-sided coefficient is calculated based on the difference in strain values recorded from zero applied field (residual strain ϵ_0) to some applied field (one-sided strain ϵ^+ against the field or ϵ^- with the field) on the loop, while the average coupling coefficient is based on strain values at the maximum positive and negative applied field (average strain ϵ^*) on the loop. Representative data points used in evaluating each coefficient are indicated in Fig. 4.4, and these coefficients are defined by the following relations

$$d^+ = \frac{\epsilon^+}{\mathcal{E}} = \frac{\epsilon_{pos} - \epsilon_0}{\mathcal{E}} \quad \text{or} \quad d^- = \frac{\epsilon^-}{\mathcal{E}} = \frac{\epsilon_{neg} - \epsilon_0}{\mathcal{E}} \quad (4.5)$$

$$d^* = \frac{\epsilon^*}{\mathcal{E}} = \frac{(\epsilon_{pos})_{\max} - (\epsilon_{neg})_{\max}}{\mathcal{E}} \quad (4.6)$$

where ϵ_{pos} is the strain recorded when the field is applied against the poling field, ϵ_{neg} is the strain recorded when the field is applied with the poling field, and ϵ_0 is the residual strain. The residual strain is found by cycling the applied field from positive to negative several times, and returning to zero applied field.

With the above definitions (Eq. 4.5 and Eq. 4.6), these coupling coefficients can be found experimentally for any value of applied field. The one-sided coefficient is useful in predicting the static induced strains due to a step input of field. This coefficient defines the change in strain (ϵ^+ or ϵ^-) for incremental increases in applied field for a particular hysteresis loop, where each hysteresis loop is defined by the maximum value, $(\epsilon_{pos})_{\max}$ or $(\epsilon_{neg})_{\max}$ of applied field, or the end points of the loop. In Fig. 4.4, the strain values measured on the 750 V/mm (19 V/mil) loop, which can be used to compute the one-sided coefficients, are shown. The average coefficient is more suited to finding the amplitude of the dynamic induced strains. The average coefficient is found from the peak to peak change in strain (ϵ^*) due to a change in the maximum and minimum applied field. In calculating this

coefficient, end point data from several loops is used. Thus, the one-sided coefficient provides information for determining one side of the hysteresis loop for a particular maximum and minimum applied field, while the average coefficient provides end point data from several hysteresis loops. Since either definition can be used, the coefficient chosen will depend only on the application. In this study, the experiments performed were quasi-static, so the coupling coefficient was evaluated using the one-sided definition (Eq. 4.5).

Strain Dependence of the Mechanical/Electrical Coupling Coefficient

In the presentation above, it was found that the effects of limited orthotropy and creep can be ignored since the effects of these non-linearities were significantly reduced by the constraints of elastic substrates found in induced strain actuator/substrate systems. However, it has been found that the relationship between the piezoceramic actuation strain and the applied field is altered by such constraints. Specifically, the mechanical electrical coupling coefficient is effected by the constraining substrates. It has been found through experimentation performed in this study and by others [Aronov, 1980] that the coupling coefficient is dependent on the actual magnitude of the induced strain in the piezoceramic. The strain dependence of the coupling coefficient is discussed below.

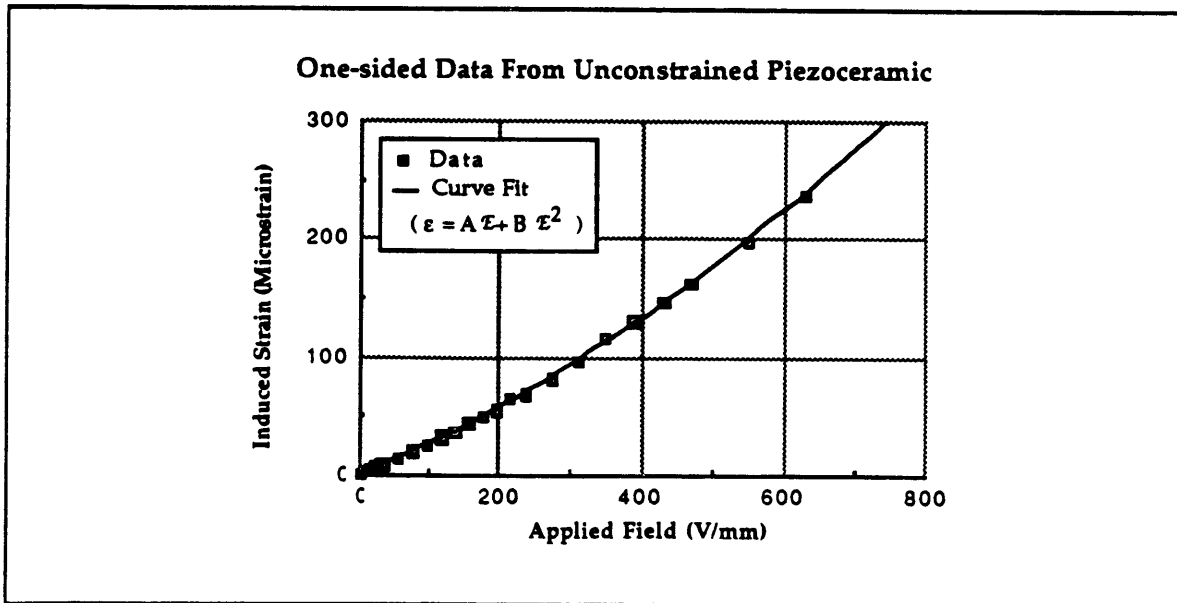


Figure 4.5 Plot of one-sided induced strain versus applied field of an unconstrained piezoceramic plate actuator.

Figure 4.5 displays the measured one-sided strain versus applied field for a typical unconstrained piezoceramic plate actuator from a 630 V/mm (16 V/mil) loop. The coupling coefficient is clearly not a constant, but it is impossible to determine from this data whether the magnitude of the coupling coefficient is a function of applied field \mathcal{E} or induced strain ϵ (which equals the actuation strain Λ in the unconstrained case).

To determine the functional dependence of the coupling coefficient an actuator/substrate system must be examined. The induced strains in such systems can be predicted by a relation in which the coupling coefficient is explicitly assumed to be either field or strain dependent

$$\text{or} \quad \epsilon = C \Lambda = C d_{31}(\mathcal{E}) \mathcal{E} \quad (4.7)$$

$$\epsilon = C \Lambda = C d_{31}(\epsilon) \mathcal{E} \quad (4.8)$$

where C is the compliance of the system, which is a function of the stiffness properties of the actuator and the substrate, and the geometry of deformation. For example, the compliance of a symmetric actuator/substrate system was found (Eq. 2.9) to be

$$C = \frac{\alpha}{\alpha + \psi} \quad (4.9)$$

Note that the strain in Eq. 4.8 is the induced strain which results from the actuation strains themselves and the forces and moments created at the boundaries, and is not dependent on any externally applied forces or moments (F_k or M_k).

The quantity on which the mechanical/electrical coupling coefficient depends can be determined by examining experimental results from simple actuator/substrate systems. The induced strains predicted in systems by a coupling parameter which is a function of applied field do not match experimental results. The poor correlation can be seen, in Fig. 4.6, from the plot of the induced strain versus applied field for the isotropic aluminum sandwich actuator specimen (discussed in chapter 5). The predictions based on a strain dependent coupling coefficient are also shown in Fig. 4.6. Notice how closely the theoretical prediction based on a coupling coefficient which is a function of induced strain, defined later in this section, matches the

experimental results shown in Fig. 4.6. It is evident that the coupling coefficient does not depend on field, but on induced strain. A method by which the strain dependent coupling coefficients are determined, and hence the actuation strains and induced strains are found, is discussed below.

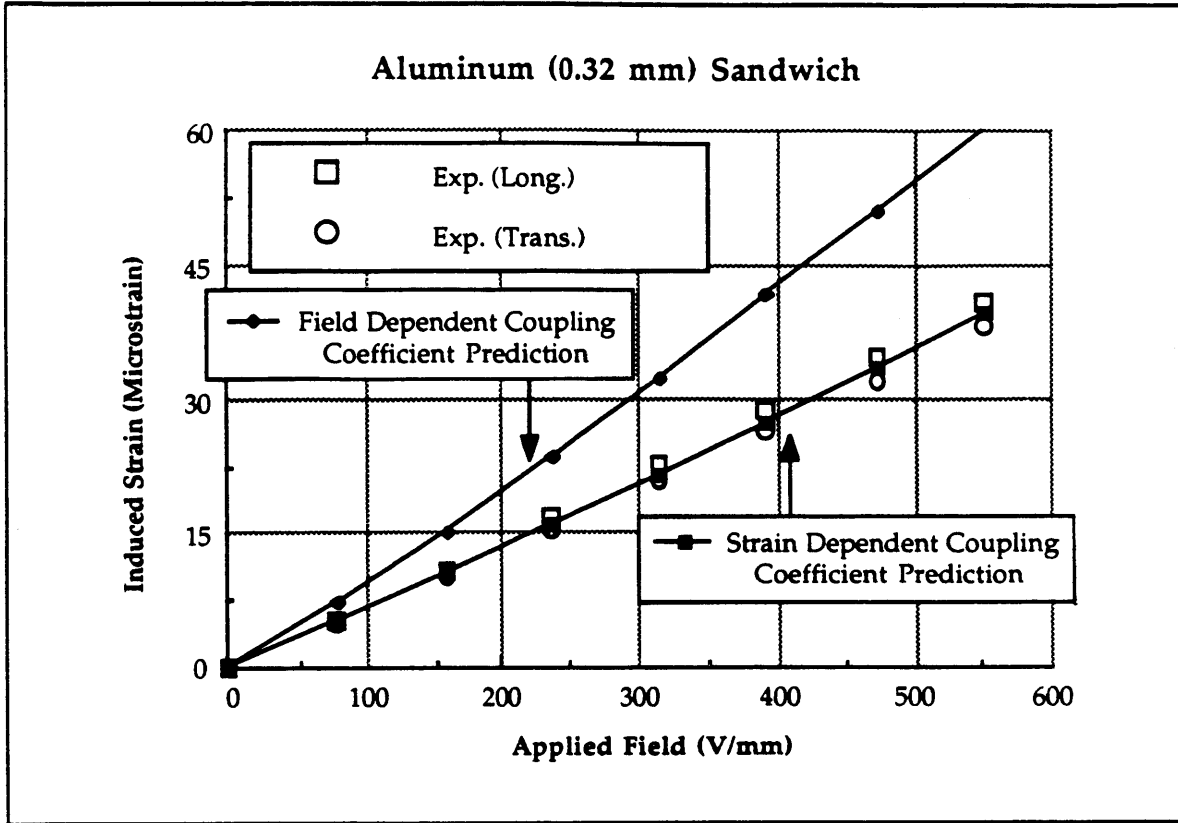


Figure 4.6 Plot of induced strain versus applied field for an aluminum sandwich system. Figure compares strains predicted with an assumed strain dependent and field dependent coupling coefficient.

The dependence of the mechanical/electrical coupling coefficient on induced strain necessitates the development of a new relationship for the actuation strains produced by an applied field. Because the substrates of actuator systems may be anisotropic, which could cause the induced strains to differ significantly in the longitudinal and transverse directions, the coupling coefficient will be different in the two directions. Hence, there will be two distinct values of the coupling coefficients, each a function of the induced strain. Thus, the relationship between the actuation strains and the applied field is given by

$$\Lambda = \begin{bmatrix} \Lambda_x \\ \Lambda_y \\ 0 \end{bmatrix} = \begin{bmatrix} d_{31}(\epsilon_x) \\ d_{32}(\epsilon_y) \\ 0 \end{bmatrix} \mathcal{E}_z \quad (4.10)$$

A semi-empirical method for predicting the coupling coefficient, which uses experimental data from unconstrained piezoceramic plate actuators, can be developed. Functional relationships for the coupling coefficients are found by fitting a curve through experimental strain versus field data of an unconstrained piezoceramic and then rearranging the equation in terms of the coupling coefficient as a function of strain. The induced strains, which are equal to the actuation strains for unconstrained actuators, as a function of field \mathcal{E} , can be approximated in each orthogonal direction by the following power series

$$\Lambda = \epsilon = A \mathcal{E} + B \mathcal{E}^2 \quad (4.11)$$

where the constants A and B are determined experimentally by fitting a curve through the strain versus field data shown in Fig. 4.5.

The coupling coefficient, either one-sided or average, can be written as

$$d = \frac{\epsilon}{\mathcal{E}} \quad (4.12)$$

where ϵ is the induced strain in the piezoceramic in each orthogonal direction. If d were non-linearly dependent on the field, Eq. 4.11 would be substituted into Eq. 4.12 to explicitly show the dependence on field as

$$d = A + B \mathcal{E} \quad (4.13)$$

However, as described above, this is not experimentally found to be the case. Instead the explicit dependence is on the induced strain ϵ . A relation showing the explicit dependence on ϵ can be found by substituting Eq. 4.12 into Eq. 4.11 for \mathcal{E} , and rearranging:

$$d^2 - A d - B \epsilon = 0 \quad (4.14)$$

Solving for coupling coefficient d yields a strain dependent expression for this coefficient in the following form

$$d(\epsilon) = \frac{A}{2} + \frac{A}{2} \sqrt{1 + \frac{4B\epsilon}{A^2}} \quad (4.15)$$

expanding the term under the radical using the first two terms of a binomial expansion yields

$$d(\epsilon) = A + \frac{B}{A}\epsilon \quad (4.16)$$

Finally, since the actuation strain is the coupling coefficient times the applied field as given in Eq. 4.10, an expression for the actuation strains is easily obtained

$$\begin{bmatrix} \Lambda_x \\ \Lambda_y \\ 0 \end{bmatrix} = \left\{ \begin{bmatrix} 1 \\ 1 \\ 0 \end{bmatrix} A + \begin{bmatrix} \epsilon_x \\ \epsilon_y \\ 0 \end{bmatrix} \frac{B}{A} \right\} \epsilon_z \quad (4.17)$$

Notice the difference between this expression for the actuation strains compared to the linear isotropic (Eq. 4.4) model. Eq. 4.17 shows the functional dependence of the actuation strains Λ on the induced strains ϵ , and how the experimentally determined constants from unconstrained actuators are used to predict the actuation strains created by piezoceramic actuators which are part of induced strain actuator systems.

4.3 Semi-Empirical Iterative Solution Procedure

Now that a relation for the accurate prediction of the coupling coefficients and the actuation strains has been found, it is desirable to combine this relation with the models developed for induced strain actuator/substrate systems in order to predict the induced strains found in actuator systems with piezoceramic actuators. The techniques developed below will be used to calculate theoretical predictions for comparison with experimental results obtained from the specimens constructed and tested (Chapters 5 and 6) in this research effort. Because the piezoceramic actuation strains are functions of the induced strains, solving for the induced strains in actuator/substrate systems requires solving coupled non-linear equations. In addition, the strain dependent coupling coefficient must be calculated in a

semi-empirical fashion. Therefore, an iterative solutions procedure, discussed below, will be used to find the induced strains in actuator systems.

The strains induced in an actuator system are, as found in Chapters 2 and 3, proportional to some compliance matrix C and the actuation strains

$$\begin{bmatrix} \varepsilon_x \\ \varepsilon_y \\ 0 \end{bmatrix} = C \left\{ \begin{bmatrix} 1 \\ 1 \\ 0 \end{bmatrix} A + \begin{bmatrix} \varepsilon_x \\ \varepsilon_y \\ 0 \end{bmatrix} \frac{B}{A} \right\} \varepsilon \quad (4.18)$$

Eq. 4.18 shows the effect of a strain dependent coupling coefficient. The equations governing the transfer of strain from the actuator to the substructure become non-linear. Because this equation has a non-linear dependence on strain and empirically determined coefficients, the strains and curvatures of the system must be obtained by an iterative procedure as follows: 1) assume the strain in the structure to be zero, 2) calculate an initial guess for the coupling coefficient and the actuation strains, 3) find the induced strains in the actuator system, 4) calculate the induced strains in the actuator, 5) calculate the new value for the coupling coefficient and the actuation strains, 6) find the new induced strains, 7) compare the new value calculated for the induced strains to the previous value. This procedure can be repeated until the solution converges.

Solving for the induced strains in actuator/substrate systems using this iterative procedure is relatively straight forward; however, care must be taken in evaluating the induce strains in the actuators. In the case of extensional actuation the induced strains are constant through the thickness of the actuator system, so the strains are given by Eq 2.30 for the "pin" force plate model or Eq. 2.40 (with M_A and M_k set to zero) for the consistent plate model. In the case of actuation in bending, the strains are constant through the thickness in the "pin" force plate model and are given by Eq. 2.38. However, the strains vary linearly through the thickness for the consistent plate model (Eq. 2.40). So, in order to estimate the magnitude of the induced strains in the actuators, the induced strains will be evaluated at the mid-thickness of the piezoceramic.

For anisotropic systems, the induced strains in the piezoceramic will be different in the longitudinal and transverse directions. Hence, there are two independent coupling coefficients as discussed above, and in order to reach a solution for systems which exhibits such anisotropic behavior, coupling coefficients which differ in the longitudinal $d_{31}(\epsilon_x)$ and transverse $d_{31}(\epsilon_y)$ directions must be accounted for. This difficulty can be handled by resolving the actuator strains into principle strains, evaluating the induced strains in each direction, and iterating simultaneously for the strains in both principle directions. The solution is reached when both strains have converged. Anisotropic induced strains may be created as a result of anisotropic system components or boundary conditions

Further consideration must be given to systems in which the induced strains are not constant along the length or width of the structure. This non-uniformity leads to the problem of where to evaluate the strains. It is quite possible to evaluate the strains at several different locations and iterate at each location. But, this added complexity is unnecessary because the static strains and curvatures found under most loading conditions vary slowly over the plate. Therefore, iterative solutions can be obtained by simply evaluating the strains at some typical point, such as the mid-point of a plate with an assumed linear curvature distribution. It will be shown in the following chapters that evaluating the induced strains in the piezoceramic at the mid-point of a typical section approximates the actual induced strains remarkably well and provides for very accurate solutions.

Solution Convergence

Since the means of obtaining actual solutions uses an iterative techniques, the convergence of the iteration scheme must be considered. The convergence can be examined by looking at the series formed by the first few terms of the iteration. The induced strains in a system which involves piezoceramic actuators is given by Eq. 4.18, which can be rewritten as an iteration equation in strain

$$\begin{bmatrix} \epsilon_x \\ \epsilon_y \\ 0 \end{bmatrix}_{i+1} = C \left\{ \begin{bmatrix} 1 \\ 1 \\ 0 \end{bmatrix} A + \begin{bmatrix} \epsilon_x \\ \epsilon_y \\ 0 \end{bmatrix}_i \frac{B}{A} \right\} \mathcal{E} \quad (4.19)$$

Beginning with an initial guess of ϵ equal to zero, the induced strain in both the longitudinal and transverse direction becomes

$$\epsilon_0 = CA \mathcal{E} \quad (4.20)$$

Substituting this as the next guess yields

$$\epsilon_1 = CA \mathcal{E} + B (C \mathcal{E})^2 \quad (4.21)$$

and successive iterations gives

$$\begin{aligned} \epsilon_2 &= CA \mathcal{E} + B (C \mathcal{E})^2 + \frac{B^2}{A} (C \mathcal{E})^3 \\ \epsilon_3 &= CA \mathcal{E} + B (C \mathcal{E})^2 + \frac{B^2}{A} (C \mathcal{E})^3 + \frac{B^3}{A^2} (C \mathcal{E})^4 \end{aligned} \quad (4.22)$$

which is a geometric series of the form

$$\epsilon_n = \sum_{j=0}^n (C \mathcal{E})^{j+1} A^{-(j-1)} B^j \quad (4.23)$$

Applying the ratio test gives

$$\lim_{j \rightarrow \infty} \frac{\epsilon_{n+1}}{\epsilon_n} = C \mathcal{E} \frac{B}{A} = R \quad (4.24)$$

If R is less than one, the iteration will always converge. It can be seen that the iteration will converge for almost any actuator system by examining typical values of the compliance, applied field, and experimentally determined coefficients A and B . The compliance found from the "pin" force model (Eq. 4.9), will always be less than or equal to one. The maximum electric field which can be sustained by a piezoceramic was found to be roughly 827 V/mm (21 V/mil), and the constants A and B were found to be $2.54 \cdot 10^{-7}$ mm/V ($10.0 \cdot 10^{-6}$ mils/V) and $1.94 \cdot 10^{-10}$ mm²/V² ($3.0 \cdot 10^{-7}$ mils²/V²), respectively. Substitution of these values leads to an upper limit on the value of R equal to roughly 0.6, which shows that the iteration will converge.

4.4 Conclusions

In this chapter the behavior of piezoceramic induced strain actuators was discussed, and the non-linear nature of these devices was assessed. It was found that the effect of the limited anisotropy and creep inherent in piezoceramics was small and can be ignored, while the effects of hysteresis and the strain dependence of the mechanical/electrical coupling coefficient must be considered. The effects of hysteresis were accounted for procedurally by cycling the applied field with and against the poling direction several times before recording data and by carefully defining the coupling coefficient in order to obtain consistent test results. On the other hand, in order to include the effects of a strain dependent coupling coefficient, it was found that this non-linearity must be incorporated directly into the actuation strain model.

A model for predicting the actuation strains produced by piezoceramics was developed. It was found that the linear isotropic model did not predict the actuation strains well, so it was necessary to calculate the actuation strains in a semi-empirical fashion using a strain dependent coupling coefficient and experimental data from unconstrained piezoceramics. This technique accounted for the strain dependence of the coupling coefficient and the effects of system constraints on the actuation strains. And, because of the strain dependence of the coupling coefficient, the coupling coefficient itself and the actuation strains became anisotropic when the actuator system included anisotropic components or boundary conditions. It was found that the actuation strains calculated, based on such strain dependent coupling coefficients, matched experimental results remarkably well.

Additionally, a procedure for combining the piezoceramic actuation strain model with the induced strain actuation models of Chapter 2 was detailed in order to predict the induced strains in piezoceramic induced strain actuator/substrate systems. Finally, it was found that an iterative solution procedure was needed to solve for the induced strains, and it was shown that this iterative solution will converge for real actuator systems.

CHAPTER 5

TESTING OF THE SANDWICH ARTICLES

5.1 Introduction

To verify the induced strain actuator models (Chapter 2), their solutions (Chapter 3), and the semi-empirical iterative procedure for predicting the actuation strains in piezoceramics (Chapter 4), two types of induced strain actuator/substrate systems were constructed. In all nine test articles were designed, built, and tested. The first set of four small specimens were made of a piezoceramic actuator sandwiched between two identical structural plates. The second, more representative set of four symmetric systems, were made of cantilever plates with multiple piezoceramics bonded on each surface. Isotropic and anisotropic plates were tested for both geometries. Construction and testing of the sandwich actuator test articles is discussed in this chapter, and construction and testing of the cantilever plate symmetric actuator/substrate specimens are presented in Chapter 6.

The sandwich actuator test articles were designed to be simple systems, so that the analytic models could be verified with as few complications as possible. Since each system contained only one piezoceramic actuator located at the neutral axis of the system, only actuation in the extensional mode was possible. In addition, these specimens were tested in a free-free, free-free configuration, and no loads were applied externally. Therefore, the results from these tests can be compared directly to the induced strains predicted by the exact solutions (Eqs. 3.9, 3.17, and 3.18) from Chapter 3. In addition, these sandwich actuators were used to verify the strain dependence of the piezoceramic mechanical/electrical coupling coefficient, and the validity of the semi-empirical iterative solution procedure discussed in Chapter 4.

5.2 Construction of the Sandwich Articles

Four sandwich plate actuator systems were constructed. Each of the four specimens was 5.1 cm (2.0 in.) square, as shown in Fig. 5.1. The actuators used were 0.25 mm (10 mils) thick Piezoelectric Products G-1195 piezoceramic plates. The structural plates of the first 3 sandwiches were made of aluminum. The fourth sandwich constructed had structural plates made of uni-directional graphite/epoxy. The Hercules AS4/3501 Graphite/Epoxy was manufactured in the Technology Laboratory for Advanced Composites (TELAC) at MIT. Because each plate consisted of only 2 plies, the fiber volume of the plates was significantly reduced. Thus the elastic moduli of the graphite/epoxy plates were found to be lower than usual. Table 5.1 lists the four sandwiches constructed along with their structural plate thickness and material properties, the total system thickness, and the relative stiffness ratio ψ of each actuator/substrate system.

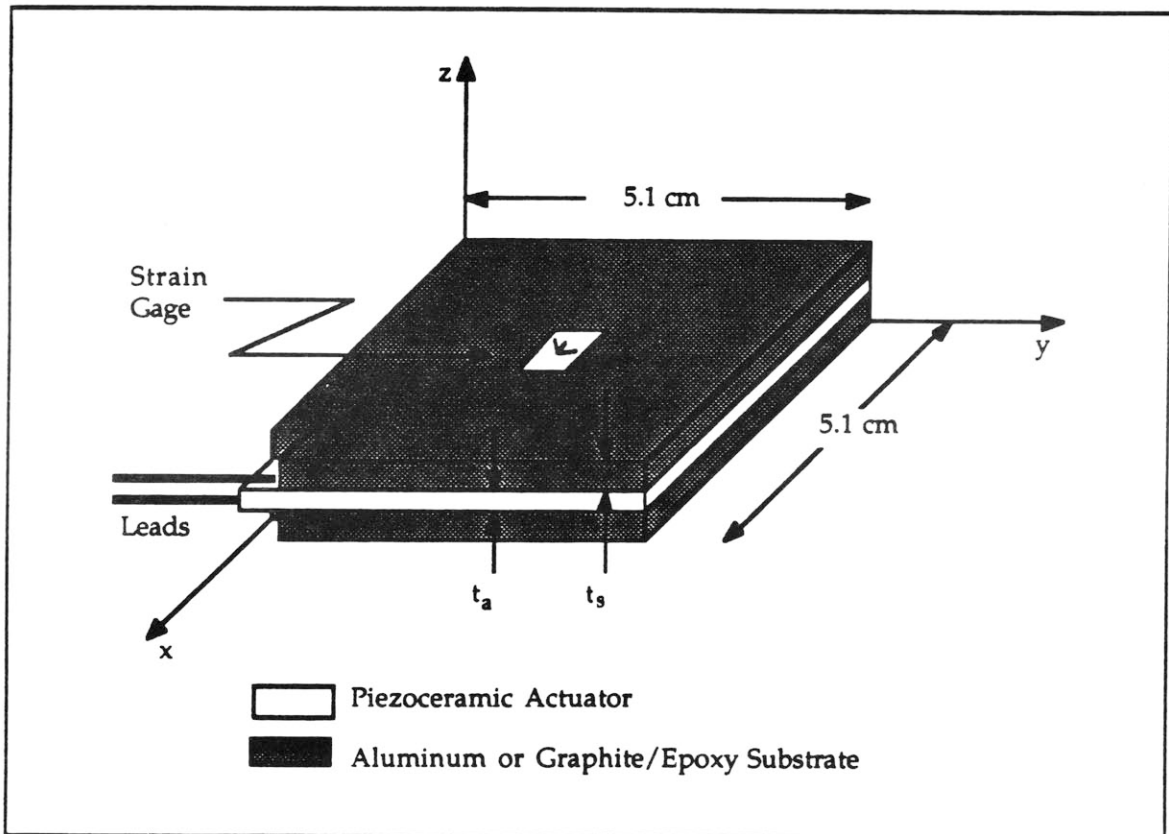


Figure 5.1 Sandwich actuator/substrate specimen geometry.

The sandwich plate actuator systems were bonded together using room temperature cure Ecobond 45 Epoxy. Each sandwich was allowed to cure for 24 hours under pressure applied by a "C" clamp. The bond layer thickness was found to be unmeasurable (less than 0.01 mm). Before bonding, cut outs were machined in the upper and lower structural plates so that wire leads could be soldered to the electrodes on the upper and lower surface of the piezoceramic. These wire leads were connected to a voltage supply to provide the necessary applied fields. Finally a BLH FAER-06B-35 S13 ET strain gage rosette was bonded to the upper surface of each actuator system to measure the induced strains, and a thin polyurethane covering was applied for protection.

Table 5.1. Sandwich Specimen Dimensions and Material Properties.

	Alum. 1	Alum. 2	Alum 3	G/E
t_s (mm)	0.84	0.51	0.32	0.41
ψ	3.67	2.22	1.39	2.23
t_{total} (mm)	1.93	1.27	0.89	1.07
E_L (GPa)	70.0	70.0	70.0	95.8
E_T (GPa)	70.0	70.0	70.0	6.7
E_a (GPa)	63.0	63.0	63.0	63.0

5.3 Experimental Procedure and Results

Each sandwich actuator system was tested up to a maximum applied field of 551 V/mm (14 V/mil), which is equivalent to 67% of the G-1195 coercive field. Before taking data, the applied field was cycled from maximum positive to maximum negative applied field, and then returned to zero applied field from an applied field with the poling direction. Then from

an applied field of zero, the field was increased against the poling direction and extensional strains were recorded at applied field increments of 79 V/mm (2 V/mil). The strains were recorded using the one-sided definition ϵ^+ given in Eq. 4.5.

This data acquisition procedure described above was identical to the procedure followed in order to obtain the experimental data used to calculate the mechanical/electrical coupling coefficient of the piezoceramic, thereby producing consistent results between sandwich data and semi-empirical analytic predictions (of the coupling coefficient, actuation strains, and induced strains) and avoiding any problems due to hysteresis. Similar experiments were done to measure the strains ϵ^- (Eq. 4.5) which resulted from applied fields with the poling direction. In all cases, ϵ^- for a given magnitude of applied field was comparable to ϵ^+ , so only ϵ^+ values will be reported.

Figs. 5.2 to 5.4 display the strains ϵ^+ measured in each orthogonal direction in the sandwich actuator system experiments, and the results of the sandwich experiments are summarized in Table 5.2. The strain measured in the longitudinal x and transverse y directions are plotted on the ordinate, versus applied field on the abscissa. The results of the aluminum sandwich actuator tests are presented in Figs 4.6, 5.2, and 5.3. Fig. 5.2 shows the measured and predicted strains of sandwich 1 which had the thickest structural plates, Fig. 5.3 presents data from sandwich 2, and Fig. 4.6 displays the result of the aluminum actuator system with the thinnest structural plates, designated sandwich 3. By comparing the magnitude of the strains for a fixed field in these three figures, it can be seen how the total strains ϵ vary with the relative stiffness ratio ψ . The total strain increased as the thickness of the structural plates t_s , and therefore the relative stiffness ratio, decreased. This trend can be shown by observing the magnitude of the total strains measured at the maximum applied field, 394 V/mm (14 V/mil), reported in Table 5.2. In aluminum sandwich 2, which has a relative thickness ratio 39% less than aluminum sandwich 1, the strains were an average of 90% larger. And, the strains found in aluminum sandwich 3, which has a relative thickness ratio 64% less than aluminum sandwich 1, were an average of 165% larger.

Table 5.2. Sandwich Specimen Results at 551 V/mm .

	Alum. 1	Alum. 2	Alum. 3	G/E
<i>Induced Strain ϵ_L (Longitudinal $\mu\epsilon$)</i>				
Experiment	14.6	28.1	38.1	23.2
Exact Solution	16.9	26.6	39.7	20.4
<i>Induced Strain ϵ_T (Transverse $\mu\epsilon$)</i>				
Experiment	15.1	28.2	40.9	183.2
Exact Solution	16.9	26.6	39.7	187.0
<i>Strain Ratio (ϵ_L/ϵ_T)</i>				
Experiment	1.03	1.00	1.07	7.90
Exact Solution	1.00	1.00	1.00	9.17
<i>Predicted Coupling Coefficients d (pm/V)</i>				
Long. d_{31}	256	263	272	258
Trans d_{32}	256	263	272	354
<i>Predicted Actuation Strains Λ ($\mu\epsilon$)</i>				
Long. Λ_x	141	145	150	142
Trans. Λ_y	141	145	150	195

Figures 4.6, 5.2, and 5.3 also clearly show the limited anisotropy associated with the piezoceramic actuators, discussed in section 4.2. The variation in total strain in the longitudinal or transverse direction from the average total strain at roughly 67% the coercive field was found to be 1.7%, 0.2%, and 3.5% for aluminum sandwich 1, 2, and 3 respectively.

The total strains recorded in the graphite/epoxy sandwich are shown in Fig. 5.4. This graph illustrates the effect of an orthotropic substrate on the resulting total strains in the system. The strains found in the graphite/epoxy

sandwich at the maximum applied field were over 7.9 times larger in the longitudinal direction perpendicular to the Graphite fibers than the strains recorded in the transverse direction parallel to the fibers, as reported in Table 5.2.

5.4 Comparison of Experimental Results with Theoretical Predictions

The agreement between the experimentally measured strains and those predicted by the analytic models with a strain dependent coupling coefficient is excellent. The analytic predictions shown in Figs. 4.6, 5.2, 5.3, and 5.4, and reported in Table 5.2 were calculated with the strain dependent coupling coefficients $d(\epsilon)$ and the actuation strains given by Eq. 4.14. The one-sided coupling coefficient definition d^+ (Eq. 4.5), and the iterative procedure discussed in section 4.3 were utilized. Since the configuration of the sandwich systems tested was that of an unconstrained, unloaded sandwich geometry actuated in extension, the solutions found by solving the "pin" force plate model equations (Eq. 3.3), the consistent plate model equations (Eq. 3.18), or the strain energy relations (Eq. 3.30) were found to be identical.

Isotropic Sandwich Actuator Systems

Under the assumption of isotropic behavior of the aluminum plates and the piezoceramic actuator, the induced strains predicted analytically for the aluminum sandwich actuator systems by Eqs 3.9, 3.19, or 3.33 were found to be identical in the longitudinal and transverse directions. This is the reason why only one theoretical curve is presented for the induced strains in Figs. 5.2, and 5.3. The geometric constant α is equal to 1/2 for the sandwich configuration as shown in Fig. 2.4.

It was found that the analytically predicted induced strains differ only by a small amount from the experimentally measured strains. The predicted and measured induced strains at the maximum applied field of 551 V/mm (14 V/mil), 67% of the coercive field, are reported in Table 5.2. At this applied field analytical predictions deviate by 11.9%, 5.3%, and 4.2% from the average measured total strains for aluminum sandwich 1, 2, and 3 respectively.

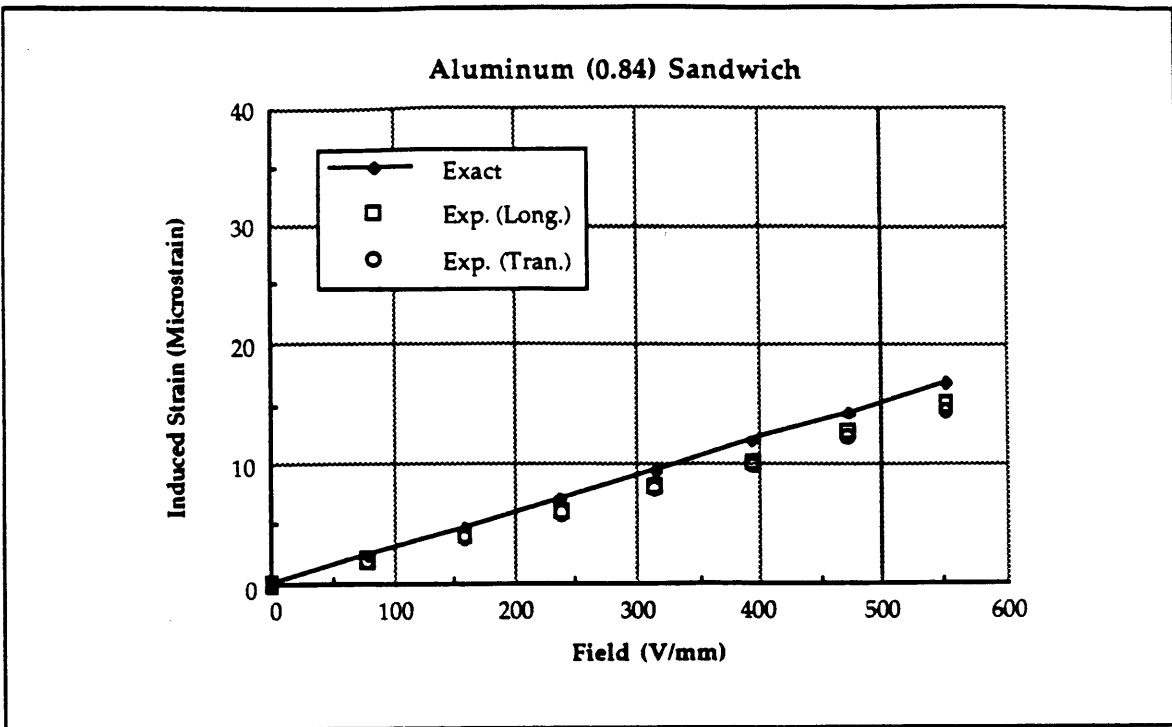


Figure 5.2 Induced strain versus applied field for the aluminum sandwich with 0.84 mm thick substrates.

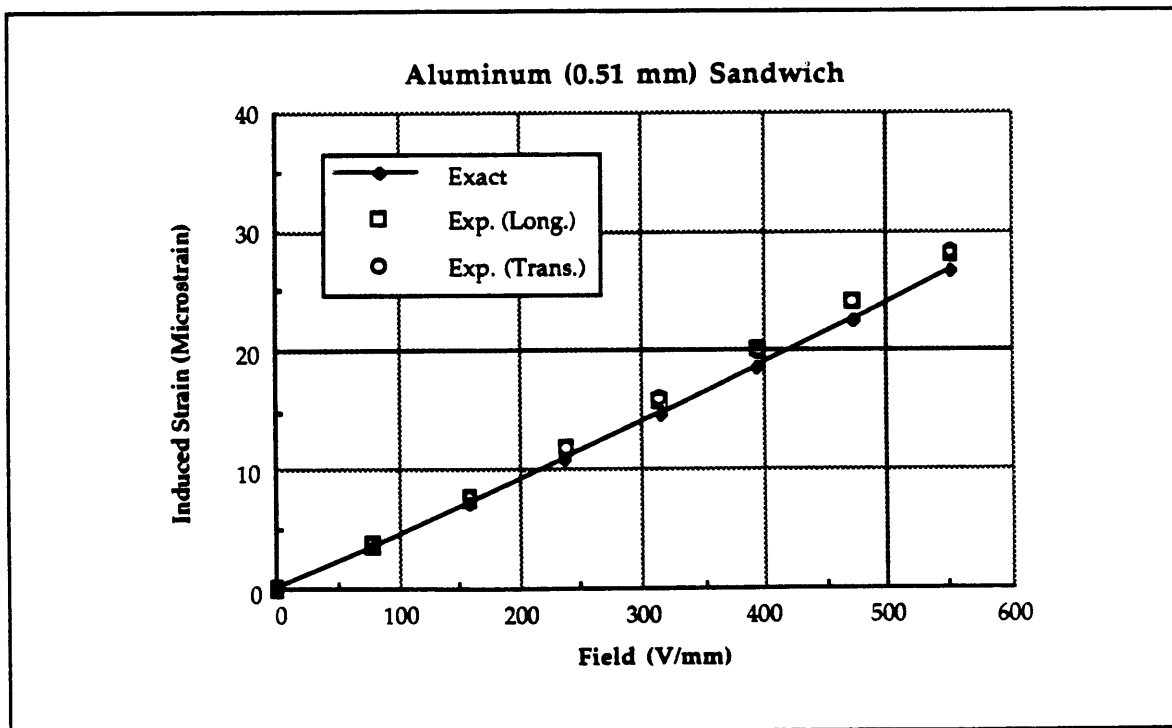


Figure 5.3 Induced strain versus applied field for the aluminum sandwich with 0.51 mm thick substrates.

The inconsistencies found were within the range of error, due to unmodelled non-linear piezoceramic effects and variations in material properties, expected.

The mechanical/electric coupling coefficient and the predicted actuation strains varied considerably over both the range of applied fields and from system to system. At the maximum applied field the coupling coefficients showed an increase of 0.8%, 3.5%, and 7.1% for aluminum sandwich 1, 2, and 3 respectively, over the nominal zero induced strain value of the coupling coefficient, which was 254 pm/V. The actuation strains which correspond to the above coupling coefficients were predicted to be 140.8 $\mu\epsilon$, 144.9 $\mu\epsilon$, and 150.1 $\mu\epsilon$, as reported in Table 5.2.

Orthotropic Sandwich Actuator Systems

Excellent agreement between theoretical predictions and experimental results was also found for the graphite/epoxy sandwich actuator system. These results are displayed in Fig. 5.4. At the maximum applied field, the theory is off by 12% in the direction parallel to the fibers and 2.1% perpendicular to the fibers. And, the predicted strains are never off by more than 3 $\mu\epsilon$ at any value of applied field even though relatively high total strains, 183 $\mu\epsilon$, were recorded in the Epoxy matrix perpendicular to the Graphite fibers.

Obviously, in addition to varying over the range of applied fields, the predicted values of the strain dependent coupling coefficient and the actuation strains differed greatly in the longitudinal direction parallel to the Graphite fibers and the transverse direction perpendicular to the fibers. Hence, two independent coupling coefficients, as described in section 4.2, were used to predict the induced strains for this orthotropic system. The coupling coefficients, actuation strains, and induced strains for the graphite/epoxy systems are also reported in Table 5.2. At the maximum applied field the theoretically predicted coupling coefficients were found to be 258 pm/V in the longitudinal direction and 354 pm/V in the transverse direction. This corresponds to a 37% difference and an increase of 1.6% and 39.4% in the longitudinal and transverse directions respectively over the nominal value of the coupling coefficient, 254 pm/V.

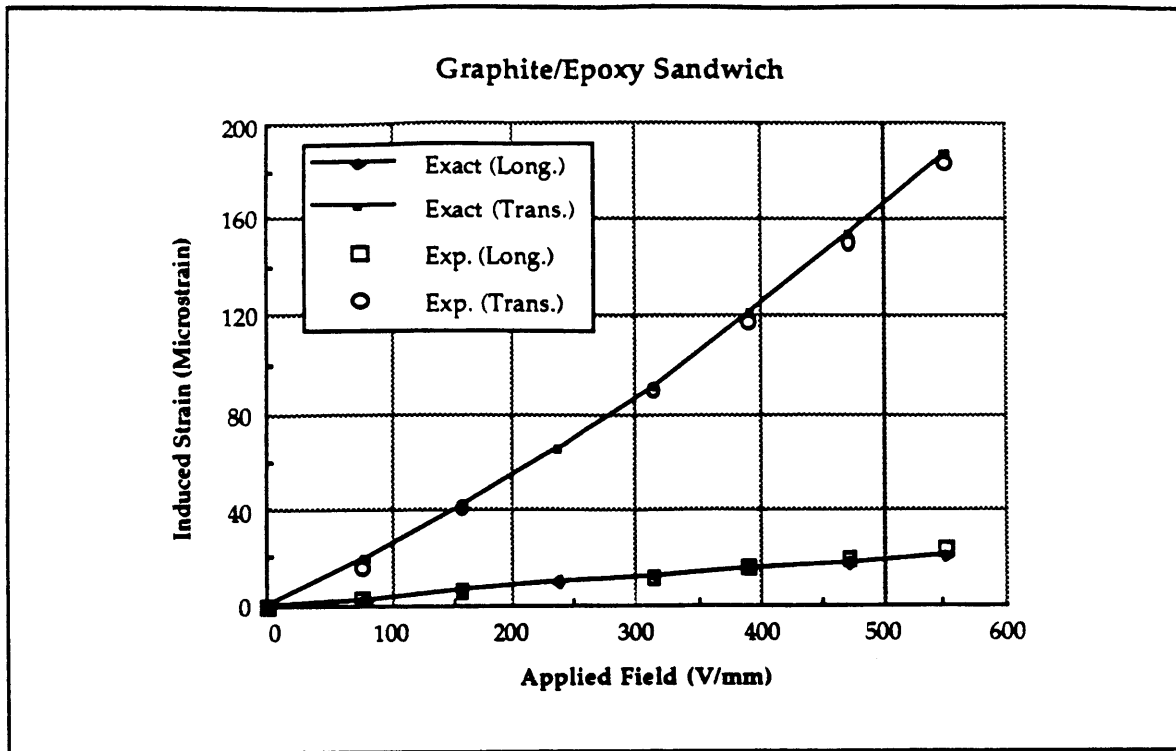


Figure 5.4 Induced strain versus applied field for the graphite/epoxy sandwich. Plotted are the theoretical and experimental results in the longitudinal and transverse dimensions.

5.6 Conclusions

The experimentally measured extensional induced strains were found to correlate extremely well with the theoretically predicted strains for the unconstrained, unforced, sandwich actuator systems tested. It was found that the coupling coefficient varied considerably due to the wide range of induced strains found in the sandwich systems.

Actuator/substrate systems with orthotropic components caused both the induced strains and the value of the coupling coefficients to differ in the longitudinal and transverse directions. The analysis of the graphite/epoxy sandwich indicates that independent analysis along the two principal directions yield orthotropic solutions which closely match experimental values for induced strain.

These tests of the simple sandwich actuator have demonstrated the validity of the strain dependence of the mechanical/electrical coupling coefficient, and of the semi-empirical iterative solution procedure. This will be applied to the analysis of the experiments performed on the more representative and cantilevered plates to be discussed in the next chapter.

CHAPTER 6

TESTING OF THE CANTILEVER PLATE ARTICLES

6.1 Introduction

As discussed in Chapter 5, simple sandwich systems were tested to validate the basic induced strain actuation models in specific geometries, and to confirm the behavior of piezoceramic induced strain actuators in constrained situations. In this chapter the construction and testing of the cantilever plate symmetric actuator/substrate systems constructed and tested are discussed. These plate systems consisted of a single structural plate with piezoceramic actuators symmetrically bonded to both the upper and lower surfaces of the plate. The purpose of these tests were to examine systems which are more representative of actual induced strain actuation systems, as might be found in members of precision pointing instruments, deformable aeroelastic lifting surfaces, and shape controlled deformable optical surfaces. The results of these test were used to verify the ability to predict the performance of systems with more complex geometries and boundary conditions, and to determine if the deflections obtained are large enough for induced strain systems to be used in practical applications.

The specific objectives of these tests were to determine the static mode shapes and the applied field/deformation relations. It was also the objective of these experiments to verify the Ritz solution developed in section 3.4. A total of four such symmetric systems were constructed and tested, and the mode shapes and deflections measured were compared to the mode shapes and deflections predicted by the analytic models. Ritz approximate solutions (Eq. 3.30) of the plate strain energy equations (2.47) were used to formulate and solve for the analytically predicted deformations since the strain and curvature relations (Eqs. 2.30, 2.37, 2.38, and 2.40) cannot be solved exactly for these cantilever systems. As was the case for the sandwich systems, the strain dependent coupling coefficients and actuation strains, and the semi-empirical iterative solution procedure were utilized in the calculations. The construction and testing of these systems is discussed below.

6.2 Construction of the Cantilever Plate Articles

The geometry of the four large cantilever plate, symmetric systems is shown in Fig. 6.1. Each plate had overall dimensions of 33.0 cm (13.0 in.) in the longitudinal x direction by 15.2 cm (6.0 in.) in the transverse y direction. The plates were clamped at the base of the longitudinal dimension ($x=0$). Each plate had 3.8 cm (1.5 in.) of the longitudinal length in the clamp itself, providing the cantilever boundary condition.

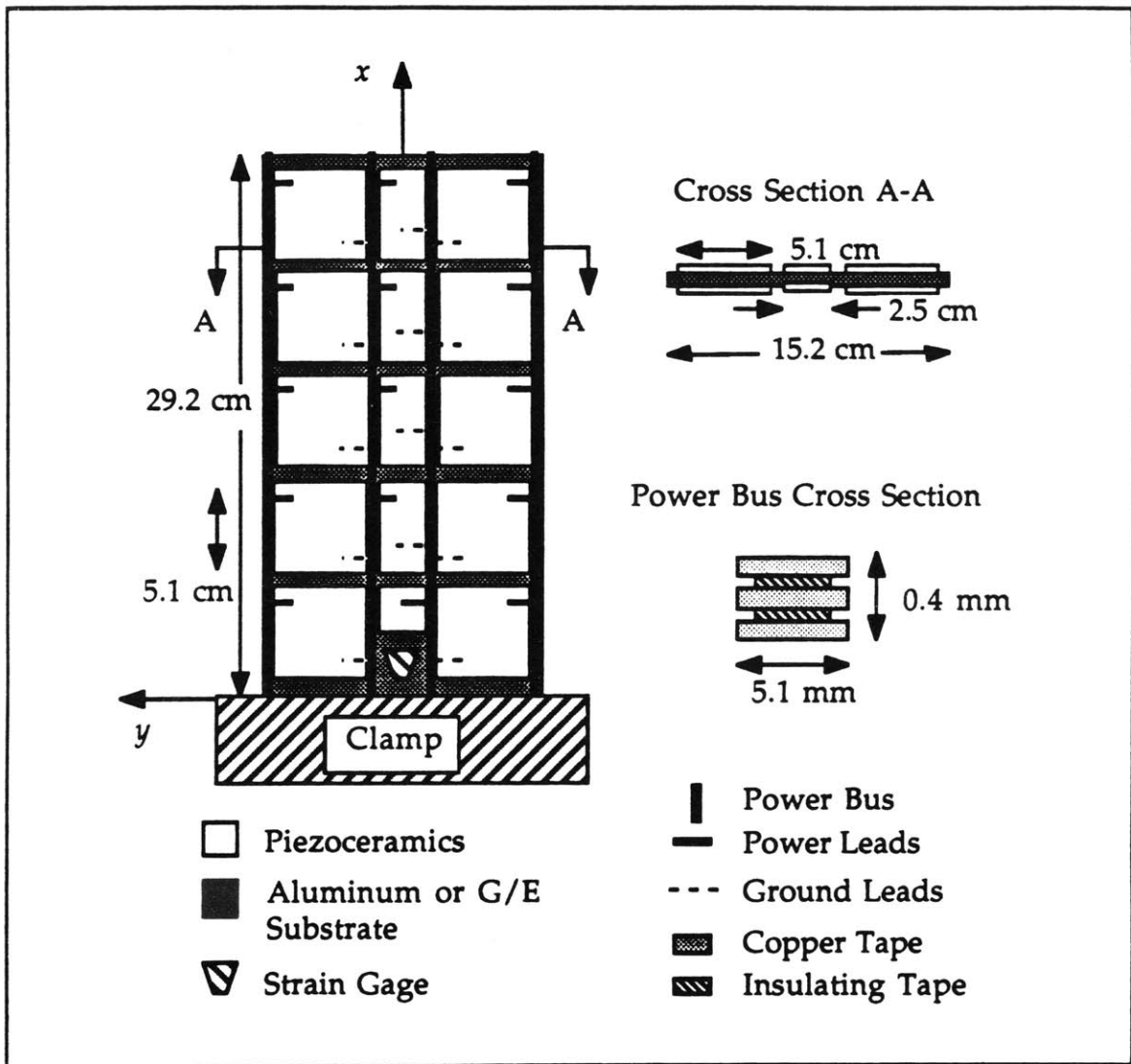


Figure 6.1 Cantilever plate symmetric actuator/substrate specimen configuration.

All 4 plates were covered with 30 surface bonded Piezoelectric Products G-1195 piezoceramic plate actuators. Each actuator had a thickness of approximately 0.25 mm (10 mils), and 1/2 of the actuators were bonded to each surface of each plate. The piezoceramics were sized and arranged so that as much of the plate surfaces were covered as possible. As shown in Fig. 6.1, the piezoceramics on the outer transverse edges were 5.08 cm (2.0 in.) square while the actuators in the middle row were 5.08 cm (2.0 in.) by 2.54 cm (1.0 in.). The middle piezoceramic nearest to the cantilever edge was cut to 2.54 cm (1.0 in.) square to make room for a BLH FAER-06B-35 S13 ET strain gage rosette which was bonded to each plate surface. The arrangement of the piezoceramic actuators was identical on the upper and lower plate surface. A space of 0.51 cm (0.20 in.) separated the piezoceramics from one another, and a space of 0.51 cm (0.20 in.) separated the outer most actuators from the transverse edges, while a gap of 0.64 cm (0.25 in.) was left between the outer rows of piezoceramics and the longitudinal edges of the plate at the clamped and free ends. The completed symmetric specimens had 71% of their upper and lower surfaces covered with piezoceramic plate actuators.

The gaps between the actuators were left to prevent the actuators from physically touching one another, and to allow enough space for the wires needed to apply electric fields to the actuators. These wires are displayed in Fig. 5.1 and labelled as power busses and power leads. Each power bus consisted of two copper strips surrounded by insulating tape as indicated in the figure. Thus on each surface there were four power busses with a total of 8 connectors (6 feeds and 2 grounds). Very thin, 0.18 mm (7 mils) wire leads were used to connect the actuators to the power busses. A schematic diagram detailing the wiring configuration of each plate is shown in Fig. 6.2.

This wiring arrangement allowed a total of 12 independent fields to be applied to each symmetric plate actuator system. The piezoceramic actuators, power busses, and wire leads were organized in such a manner so that the plates could be actuated in a static extension mode, a static bending mode, or the first three plate dynamic modes (1st bending, 1st torsion, and 2nd bending). In order to accomplish the above, the actuators were arranged into 12 groups, 6 on each surface, and the actuators were connected to the power busses so that the fields applied to each group could be controlled

independently. The actuator groups and the strain node lines of the first three dynamic modes are displayed in Fig. 6.3. Notice that the 2nd bending node line occurs at approximately the 20% point in the longitudinal x direction [Crawley and de Luis, 1987].

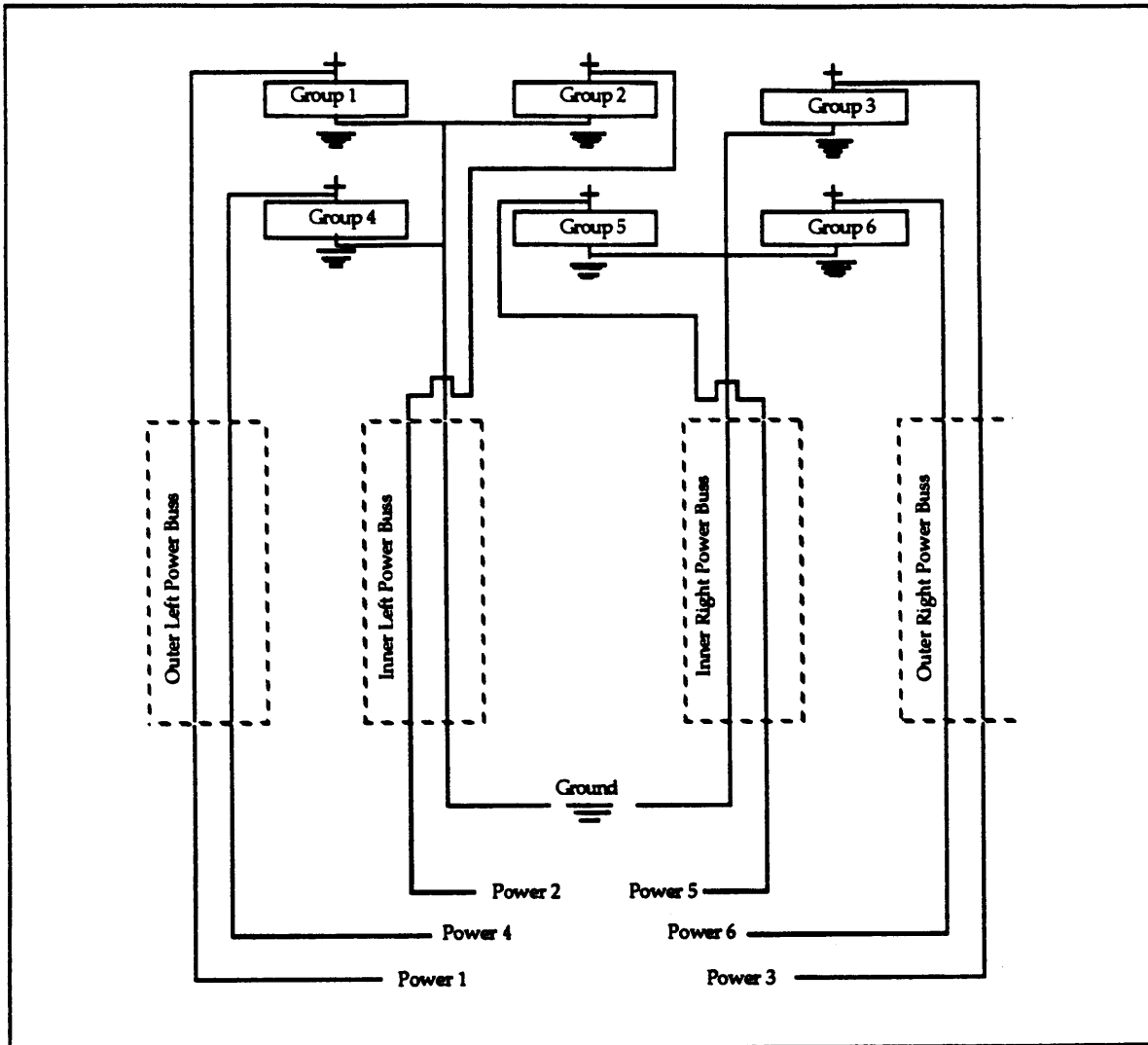


Figure 6.2. Cantilever plate symmetric actuator/substrate specimen wiring schematic.

Details of the structural plates used and the actual construction procedures followed are now discussed. Of the four plate systems constructed, one was made of aluminum and the remaining three were constructed from Hercules AS4/3501 Graphite/Epoxy. Each plate was designed for a different purpose. The 0.79 mm (0.031 in.) aluminum plate served as an isotropic bench mark specimen, while each of the graphite/epoxy plates were designed

to exploit a specific directional stiffness and to produced certain desired deformations. The first was designed for increased transverse bending. The second was designed to produced twist though bending/twist coupling. And the third was designed to take advantage of extension/twist coupling to produce twist. The thicknesses, material properties, and important extensional **A**, coupling **B**, and bending **D** stiffnesses of these plates are given in Table 6.1.

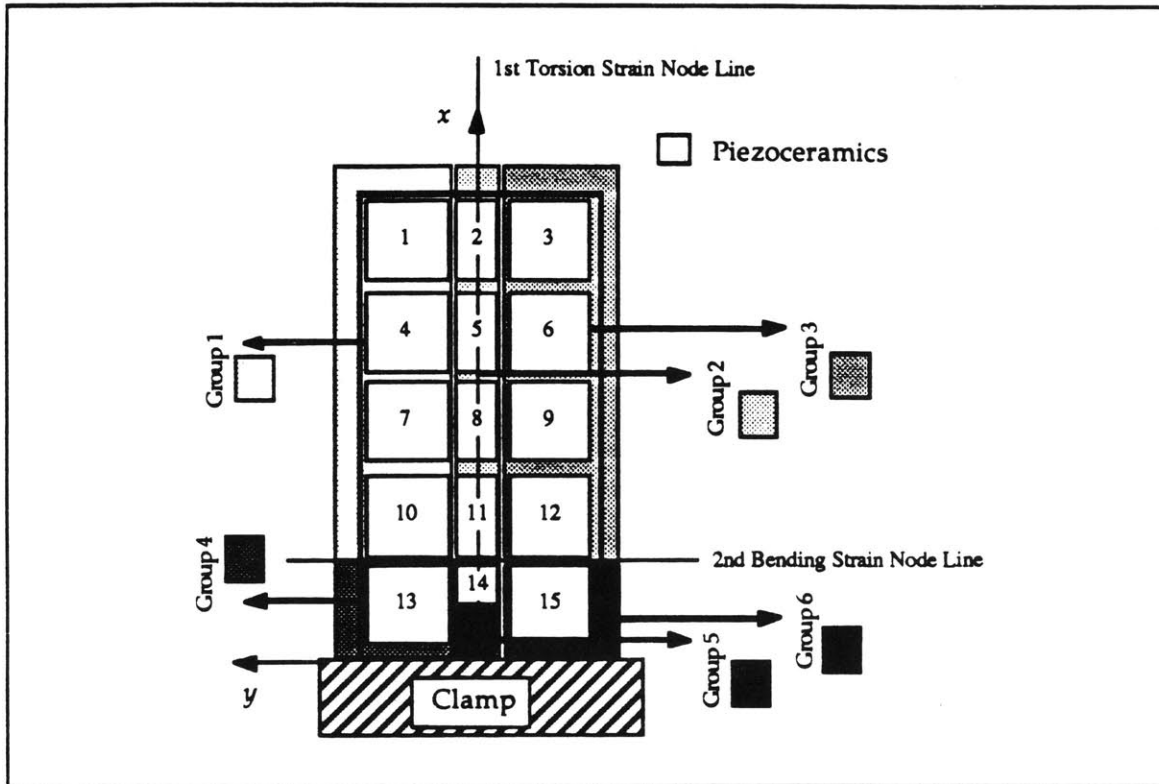


Figure 6.3. Cantilever plate symmetric actuator/substrate specimen actuator groupings.

Each of the 3 graphite/epoxy structural plates were manufactured in the MIT TELAC facility. The first composite plate constructed, which had a lay-up of $[0/\pm 45]_s$, possessed a higher, by 28.2%, longitudinal bending stiffness than the aluminum specimen and a lower, 19.6%, transverse bending stiffness. Thus, this plate was designed to have smaller longitudinal deflections and increased transverse bending deformations compared to the aluminum plate system. It should also be noted that although the $[0/\pm 45]_s$ plate was not designed specifically for the purpose of creating twist curvature, the laminate possessed a slight bending/twist coupling, with ψ_D equal to 0.06

(Eq. 3.39). The second and third composite plates were design to produce twist curvature by exploiting an entry of the **B** or **D** stiffness matrixes. A $[+30_2/0]_s$ graphite/epoxy laminate was constructed to produce twist curvature from bending actuation. This plate made use of bending/twist coupling (D_{16}) and had a bending/twist coupling parameter ψ_D of 0.31. A $[+45_3/-45_3]$ laminate was built to produce twist curvature from extensional actuation. This plate exploited extension/twist coupling (B_{16}) and had a extension/twist coupling parameter ψ_B of 0.36 (Eq. 3.42).

Because of the extension/twist coupling of the $[+45_3/-45_3]$ laminate, a special manufacturing procedure was required. Rather than curing the entire laminate all at once, as was done for the other two graphite/epoxy plates, the upper three plies and the lower three plies were cured separately and then bonded together in vacuo. The two plates were bonded together using Dexter Hysol EA 9330 Epoxy, and the thickness of the bond was unmeasurable (less than 0.01 mm). This was done to avoid any initial twist in the laminate which would have resulted from residual thermal stresses created by the process of curing an unsymmetric laminate.

Table 6.1 Cantilever Plate Specimen Dimensions and Material Properties.

	Alum.	G/E	G/E	G/E
Ply Sequence	----	$[0/\pm 45]_s$	$[30_2/0]_s$	$[+45_3/-45_3]$
t_s (mm)	0.79	0.83	0.83	0.83
ψ	4.90	9.36	9.36	9.36
A_{11} (MN/m)	86	89	110	62
A_{22} (MN/m)	86	52	38	62
B_{16} (KN)	0.00	0.00	0.00	5.64
D_{11} (N-m)	9.18	11.8	10.6	8.56
D_{22} (N-m)	9.18	7.38	7.34	8.56
D_{16} (N-m)	0.00	0.35	1.90	0.00
D_{66} (N-m)	3.21	2.96	3.57	3.97
ψ_D	0.00	0.06	0.31	0.00
ψ_B	0.00	0.00	0.00	0.36

The aluminum structural plate and the graphite/epoxy plates, once cured, were cut to the required plate dimensions and small grooves, 0.46 cm (0.18 in.) wide by 0.13 mm (5 mils) deep, were machined on both sides of the plates. Long longitudinal grooves running the length of the plate were machined for the busses and short, 1.3 cm (0.5 in.) transverse grooves were machined for the leads, so that the busses and leads would fit smoothly under and around the piezoceramic actuators. Once the grooves were machined the busses, which consisted of copper tape and insulating tape, were laid down. The actuators were then placed in position and the leads were soldered to the piezoceramics and the appropriate busses. Room temperature cure Ecobond 45 Epoxy was spread on the piezoceramics and the plate. A Teflon sheet and a metal covering were placed over the plate and pressure was applied with "C" clamps in order to ensure a strong bond and a thin bond layer. The epoxy was allowed to cure for 24 hours, and wax coated strings were used to keep the actuators in position during the 1st hour of the curing process. Each plate surface was built separately, and coated with polyurethane for protection.

5.3 Experimental Procedure and Results

Each cantilever plate system was tested to determine the shape of deformation, deflection versus applied field, and maximum deflection. The cantilever plates were actuated in either bending or extensional modes depending on the design of the particular plate. The tests were conducted in a manner similar to the procedure used for the sandwich tests, as described in section 5.3. The applied field was cycled from maximum positive to maximum negative field and returned to zero before beginning each test. One-sided data was recorded as the field was increased from zero applied field to the maximum field. As before, a strain dependent coupling coefficient $d+$ (Eq. 4.5) and the iterative solution procedure (section 4.3) was used. However the solutions for these plate systems were determined using the Ritz solution (Section 3.4) and the assumed mode shapes illustrated in Fig. 3.4.

The deflection mode shape and deflection magnitude data was obtained using three non-contacting proximity sensors. A total of 33, 1.3 cm (0.5 in.) square, steel targets were attached to one surface of each plate. Fig. 6.4

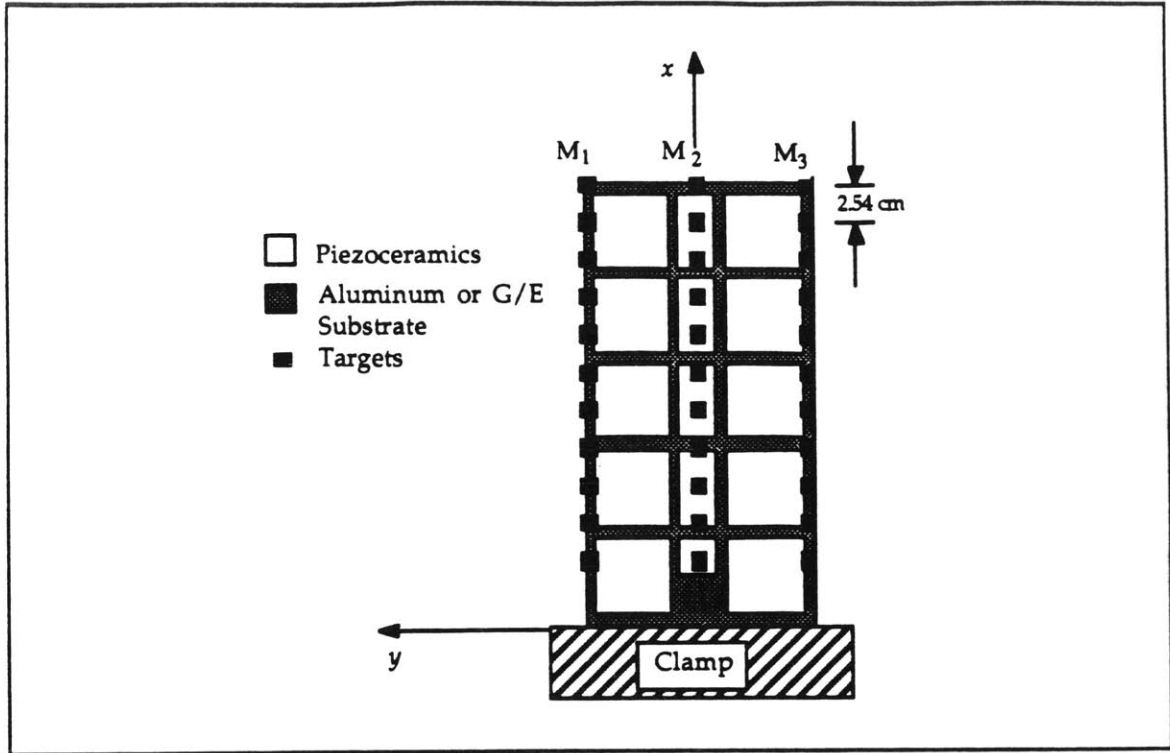


Figure 6.5. Cantilever plate symmetric actuator/substrate specimen target locations.

shows the target locations. As illustrated in this figure, three targets were placed along the transverse dimension at eleven longitudinal stations which were 2.54 cm (1.0 in.) apart. Three targets were used in the transverse direction in order to resolve out-of-plane deflections due to longitudinal bending, twist, and transverse bending. The position of these measurements were at the outer transverse edges (M_1 and M_3) and at the center of the plate (M_2) as indicated in Fig. 6.4. The procedure of cycling the applied field and recording one-sided data was carried out with the three sensors at one station. Then the sensors were moved to the next station and the test was repeated. The raw data obtained was resolved into three non-dimensional out-of-plane displacements: longitudinal bending deflection W_1 , twist deflection W_2 , and transverse bending deflection W_3 . These displacements are defined as

$$W_1 = \frac{M_2}{C} \quad W_2 = \left[\frac{M_1 - M_3}{C} \right] \quad (6.1)$$

$$W_3 = \frac{M_2 - \left[\frac{M_1 + M_3}{2} \right]}{C} \quad (6.2)$$

where C denotes the width, in the transverse direction, of the plate systems. Physically W_1 is the non-dimensional longitudinal bending, W_2 is the twist in radians, and W_3 is the fractional transverse curvature. The mode shape displacements are reported below for each plate, and following these results the magnitude of the deformations recorded for each plate, at typical locations, versus applied field will be presented. The deflections measured experimentally will also be compared to analytically predicted deflections.

Static Mode Shape Tests

The aluminum plate system was tested in the bending actuation mode. Since this system had no bending/twist coupling, no twist deformation was expected. The mode shapes measured at a maximum applied field of 630 V/mm (16 V/mil) are shown in Fig. 6.5 for longitudinal bending W_1 and in Fig. 6.6 for transverse bending W_3 . In both figures the deflection is plotted versus the non-dimensional longitudinal plate dimension. It can be seen from Fig. 6.5 that the longitudinal deformation was approximately quadratic. In contrast the transverse bending displacement displayed in Fig. 6.6 appeared to be a more complicated function. The transverse bending deflection is zero at the fixed end and climbs approximately linearly, but then drops off sharply at the free end. The transverse deformations were found to be significantly smaller than the longitudinal deformations. It was observed that the maximum longitudinal deformation was over 10 times the maximum transverse deformations. This is due to the smaller transverse length and the cantilever boundary condition. The Ritz assumed modes used for the analytical predictions are given in Fig. 3.4 and shown in the figures (Figs. 6.5 to 6.13). Notice that the mode shapes assumed approximate the shape of the actual modes quite well. In addition, the amplitude of the deformations predicted by the Ritz analysis closely matches the measured values.

The poor signal to noise ratio observed in Fig. 6.6 is primarily due to metrology difficulties. Although the sensors used were quite accurate (± 0.005 mm), the range was relatively small 6.4 mm (0.25 in.). And, because of their small range, the sensors had to be moved several times during each test in order to measure the large longitudinal deflections. Moving the sensors introduced additional errors, over that of the sensor accuracy, which can be seen in the plots of the transverse bending data.

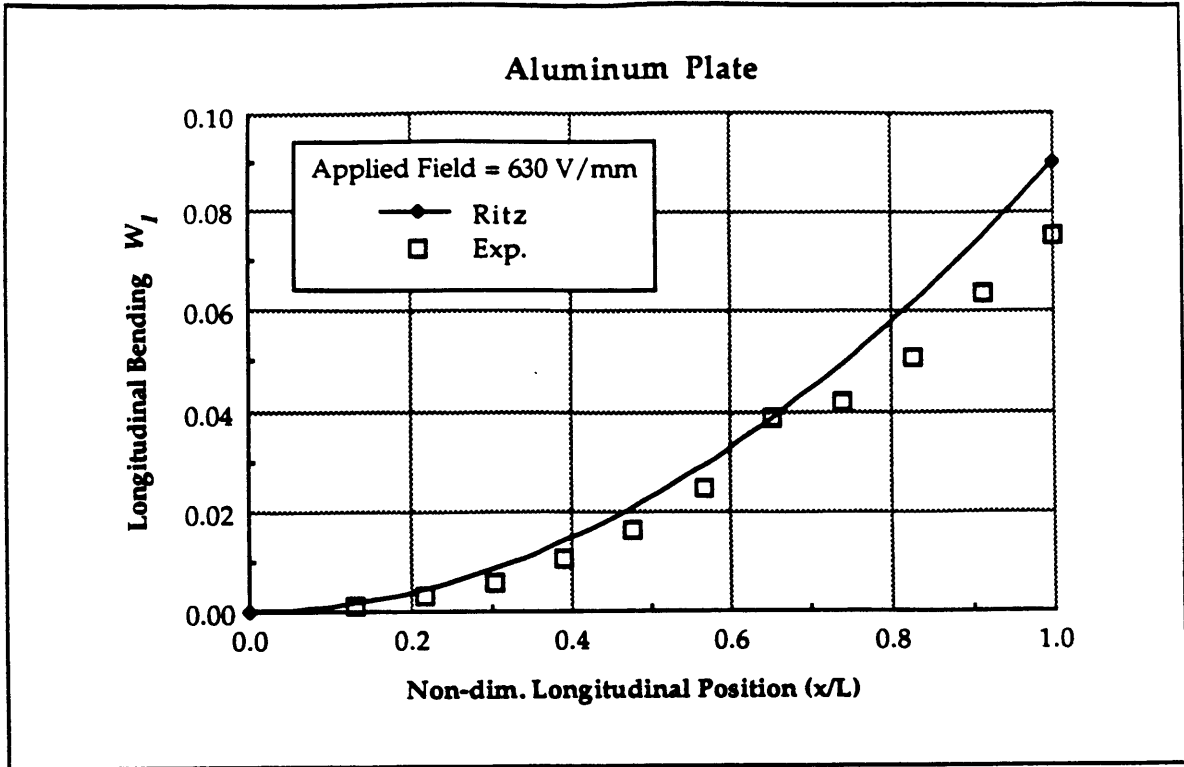


Figure 6.5 Aluminum plate longitudinal bending mode shape.

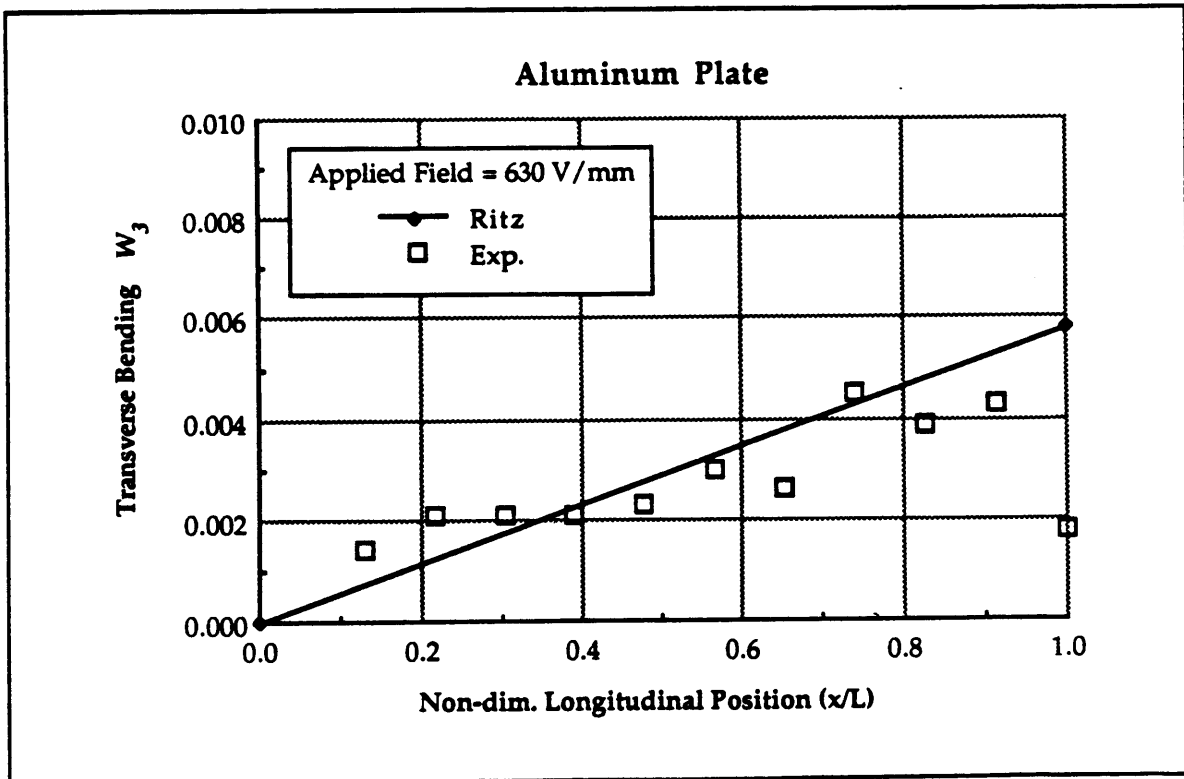


Figure 6.6 Aluminum plate transverse bending mode shape.

The results of the mode shape tests from the $[0/\pm 45]_s$ graphite/epoxy plate actuated in bending are displayed in Figs. 6.7, 6.8, and 6.9. These mode shapes were measured at the maximum applied field which was 394 V/mm (10 V/mil) for this plate. The longitudinal bending deflections, presented in Fig. 6.7 are more than an order of magnitude larger than the twist deflections W_2 , illustrated in Fig. 6.8, or the transverse bending deflections, shown in Fig 6.9. As in the case of the aluminum plate, the quadratic distribution assumed in the Ritz analysis showed good agreement in terms of shape and amplitude.. Data with appreciable scattered was recorded for the twist and transverse bending modes due to the metrology difficulties discussed above. However it can be observed that twist deformations, displayed in Fig. 6.8, were induced due to the slight bending/twist coupling and the magnitude of the transverse bending, shown in Fig. 6.9, dropped off significantly at the free edge as before. Figs. 6.8 and 6.9 also show that the linear modes assumed in the Ritz analysis for twist and transverse bending approximate the mode shapes and amplitudes measured with relatively good accuracy.

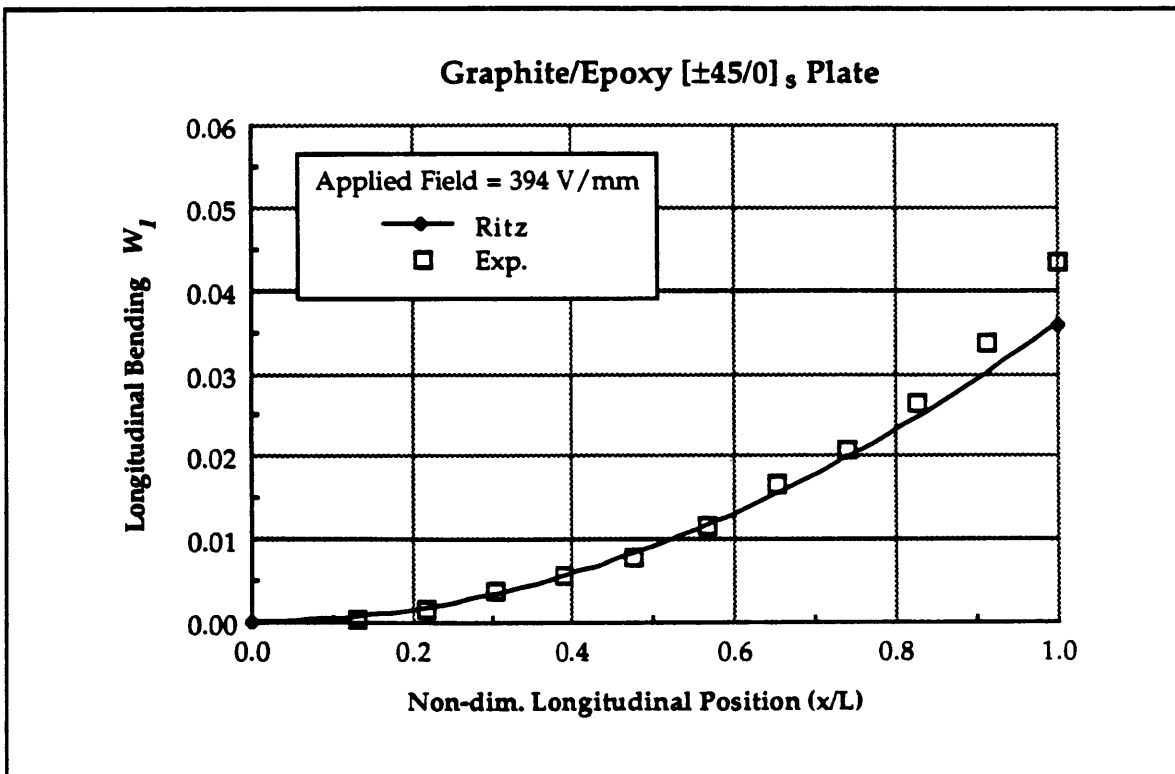


Figure 6.7 Graphite/epoxy $[\pm 45/0]_s$ plate longitudinal bending mode shape.

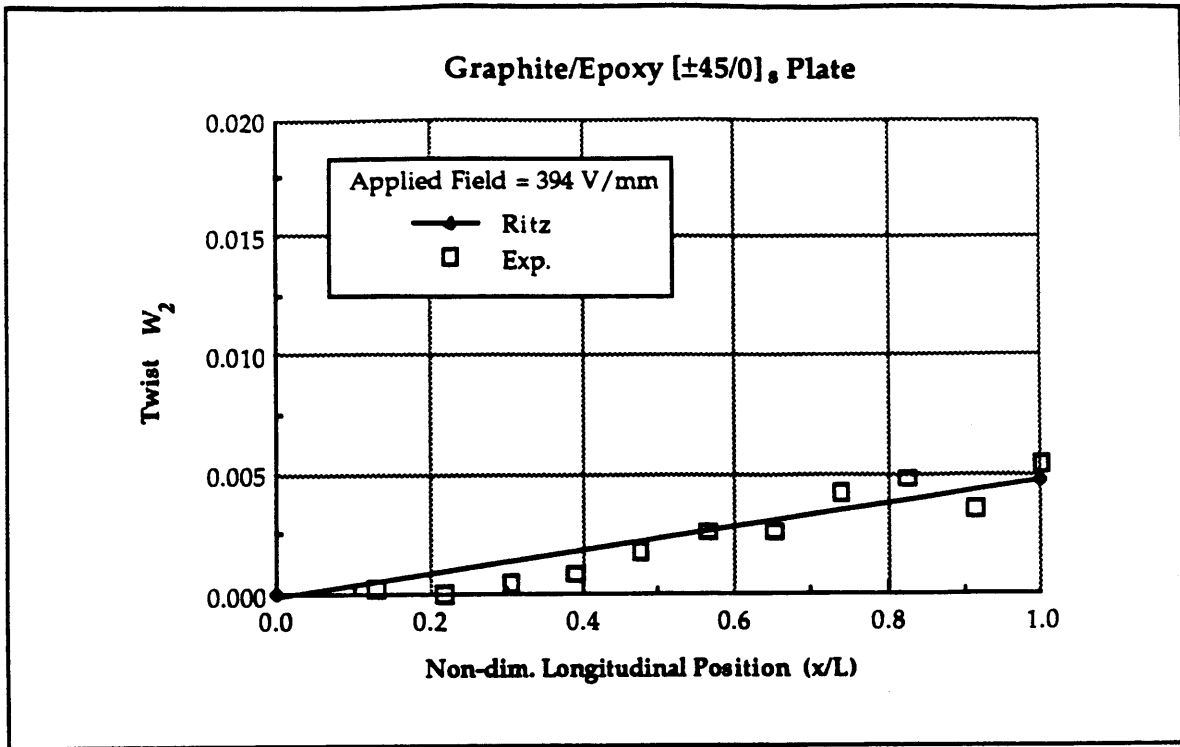


Figure 6.8 Graphite/epoxy $[\pm 45/0]_s$ plate twist mode shape.

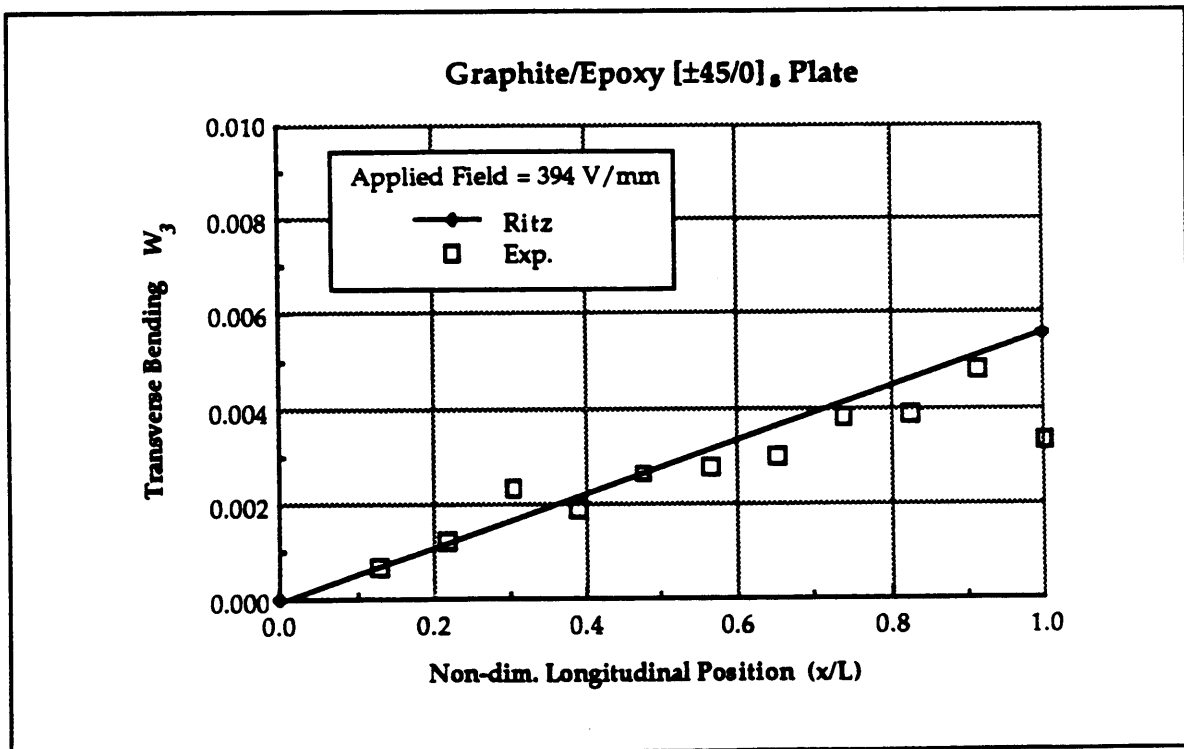


Figure 6.9 Graphite/epoxy $[\pm 45/0]_s$ plate transverse bending mode shape.

The maximum field applied to the $[+30_2/0]_s$ graphite/epoxy plate was 472 V/mm (12 V/mil). This plate was also actuated in bending. The mode shapes found for the $[+30_2/0]_s$ plate system were similar to those recorded for the previous plates, except that the twist deformation was significantly more pronounced due to the larger bending/twist coupling parameter associated with this plate. Notice the agreement between the Ritz prediction and the measured quadratic longitudinal bending mode shape in Fig 6.10. The twist mode shape W_2 , presented in Fig. 6.11, was found to be nearly linear, which indicates that the linear mode shape assumed for the twist distribution, presented in Fig. 3.4 and illustrated in Fig 6.11, was a reasonable selection. Once again the magnitude of the transverse bending deflection was found to drop off sharply at the free edge, as shown in Fig. 6.12. As above, good agreement was found between the Ritz and experimental mode shapes and amplitudes for twist and transverse bending deformation.

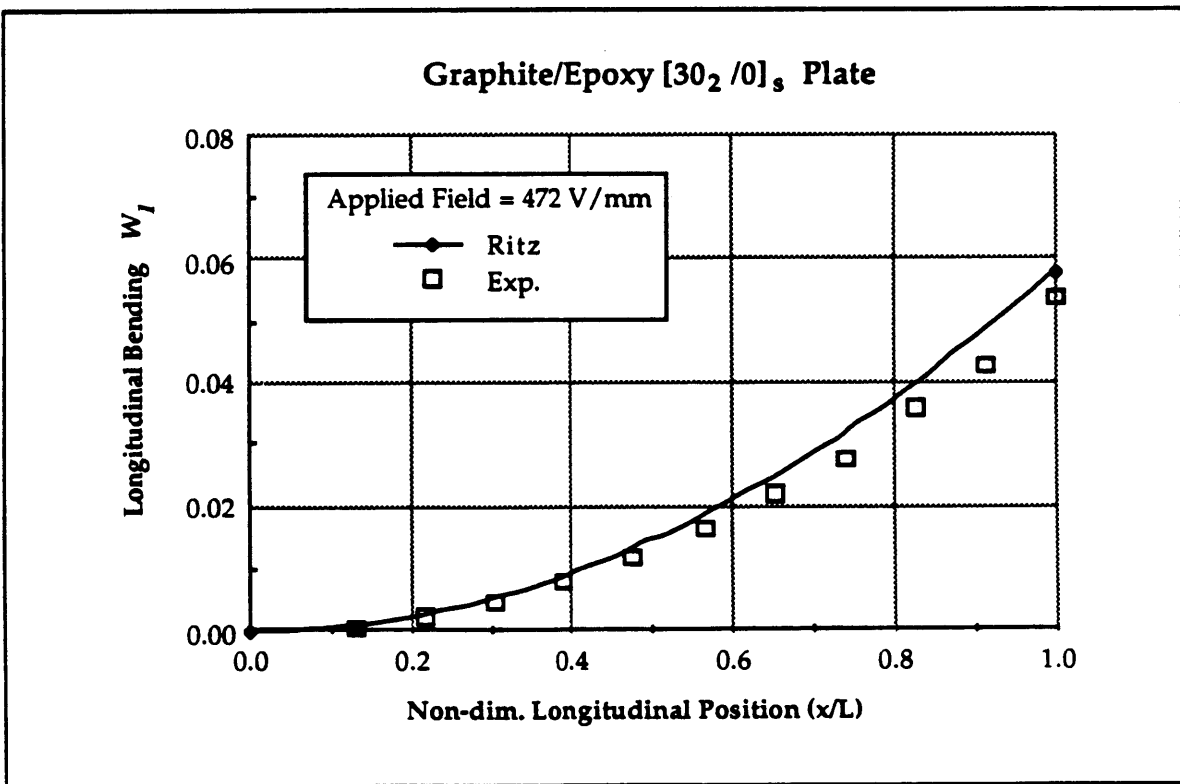


Figure 6.10 Graphite/epoxy $[30_2/0]_s$ plate longitudinal bending mode shape.

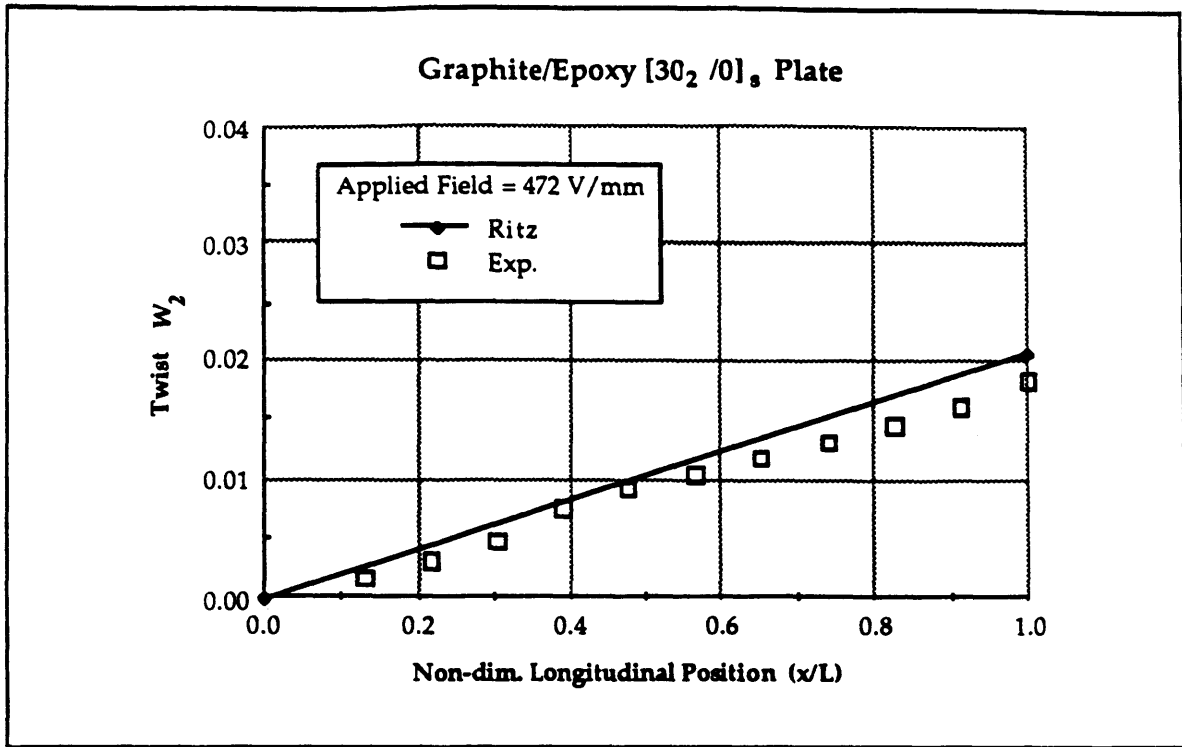


Figure 6.11 Graphite/epoxy $[30_2/0]_s$ plate twist mode shape.

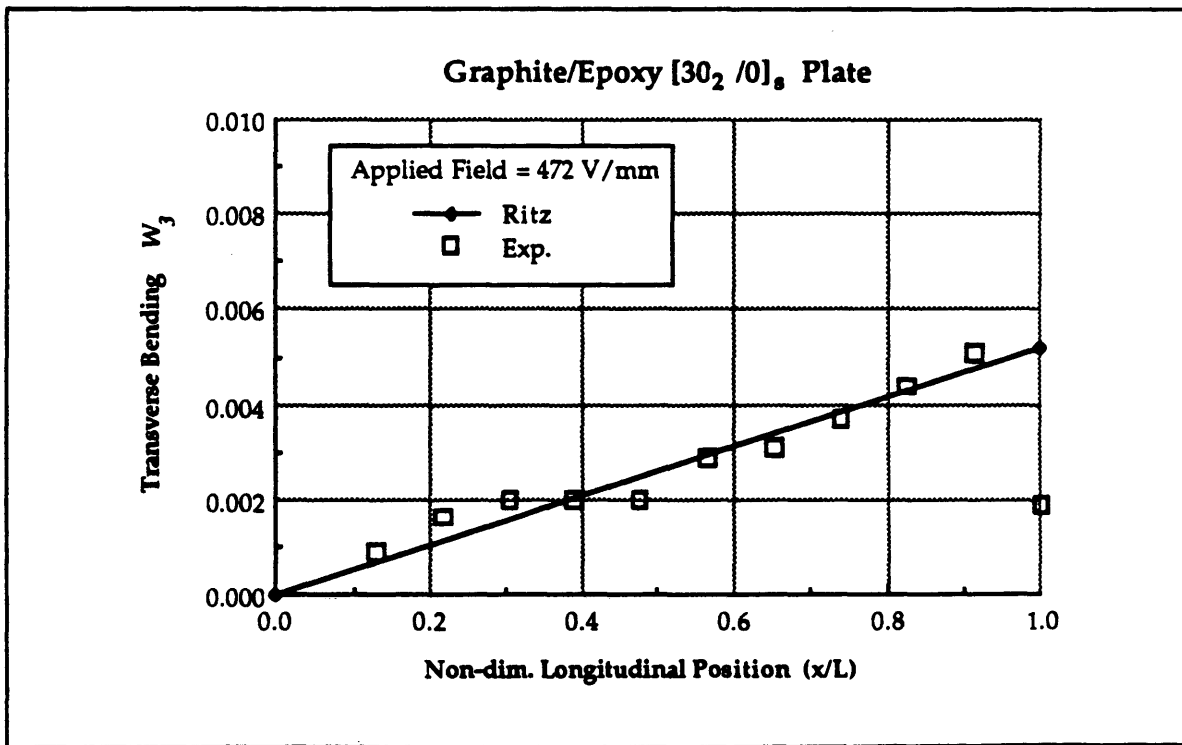


Figure 6.12 Graphite/epoxy $[30_2/0]_s$ plate transverse bending mode shape.

The final plate tested to determine the experimentally measured static mode shapes was the $[+45_3/-45_3]$ graphite/epoxy plate. This plate was actuated in an extensional mode. Because the $[+45_3/-45_3]$ graphite/epoxy plate possessed a high extension/twist coupling parameter and no extension/bending coupling, twist deformations were the only deflections expected and were in fact the only significant deflections measured. Fig. 6.13 displays the nearly linear twist mode shape observed at an applied field of 472 V/mm (12 V/mil). Notice the deflection is not quite linear near the clamped edge due to the zero slope conditions enforced by the cantilever boundary, and the Ritz analysis predicts both the twist mode shape and the magnitude of twist deformation quite accurately.

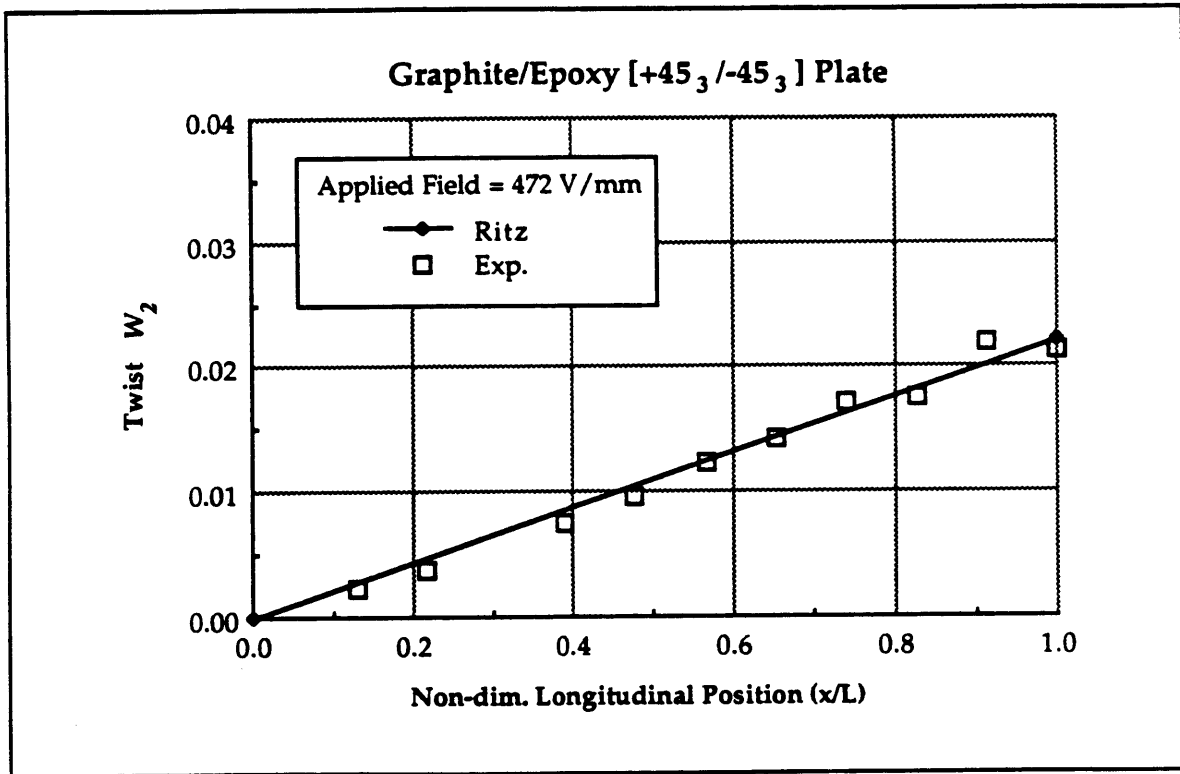


Figure 6.13 Graphite/epoxy $[+45_3/-45_3]$ plate twist mode shape.

Deflection versus Applied Field Tests

The results of the deflection versus applied field tests are presented as deflection in terms of the normalized longitudinal bending W_1 , twist W_2 , and transverse bending W_3 deflections, as defined by Eqs. 6.1, 6.2, and 6.3 respectively, versus applied field. The deflection measurements shown are for a representative section of each plate. The section chosen for longitudinal bending and twist was the tip. And, due to the consistent decrease in transverse bending at the tip, the section chosen for this deflection was the 3/4 span (longitudinal x dimension). Each figure (Figs. 6.14 to 6.20) shows the experimentally measured deformations along with the Ritz predictions. The data symbols on the Ritz curves indicates the applied fields at which the iterations required to reach a solution were performed.

The longitudinal bending tip deflections measured experimentally and calculated analytically are plotted for the aluminum plate in Fig. 6.14. The agreement between the measured data and the Ritz predictions was very close at low applied fields. At higher fields, greater than 315 V/mm (8 V/mil), deflections greater than 10 times the plate thickness were observed. The deflections in terms of the plate thickness can be obtained by multiplying the reported values by the inverse of the thickness ratio C/t_s , which was 192 for the aluminum plates and 182 for the graphite/epoxy plates. These large plate deflections probably cause the non-linear plate stiffening terms to become significant and the Ritz predictions to overestimate the actual deflections. Table 6.2 summarizes the results of the deflection measurement experiments. Because of inaccuracies due to large plate deflections, all comparisons are made at 315 V/mm (8 V/mil). At this applied field the Ritz solution over-predicted a longitudinal bending deflection by only 5% for the aluminum plate.

The transverse bending deflections measured at the 3/4 span for the aluminum plate are plotted, along with the Ritz predictions, in Fig. 6.15. The agreement is excellent and the Ritz solutions is off by only 4% at the reference applied field 315 V/mm (8 V/mil), as shown in Table 6.2.

Table 6.2 Cantilever Plate Specimen Results at 315 V/mm.

	Alum.	G/E	G/E	G/E
Ply Sequence	----	[0/±45] _s	[30 ₂ /0] _s	[+45 ₃ /-45 ₃]
<i>Longitudinal Bending W₁</i>				
Experiment	0.036	0.034	0.035	----
Ritz	0.038	0.028	0.036	----
<i>Twist Deformation W₂</i>				
Experiment	----	0.0038	0.0106	0.0140
Ritz	----	0.0036	0.0128	0.0141
<i>Transverse Bending W₃</i>				
Experiment	0.0021	0.0028	0.0026	----
Ritz	0.0020	0.0032	0.0028	----

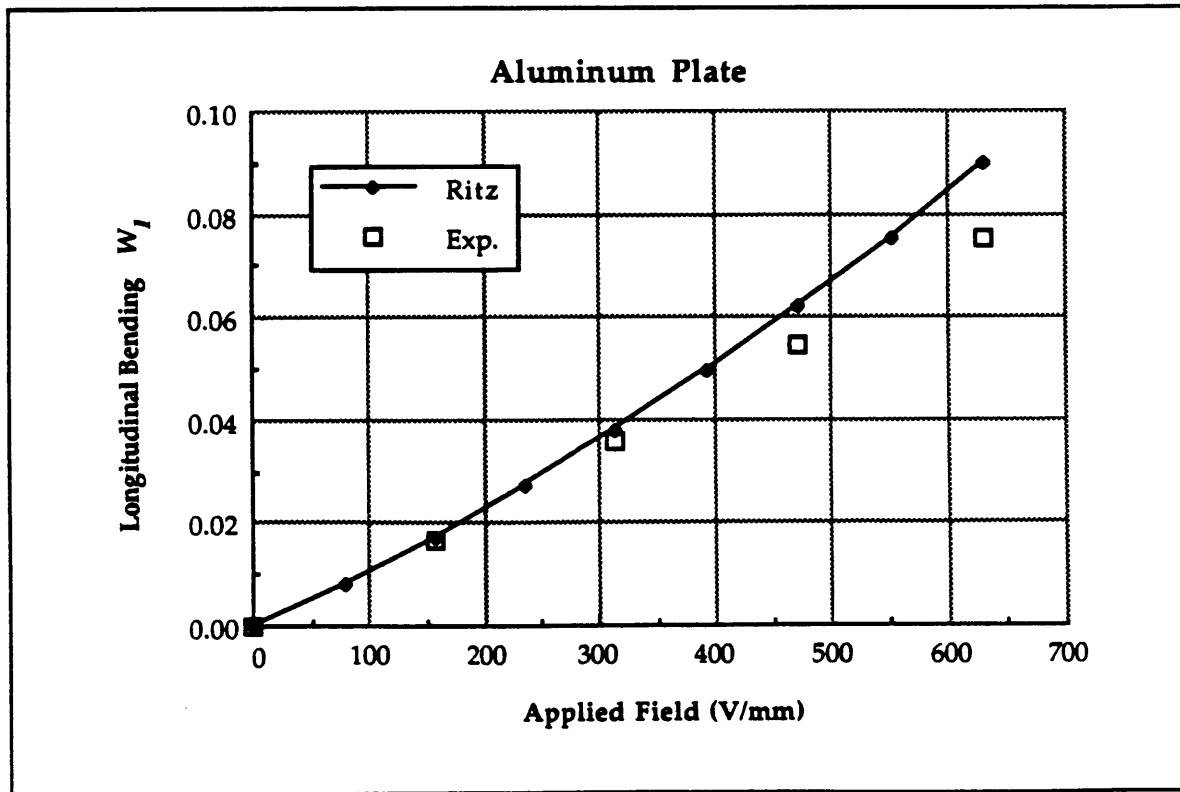


Figure 6.14 Aluminum plate longitudinal bending versus applied field.

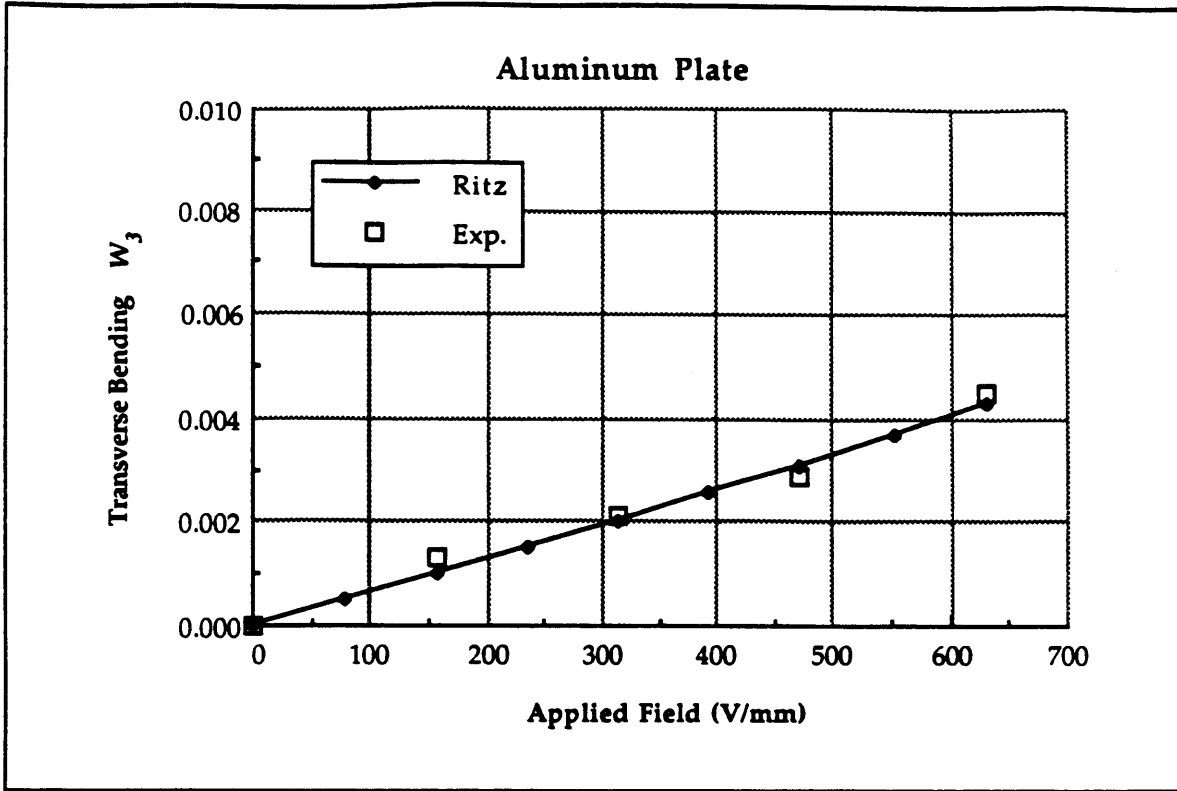


Figure 6.15 Aluminum plate transverse bending versus applied field.

The measured and analytically predicted deflections are plotted for the $[0/\pm 45]_s$ graphite/epoxy plate in Fig. 6.16 for longitudinal bending and Fig. 6.17 for transverse bending. This plate was designed for increased transverse bending with a longitudinal bending stiffness 28% higher than the aluminum plate and a transverse bending stiffness 20% less. As expected, Table 6.2 shows that the magnitude of the deflections recorded for this plate were less in longitudinal bending, by 6%, and greater in transverse bending, by 33%, than the aluminum plate deformations at the reference applied field.

Good agreement between experimental results and theoretical predictions was also found for the $[+30_2/0]_s$ graphite/epoxy plate which was designed to produce twist deformations from bending actuation. The results are presented in Fig. 6.18 for longitudinal bending and Fig. 6.19 for twist deflection. At the reference applied field the Ritz solution predicted deflections which were 3% and 20% higher than the measured values for longitudinal bending and twist deformation, respectively (Table 6.2).

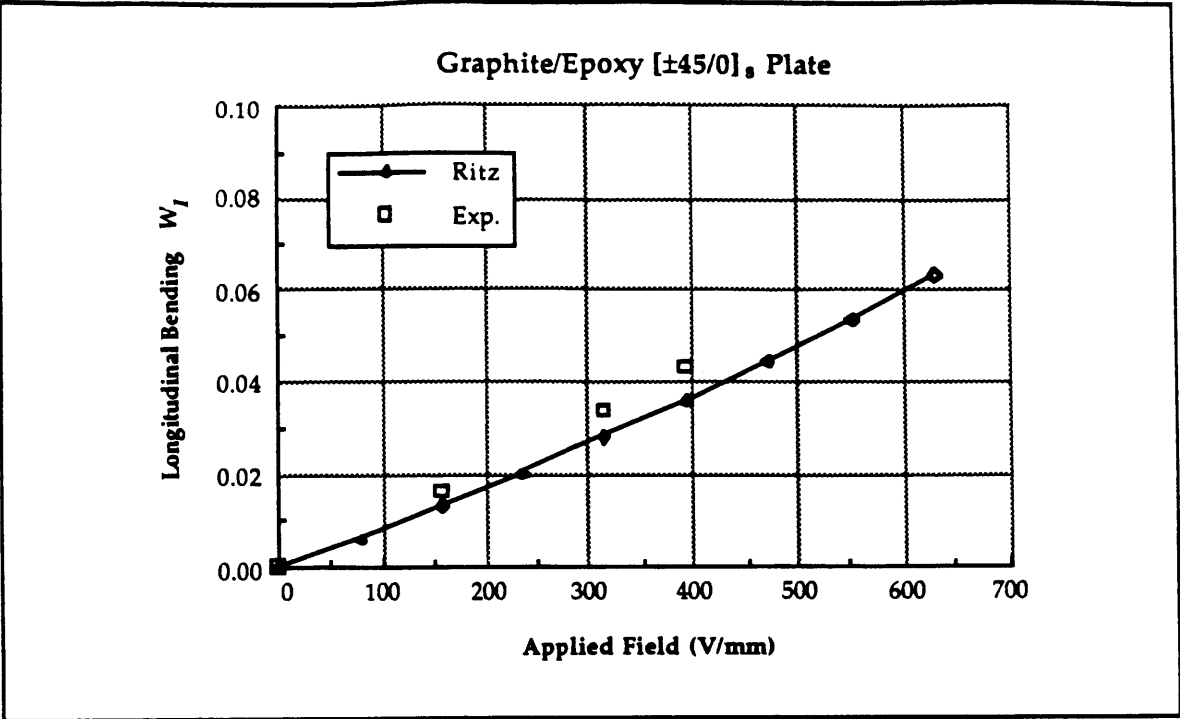


Figure 6.16 Graphite/epoxy $[\pm 45/0]_s$ plate longitudinal bending versus applied field.

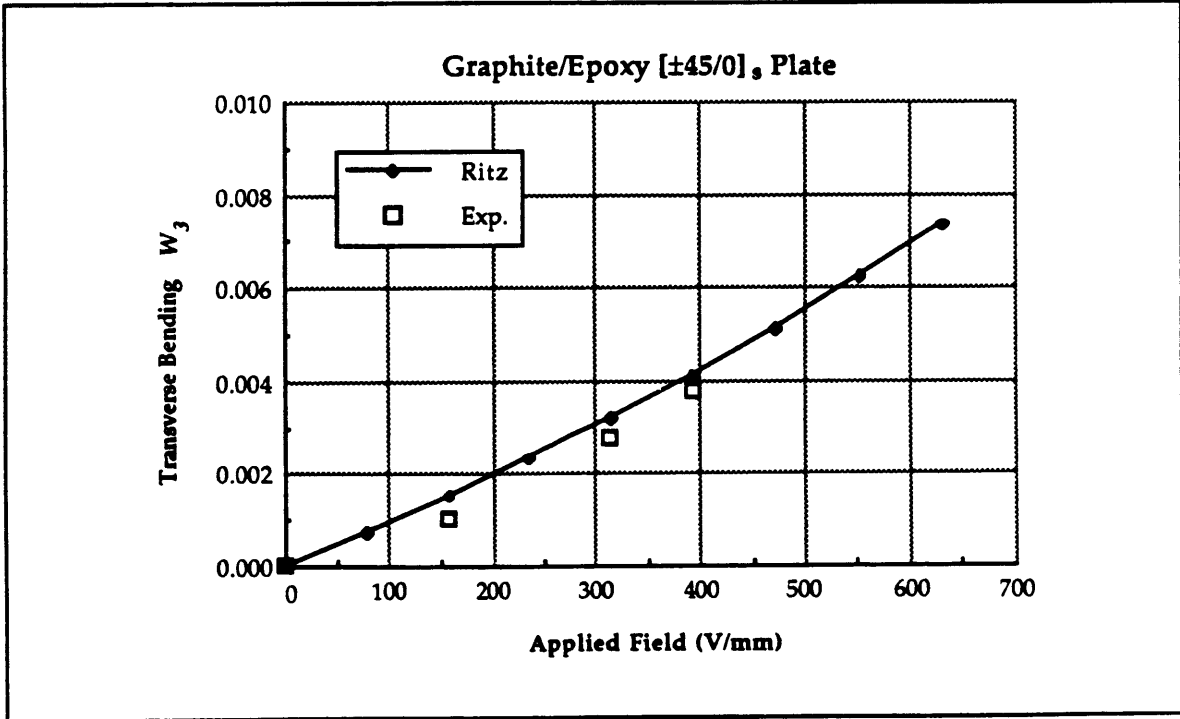


Figure 6.17 Graphite/epoxy $[\pm 45/0]_s$ plate transverse bending versus applied field.

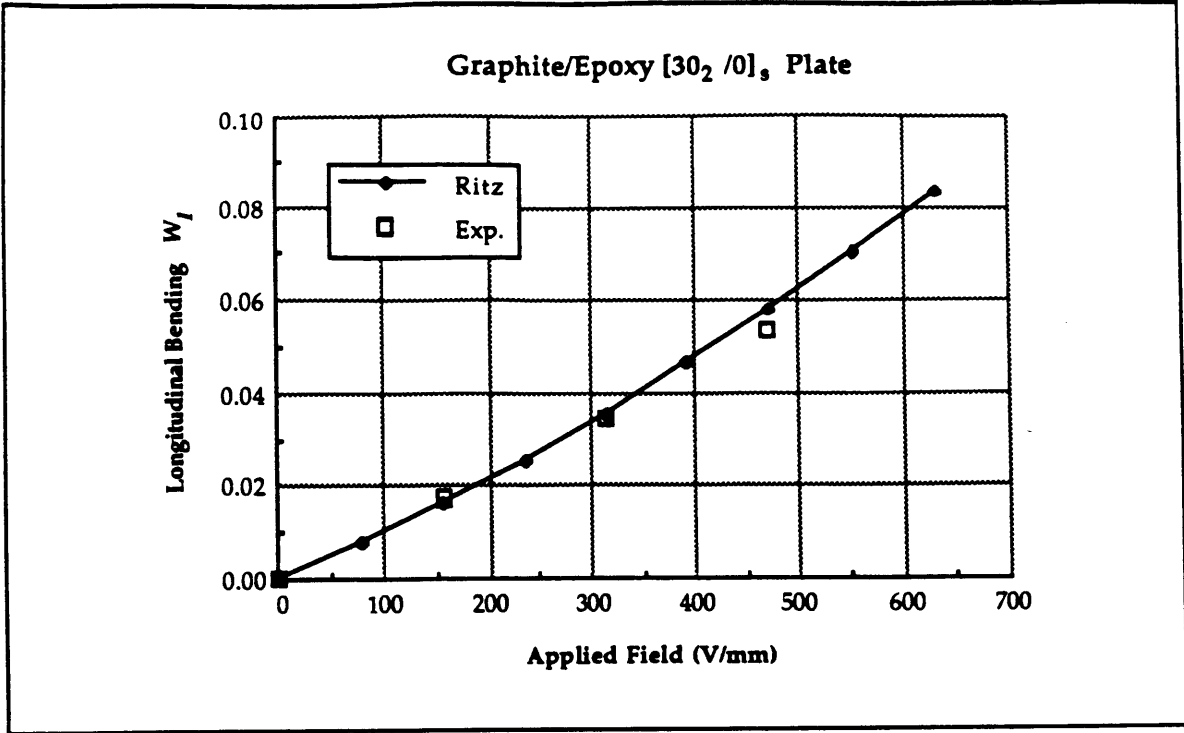


Figure 6.18 Graphite/epoxy [30₂/0]₃ plate longitudinal bending versus applied field.

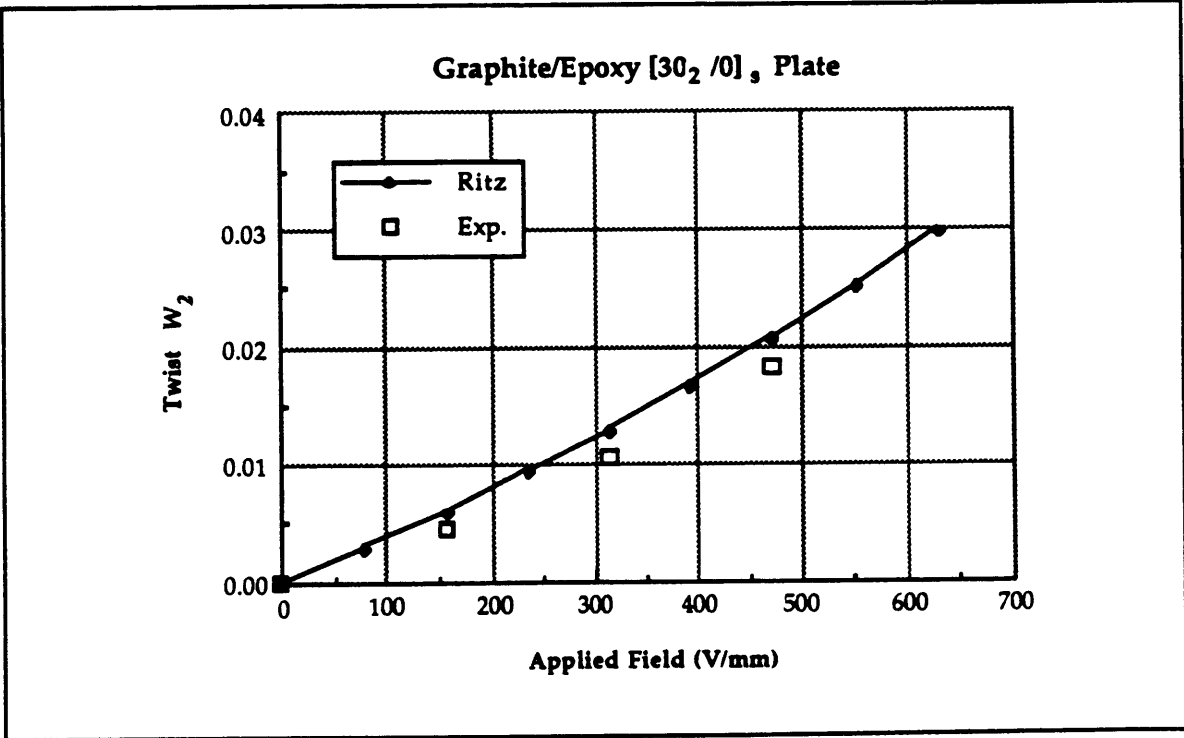


Figure 6.19 Graphite/epoxy [30₂/0]₃ plate twist versus applied field.

The final plate tested was the $[+45_3/-45_3]$ graphite/epoxy actuator system. This plate was actuated in extension and was designed to deform only in a twisting mode due to extension/twist coupling. It was observed that the $[+45_3/-45_3]$ graphite/epoxy plate produced twist deformations which were 32% larger than the deformations produced by bending/twist coupled $[+30_2/0]_s$ plate, even though the torsional stiffness of the $[+45_3/-45_3]$ plate was 11% higher. In addition, because this plate did not bend in the longitudinal or transverse directions there were no measurement complications due to large longitudinal bending, and the twist deformations predicted by the Ritz solution were virtually identical to the experimentally measured values, as reported in Table 6.2. Fig. 6.20 displays the experimentally measured and analytically predicted twist deformations versus applied field.

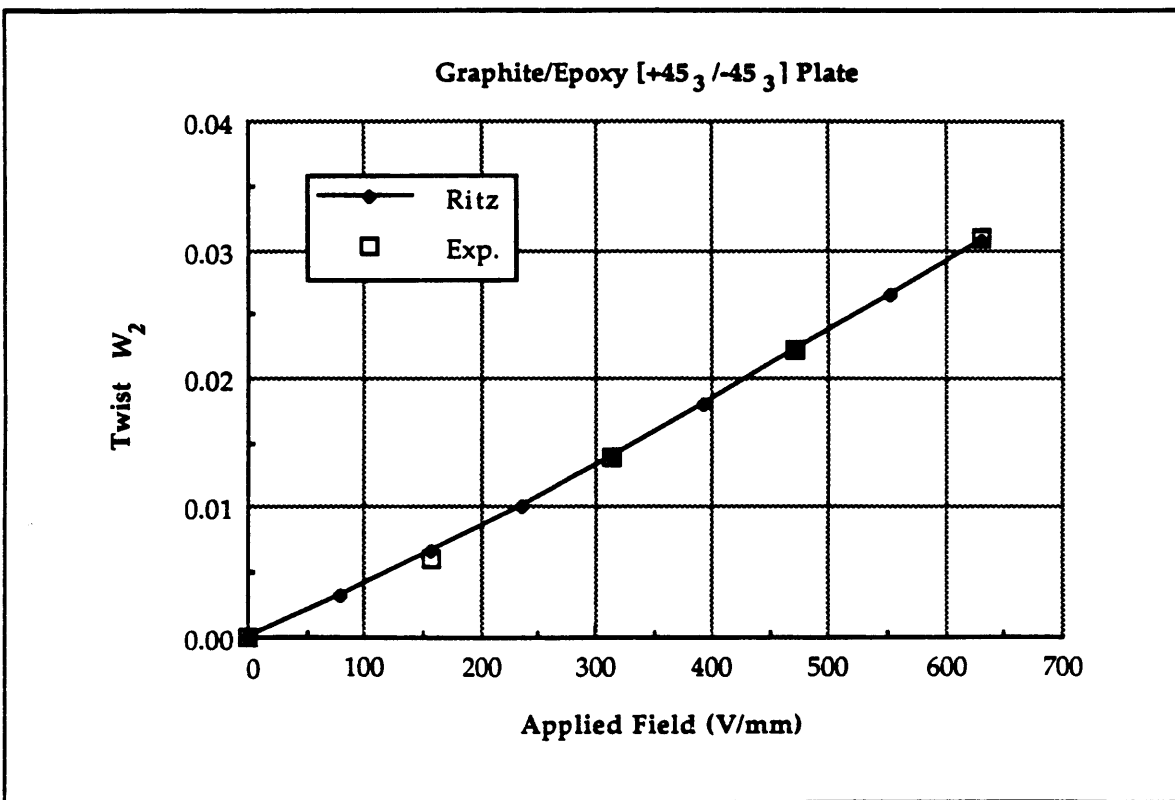


Figure 6.20 Graphite/epoxy $[+45_3/-45_3]$ plate twist versus applied field.

6.4 Conclusions

As was the case for the sandwich actuator specimens, the correlation between the experimental results and the analytically predicted deformations was excellent for the large cantilever plate, symmetric systems. Substantial agreement was found between the experimentally measured mode shapes and the mode shapes assumed in the Ritz analysis, and the magnitude of the deflections observed experimentally were in close agreement with the deflections predicted.

The longitudinal bending mode shapes were found to be well modelled by the quadratic function of the longitudinal coordinate, as was assumed in the Ritz analysis. Some noise was observed in the experimentally determined twist and transverse bending mode shapes due to metrology difficulties. However, it was observed that a simple linear function of the longitudinal coordinate approximated these modes quite well.

It was found that the Ritz solution predicted the experimentally measured deformations best in the low field range where the effects of large plate deformation non-linear terms were small, although good agreement was found throughout the range of applied fields tested. Finally it was observed that the $[0/\pm 45]_s$ graphite/epoxy plate produced greater transverse bending deformations than the aluminum plate and that actuation of the $[+45_3/-45_3]$ graphite/epoxy plate in extension created more pronounced twist deflections than actuation of the $[+30_2/0]_s$ plate in bending as expected.

CHAPTER 7

CONCLUSIONS

Two models of induced strain plate actuator/substrate systems were developed and verified experimentally. Equations relating the actuation strains produced by the strain actuators to the strains induced in the system were derived for the "pin" force plate and the consistent plate model. The plate strain energy relations were also developed for induced strain actuator/substrate systems using the consistent plate model. In addition, a model for the actuation strains created in piezoceramic plate actuators was developed. Induced strain plate actuation test articles with piezoceramic plate actuators were constructed, and experiments were performed to measure the deformations induced. Substantial agreement between the experimentally measured and analytically predicted deformations was found, verifying the models developed, and demonstrating that induced strain actuation is an effective means of controlling plate deflections.

Exact solutions to the equations derived from the induced strain plate models were formulated for isotropic and anisotropic plate systems. Exact solutions were found for systems with free-free, free-free boundary conditions. These solutions showed the resulting induced strains and curvatures produced through strain actuation are dependent on the actuation strains, the relative stiffness ratio and the geometry of the system. It was also shown that the curvatures induced were inversely proportional the plate thickness.

Since exact solutions could only be found for a limited class of actuator/substrate systems, the plate strain energy equations were derived and a Rayleigh-Ritz approximate solution method was developed. Development of the Ritz solution to the energy equations was found to be straight forward using the consistent plate model and allowed easy analysis of systems with complicated stiffness coupling, arbitrary boundary conditions, and external loads. A seven mode Ritz solution was used to analyze the test articles constructed. Although mode shapes assumed were simple functions of the

plate dimensions, these modes were found to approximate the actual experimentally determined modes quite accurately.

Additionally, a simplified Ritz analysis was performed to reveal important design parameters. Specifically, a three mode Ritz solution was used to examine the parameters which govern the creation of twist deformations. It was found that the maximum twist deformation obtainable was dependent on the bending/twist coupling parameter for bending actuation and on the extension/twist coupling parameter for extensional actuation. Examination of these parameters showed that exploiting extension/twist coupling rather than bending/twist coupling was a desirable alternative for creating twist in some applications.

A model for predicting the actuation strains produced by a specific class of induced strain actuators, piezoceramic actuators, was also developed. The non-linear properties of piezoceramics were discussed and it was found that the important effects of such non-linearities were due to hysteresis, and the dependence of the mechanical/electrical coupling coefficient and the actuation strains on the induced strain. Thus the strain dependence of the coupling coefficient was incorporated into the actuation strain model. This strain dependent coupling coefficient allowed for anisotropic actuation strains to be created in piezoceramic actuators even though piezoceramics are nominally isotropic materials. It was found that this anisotropy resulted from anisotropic induced strains produced by anisotropic substrates or boundary conditions. In addition, a semi-empirical iterative solution procedure was required to solve for the strains induced in systems with piezoceramic actuators, and the iteration required to reach a solution was found to converge for typical actuator/substrate systems.

The models developed were verified through experimentation. Two sets of plate test articles were constructed and tested. The first set of simple test articles showed the validity and accuracy of the basic induced strain actuation models, the strain dependence of piezoceramic actuation strains, and the semi-empirical solution procedure. In addition the orthotropic test specimen showed that actuation strains do in fact vary in each principle direction due to the orthotropy of the actuator/substrate system. The resulting induced strains predicted for the isotropic test specimens, in which

isotropic actuation strains were predicted, and the induced strains predicted for the orthotropic specimen, in which orthotropic actuation strains were predicted, correlated well with the induced strains measured.

The second, more representative, set of large cantilever plate test articles built and tested verified the ability of the models to predict the strains induced in systems with heavy stiffness cross couplings and complicated boundary conditions, and to verify the Ritz approximate solution method. It was found from these experiments that systems could be constructed to produce specific desired deformations such as longitudinal bending, twist, or transverse bending. The test articles designed to produce twist deformation and those constructed for augmented transverse bending all performed as expected and produced significant deformations. Agreement between the solutions predicted by the Ritz model and the experimentally measured deformations of these plates was found to be excellent.

The sandwich and cantilever plate test articles, which were proof of concept deformable structures, showed that induced strain actuation is a viable means of effecting control. These individual systems could be used in themselves or as part of a larger system to effect control for a wide variety of applications. The models and analysis techniques developed in this report provide the designer of induced strain actuator systems with the tools necessary to incorporate induced strain actuators into specific actuator systems in order to control structural deformations.

The cantilever plate test articles also showed that significant deformations, which can be used in the control of real structures, are obtainable from induced strain actuation. At 67% of the coercive field, a one-sided non-dimensional tip deflection of 0.076, or over 15 times the plate thickness, was recorded for the aluminum specimen. A 0.5% curvature change was measured at 50% of the coercive field for the $[\pm 45/0]_s$ graphite/epoxy plate. And at 67% of the coercive field, the one-sided non-dimensional twist was found to be 0.031, or 1.8 degrees, for the $[+45_3/-45_3]$ graphite/epoxy plate. The reader is reminded that these relative large reported values are roughly doubled for applications in which average, or peek-to-peek, deformations are the quantity of interest.

The plate structures tested in this research were controlled using induced strain actuation in an open-loop manner. Methods were described by which specific deformations could be commanded by applying fields to piezoceramics. Of course, in real world situations all the various forces acting on a structure cannot be predicted in advance, thus even perfect models will not be able to predict the actual resulting deformations observed. Therefore, future work should include the development of closed loop active control schemes for induced strain plate actuation.

An obvious extension of the static induced strain actuation models developed is for the dynamic control of plate like structures. Induced strain actuation can be used in dynamic applications in order to increase damping both passively and actively [Hagood and Crawley, 1988] and to effect a variety of control algorithms, including continuous [Gibson, 1979], hierarchical [Ward and Crawley, 1985], or wave control [von Flotow, 1985]. The same plate strain energy relations and modal stiffness formulation can be used, along with modal mass terms, to formulate and solve such dynamic problems. Also, the design parameters identified can be used to design induced strain actuator systems for controlling specific dynamic mode shapes and dynamic deflections in plates.

REFERENCES

Atluri, S.N. and Amos, A.K., ed., *Large Space Structures: Dynamics and Control*, Springer Verlag, 1988.

Anderson, E.H., "Piezoceramic Induced Strain Actuation for One-and Two-Dimensional Structures," S.M. Thesis, Massachusetts Institute of Technology, Cambridge, MA, 1989.

Antonyak, Y.T. and Vassergiser, M.E. "Calculation of the Characteristics of a Membrane-Type Flexural-Mode Piezoelectric Transducer," *Sov. Phys. Acoust.* 28, pp. 294-302, 1980.

Aronov, B. S., "Effective Coefficients of Electromechanical Coupling in Piezoceramic Bodies," translated from *Prikladnaya Mekhanika*, Vol. 16, No. 10, 1980.

Ashton, J.E. and Whitney, J.M., *Theory of Laminated Plates*, Technomic Publishing Company, 1970.

Boriseiko, V.A., Grinchenko, V. T., and Ulitko, A. F., "Relations of Electroelasticity for Piezoceramic Shells of Revolution," translated from *Prikladnaya Mekhanika*, Vol. 12, No. 2, 1976.

Burke, S. and Hubbard, J.E., "Active Vibration Control of a Simply-Supported Beam Using a Spatially Distributed Actuator," *IEEE Control Systems Magazine*, Vol. 7, No. 6, 1987.

Butler, J.L., *Application Manual for the Design of ETREMA Terfenol-D Magnetostrictive Transducers*, Edge Technologies, Inc., 1988.

Chiarappa, D.J. and Claysmith, C.R., "Deformable Mirror Surface Control Techniques," *J. of Guidance and Control*, Vol. 4, No. 1, 1981.

Crawley, E.F. and de Luis, J., "Use of Piezoelectric Actuators as Elements of Intelligent Structures," *AIAA Journal*, Vol. 25, No. 10, 1987.

Crawley, E.F., de Luis, J., Hagood, N.W., and Anderson, E.H., "Development of Piezoelectric Technology for Applications in Control of Intelligent Structures," paper presented at the American Control Conference, June, 1988.

Crawley, E.F., Warkentin, D.J., and Lazarus, K.B., "Feasibility Analysis of Piezoelectric Devices," Space Systems Laboratory, Massachusetts Institute of Technology, Cambridge, MA, Rept. MIT-SSL #5-88, Jan. 1988.

Forward, R.L. and Swigert, C.J., "Electronic Damping of Orthogonal Bending Modes in a Cylindrical Mast-Theory," *J. of Spacecraft and Rockets*, Jan. - Feb., 1981.

Gibson, J.S., "The Riccati Integral Equations for Optimal Control Problems on Hilbert Spaces," *SIAM Journal on Control and Optimization*, Vol. 17, No. 4, July 1979, pp. 537-565.

Hanagud, S., Obal, M.W., and Meyyappa, M., "Electronic Damping Techniques and Active Vibration Control," AIAA paper 85-0752, presented at the 26th Structures, Structural Dynamics and Materials Conference, April, 1985.

Jensen, D.W. and Crawley, E.F., "Comparison of Frequency Determination Techniques for Cantilevered Plates with Bending-Torsion Coupling," *AIAA Journal*, Vol. 22, No. 3, p 415, 1984.

Jones, R.M., *Mechanics of Composite Materials*, Scripta Book Company, Washington, D. C., 1975.

Shimuzu, K., *et al.*, "Pseudoelasticity and Shape Memory Effects," *International Metals Review*, Vol. 31, No. 3, pp. 93-114, 1986.

Tsai, S.W. and Hahn, H.T., *Introduction to Composite Materials*, Technomic Publishing Co., Stamford, CT, 1980.

Uchino, K., "Electrostrictive Actuators: Materials and Applications," *American Ceramic Society Bulletin*, Vol. 65, No. 4, pp. 647-652, April 1986.

von Flotow, A.H., "Low-Authority Control Synthesis for Large Space Structures Using Disturbance Propagation Concepts," AIAA Paper 85-0630, April 1985.

Ward, B. A. and Crawley, E.F., "A Hierarchical Control Architecture for Large Flexible Structures," Space Systems Laboratory, Massachusetts Institute of Technology, Cambridge, MA, MIT-SSL #18-85, Aug. 1985.